# Application of multiple unmanned aircraft systems (UAS) for bushfire mitigation

**Author:**
Homainejad, Nina

**Publication Date:**
2019

**DOI:**
https://doi.org/10.26190/unsworks/21426

# APPLICATION OF MULTIPLE UNMANNED AIRCRAFT SYSTEMS (UAS) FOR BUSHFIRE MITIGATION

**Nina Homainejad**

A thesis in fulfilment of the requirements for the degree of

Master by Research


School of Civil and Environmental Engineering

Faculty of Engineering

The University of New South Wales

March 2017

**PLEASE TYPE**

**THE UNIVERSITY OF NEW SOUTH WALES**

**Thesis/Dissertation Sheet**

Surname or Family name: **Homainejad**

First name: **Nina** Other name/s:

Abbreviation for degree as given in the University calendar: **MRes**

School: **School of Civil and Environmental Engineering** Faculty: **Faculty of Engineering**

Title: **Application of Unmanned Aircraft Systems (UAS) for Bushfire Mitigations**


**Abstract**

When a disaster threatens lives and livelihoods, emergency responders require high resolution, near-real-time, accurate data about the impact of the disaster to aid them during the response and decision making phases. Currently in the case of bushfires disaster response services rely on watchtowers, manned aircraft and satellite data for information. Advances in technology such as the development of sense-and-avoid systems will soon allow Unmanned Aircraft Systems (UAS) to be flown alongside manned aircraft in non-segregated airspace.

This research thesis explores how the simultaneous deployment of a low altitude UAS along with a high medium altitude UAS in different airspaces can aid bushfire mapping and surveillance. Each UAS category can supply a different set of valuable geospatial data in (near-)real-time to emergency service. The high/medium altitude UAS is fitted with satellite-like sensors and could be used for hot-spot detection, while the low altitude UAS is typically fitted with a video sensor and is utilised for object tracking and real-time site assessment. This research investigates the different UAS categories and their characteristics, and makes recommendations on the most useful UAS for monitoring bushfire behaviour. Subsequently a multiple UAS mission flight is proposed.

To support the implementation of a multiple UAS mission for data acquisition and analysis of fire behaviour, two sets of sample data were analysed. The first exercise compares the spatial-temporal advantage of the Predator B Ikhana UAS to MODIS satellite multispectral data. The second exercise explores the advantage of spatial video during bushfire emergencies. A series of video streams collected by a UAS were processed and integrated within a GIS database. The advantages of motion video, both as raw frames or as geo-referenced frames, with other layers of geospatial data are discussed.

The results from these exercises support the use of a combination of UAS during bushfire emergencies, and are a suitable alternative to traditional methods of data acquisition because of their ability to be used in dangerous environments thereby eliminating or reducing risks for firefighters and first responders.




FOR OFFICE USE ONLY Date of completion of requirements for Award:

**ORIGINALITY STATEMENT**

'I hereby declare that this submission is my own work and to the best of my knowledge it contains no materials previously published or written by another person, or substantial proportions of material which have been accepted for the award of any other degree or diploma at UNSW or any other educational institution, except where due acknowledgement is made in the thesis. Any contribution made to the research by others, with whom I have worked at UNSW or elsewhere, is explicitly acknowledged in the thesis. I also declare that the intellectual content of this thesis is the product of my own work, except to the extent that assistance from others in the project's design and conception or in style, presentation and linguistic expression is acknowledged.'

Signed .....

Date .....

**INCLUSION OF PUBLICATIONS STATEMENT**

UNSW is supportive of candidates publishing their research results during their candidature as detailed in the UNSW Thesis Examination Procedure.

**Publications can be used in their thesis in lieu of a Chapter if:**

- The student contributed greater than 50% of the content in the publication and is the "primary author", ie. the student was responsible primarily for the planning, execution and preparation of the work for publication
- The student has approval to include the publication in their thesis in lieu of a Chapter from their supervisor and Postgraduate Coordinator.
- The publication is not subject to any obligations or contractual agreements with a third party that would constrain its inclusion in the thesis

Please indicate whether this thesis contains published material or not.

☐ *This thesis contains no publications, either published or submitted for publication*

☒ *Some of the work described in this thesis has been published and it has been documented in the relevant Chapters with acknowledgement*

☐ *This thesis has publications (either published or submitted for publication) incorporated into it in lieu of a chapter and the details are presented below*

**CANDIDATE'S DECLARATION**

I declare that:

- I have complied with the Thesis Examination Procedure
- where I have used a publication in lieu of a Chapter, the listed publication(s) below meet(s) the requirements to be included in the thesis.

| **Name** | **Signature** | **Date (dd/mm/yy)** |
|---|---|---|
| | | |

# ACKNOWLEDGMENTS

First and foremost, I would like to thank my parents for all their encouragement, support and guidance. It is because of their hard work and many sacrifices in life that I am able to pursue my dreams. To my father, who is my greatest supporter, advisor, inspiration and my number one mentor, thank you for introducing me to the field of Surveying and Geospatial Engineering. It was your joy and passion for research that influenced me to undertake research work. To my mother, you are my biggest female inspiration, role model, mentor, and idol, but most importantly my best friend. Thank you for shaping me into strong minded and independent person. I hope I make the two of you proud with every step that I take in life.

I would like to extend my gratitude to my supervisor, Professor Chris Rizos, the most supportive, hardworking, and encouraging of supervisors. Thank you for believing in me, teaching me the "ropes" associated with research, and for pushing me to learn and achieve more every day. I appreciate all of the gruelling time that you have spent in helping me. I have learnt a great deal, and I feel blessed that I have had the opportunity to learn from you.

My gratitude is also extended out to my co-supervisor Dr Craig Roberts, for all his encouragement and support throughout my research. You have always provided me with helpful advice and recommendations.

I'd like to also thank Professor John Trinder for all his support. You are one of the most intelligent people that I have met. Your passion for research has inspired me. I'm so thankful that I have had the privilege to meet you and to learn from you, and I hope to learn more from you in the future.

To Professor Bruce Forster, thank you for your guidance, support and teachings. Your warm personality has made learning enjoyable.

This research would not have been possible without the assistance of many other people. First and foremost I'd like to thank Reza Homainejad for all of his assistance. I'd like to thank Vincent G. Ambrosia from NASA for guiding me to the correct channel in NASA and for

providing me access to the NASA Ikhana data. Many thanks to Katie Vandine and Anthony Fergusson from the NSW Rural Fire Services, who provided me with an incredible amount of helpful information. Rhys G. Bittner, Business Development Manager from Hexagon Geospatial, thank you for providing me access to the GeoMedia software. Thank you to WGCDR Jonathan McMullan and Heron 1 MALE category RPAS operator, and Janelle Sheridan from the Royal Australian Air Force for providing me access, and the opportunity, to visit their Woomera base station and to inspect the IAI Heron (Machatz-1) MALE category UAS up close.

# Table of Contents

# List of Acronyms

| Acronym | Description |
|---|---|
| ABSAA | Airborne Sense and Avoid |
| ALI | Advanced Land Imager |
| AMS | Autonomous Modular Scanner |
| ATC | Air Traffic Control |
| ATM | Air Traffic Management |
| ASTER | Advanced Spaceborne Thermal Emission and Reflection Radiometer |
| AVHRR | Advanced Very High Resolution Radiometer |
| BIRD | Bispectral InfraRed Detection |
| BIROS | Berlin InfraRed Optical System |
| BLOS | Beyond Line-of-Sight |
| C2 | Command and Control |
| C3 | Command, control and communications |
| CASA | Civil Aviation Safety Authority |
| CR | Close Range |
| DAA | Detect and Avoid |
| DSM | Digital Surface Model |
| EM | Electro-magnetic |
| ENVI | Environment for Visualising Images |
| EO | Electro Optical |
| ETM+ | Enhanced Thematic Mapper Plus |
| FDI | Fire Danger Index |
| FFDI | Forest Fire Danger Index |
| FDR | Fire Danger Rating |
| GBSAA | Ground Based Sense and Avoid |
| GCS | Ground Control Station |
| GFDI | Grassland Fire Danger Index |
| GIS | Geographic Information System |
| GNSS | Global Navigational Satellite System |
| GPS | Global Positioning System |
| GSD | Ground Sampling Distant |

| | |
|---|---|
| HALE | High Altitude Long Endurance |
| ICAO | International Civil Aviation Organisation |
| IMU | Inertial Measurement Unit |
| INS | Inertial Navigational System |
| IR | Infrared |
| ITU | International Telecommunications Union |
| LALE | Low Altitude Long Endurance |
| LASE | Low Altitude Short Endurance |
| LOS | Line Of Sight |
| MALE | Medium Altitude Long Endurance |
| MAV | Micro- UAS |
| MOA | Memorandum of Agreement |
| MODIS | Moderate Resolution Imaging Spectro-radiometer |
| MTOW | Maximum take-off Weight |
| MR | Medium Range |
| MRE | Medium Range Endurance |
| NAS | Nano – UAS |
| NATO | North Atlantic Treaty Organization |
| NASA | National Aeronautics and Space Administration |
| NAV | Nano-UAS |
| PAV | Pilotless Aerial Vehicle |
| RAAF | Royal Australian Air Force |
| RF-LOS | Radio-Frequency Line of Sight |
| ROA | Remotely Operated Aircraft |
| RP | Remote Pilot |
| RPA | Remotely-piloted aircraft |
| RPAS | Remotely-piloted aircraft system |
| RPS | Remote Pilot Station |
| RPV | Remotely Piloted Vehicle |
| RTCA | Radio Technical Commission for Aeronautics |
| SAR | Synthetic Aperture Radar |
| SARP | Standards and Recommended Practices |
| SATCOM | Satellite Communications |
| SR | Short Range |

| | |
|---|---|
| TET-1 | Technology Testing Device-1 |
| TM | Thematic Mapper |
| UA | Unmanned Aircraft |
| UAS | Unmanned Aircraft System(s) |
| UAV | Unmanned Aerial Vehicle- (obsolete term) |
| UN | United Nations |
| UOC | Unmanned Aircraft System Operator’s Certificate |
| UVS | Unmanned Vehicle System |
| VLOS | Visual Line of Sight |
| VMC | Visual Meteorological Conditions |
| VTOL | Vertical Take-off and Landing |

# List of Figures

# List of Tables

# CHAPTER 1: INTRODUCTION

## 1.1 Overview

Australia's environmental conditions make it one of the most fire-prone countries in the world. Furthermore, a large number of people reside or work in high-risk suburban and rural areas. When bushfires strike they can pose serious threats to lives and property, and hence place a large economic burden on the Australian community. It was reported by News Corp Australia that in the past 13 years bushfires have caused about $2.6 billion in damages (Cornish, 2014).

In Australia the term 'bushfire' is commonly used to describe fires burning in the landscape, and therefore includes forest, scrub or grass fires (Cheney and Sullivan, 2008). The three factors that determine whether a bushfire will occur include the presence of fuel, oxygen and an ignition source. Fire-rate and fire intensity can change within a short period of time. The factors that stimulate the acceleration of fires include the moisture content of fuel, presence of large volumes of dead vegetation and, to a lesser extent, the nature of living vegetation. Additional factors include fuel surface area, distribution of fuel in the vertical plane, combustion rate, burnout times of fuel, atmospheric instability, ground wind speed, terrain slope, and conditions for promoting the "spotting" process. The time of day also plays a role as the factors that increase the rate of fires are linked to the diurnal regime of wind, humidity and temperature.

To combat bushfires effectively, early detection and continuous monitoring is vital (Casbeer et al., 2005). Currently a number of methods are used for bushfire detection and monitoring, and emergency response, including watchtowers, fixed-wing aircraft and satellites. Due to the hazardous and unpredictable nature of bushfires, firefighters prefer (near-) real-time information about the affected area in order to plan and execute an effective and safe firefighting mission (Graml and Wigley, 2008).

Unmanned Aircraft Systems (UAS) equipped with appropriate bushfire imaging sensor payloads can play an important role in bushfire disaster situations. Due to their ability to fly at different flight altitudes and during hazardous conditions they are able to provide changes

in the fissures and allow emergency services to draw conclusions they would have had difficulty reaching generally (Harriman L and J., 2013). The objective of acquiring frequent, up to data intelligence is to image the perimeters of the fire, as well as updates of the location of the fire perimeters (Meyer et al., 2009). Among the most important parameters for bushfire emergency management are the shape and position of the fire front, its rate of spread (how this front evolves with time) and the maximum height of the flames (Cheney and Sullivan, 2008). When this information, along with other critical data, is integrated into a geographic information system (GIS) database it can provide powerful analytical advantages for emergency responders. This information can be used by emergency services in fire monitoring, predicting the evolution of the fire, determining safe fire combat locations, planning deployment of firefighting assets, broadcast of warnings, evacuation of civilian populations, etc.

With great interest in the application of UAS during bushfires, better understanding of suitable UAS categories for different bushfire missions is essential. Furthermore, it is important to recognise important bushfire imaging and navigations sensors. This thesis will review the advantages and limitations of aerial and satellite bushfire data. Along with an extensive review of different UAS categories is explored to demonstrate the advantages of UAS, with the intention of making recommendations on the most suitable UAS categories for different bushfire missions. This includes taking into account such issues as endurance, sensor payload, communication system (data link), and operational constraints and challenges. A further objective of the thesis will be to speculate on how to coordinate the simultaneous operations of different types of UAS, for different categories of data acquisition, operating in different airspaces for effective bushfire mission planning and disaster response management.

To support this research, two investigations were carried out. The first explored how UAS acquired data can replace satellite imagery. The purpose for this research is to explore the many advantages of high altitude UAS fitted with ‘satellite like’ sensors compared to satellite data such as the resolution of the sensors along with its (near) real-time application and the value of such technology for firefighters and emergency services. Two sets of Predator B Ikhana data were processed in Matlab and ENVI to identify the hotspot regions and furthermore the hotspot pixels of the two fires are compared with MODIS (Moderate Resolution Imaging Spectroradiometer) satellite data from the same day. The second

explored how a low altitude UAS can be applied in site assessment, object tracking and identifying access routes for firefighters during a bushfire replacing ground and manned aerial surveying and reconnaissance.

## 1.2 Unmanned Aircraft Systems (UAS)

UAS have been operating since almost the dawn of aviation, however the defence industry has dominated their development and use for many years (Wong and Bil, 1998, NOVA Science Programming on Air and Online, 2002). This can be attributed to the complexity and cost of designing, constructing and operation of these systems, along with their unsuitability for operations in civil airspace, also referred to as non-segregated airspace, due to safety concerns (Meyer et al., 2009). In the past decade or so interest in UAS has rapidly increased, in both the military and civil sectors, with high demands for UAS for reconnaissance, surveillance, surveying and mapping, and geophysics exploration (Wang et al., 2008).

The primary difference between an UAS and a manned aircraft is the presence of the pilot on the latter. A UAS is operated by a remote pilot (RP) and does not necessarily fly 'autonomously'. In many cases the process of operating a UAS is more complicated than flying a manned aircraft as the RP lacks physical cues, such as visibility, motion, sound, feel and smell, and the crew (operator, backup-pilot etc.) responsible for the operation of a UAS may be larger than that of conventional aircraft (Everaerts, 2008; (Eisenbeiß, 2009).

### 1.2.1 Definition and terminology

The International Civil Aviation Organisation (ICAO) has adopted the Global Air Traffic Management Operational Concept (Doc 9854) definition of a UAS (ICAO, 2011, ICAO, 2005):

*"An unmanned aerial vehicle is a pilotless aircraft, in the sense of Article 8 of the Convention on International Civil Aviation, which is flown without a pilot-in-command on-board and is either remotely and fully controlled from another place (ground, another aircraft, space) or programmed and fully autonomous."*

Different taxonomies can be used to describe or classify a UAS. Familiar and synonymous terminologies used to refer to such systems include Unmanned Aerial Vehicle (UAV), Remotely Piloted Aircraft System (RPAS), Pilotless Aerial Vehicle (PAV), Unmanned Aircraft (UA) and 'drones'. The term 'Unmanned Aerial Vehicle' was retired by ICAO at the second international informal ICAO meeting held in Palm Coast, Florida, USA in January 2007. It was replaced by the more appropriate terminology 'Unmanned Aerial System' as it now refers to the whole "system", which includes the UA and the Ground Control Station (GCS). Terms such as 'Remotely Piloted Aircraft' or iterations thereof refer only to the UAS subset that requires direct control by the RP. Furthermore, this change now aligns terminologies used in Radio Technical Commission for Aeronautics (RTCA) and EUROCAE agreements.

The Civil Aviation Safety Authority of Australia (CASA) was quick to adopt the international UAS terminology standardisations recommended by ICAO, and replaced UAV with UAS, or RPA/RPAS, as appropriate (CASA, 2014a, CASA, 2014b). CASA also recognised the stigma that is associated with the label 'drone' and has acknowledged that this term is misleading (CASA, 2013).

### 1.2.2 Definition of RPAS

An RPA is a subset of UA (ICAO, 2011). As per (CASA, 2014b) an RPA is defined as "An unmanned aircraft where the flying pilot is not on board the aircraft", and an RPAS as "A set of configurable elements consisting of a remotely piloted aircraft, its associated remote pilot station(s), the required command and control links and any other system elements as may be required at any point during flight operation". Similarly the terms used for the ground crew members who operate the RPA have been changed to reflect their role by the introduction of the term "remote" before the noun (CASA, 2014a). It should be noted that ICAO has only approved the integration of RPA into the non-segregated airspace by 2030 (Light, 2016). Throughout this document, "UA" or "UAS" will be used as all-encompassing terms, whereas "remotely-piloted aircraft"(RPA) or iterations thereof will refer only to the piloted subset.

## 1.3 Aviation Rules and Regulations

The growth in number and applications of UAS has been recognised with the development of rules and regulations to ensure the safe integration of UAS into non-segregated airspace alongside manned aircraft. Rules and regulations for the safe operation of UAS have been implemented for the benefit of UAS operators, manufacturers and clients.

### 1.3.1 International Civil Aviation Organisation

ICAO is a UN (United Nations) agency whose primary mission is to develop international Standards and Recommended Practices (SARPs) for the safe, secure, efficient and environmentally-friendly operation of international civil aviation. ICAO recognised early that the international civil UAS activities had reached a level where there was a need for UAS regulatory development to address any danger to civil aircraft posed by UAS (ICAO, 2011). This means ensuring the safety of any other airspace user, as well as the safety of personnel and property on the ground and aloft in the case of integration of UAS in segregated and non-segregated airspace.

The rules and regulations are based on present and foreseeable activities of UAS and apply for the safe integration of UAS into the international non-segregated airspace, and can be used by States as a basis for developing national civil aviation regulations. In accordance with ICAO standards UAS will operate in accordance with standards that exist for manned aircraft, as well as any specific standards that address the operational, legal and safety differences between manned and unmanned aircraft operations. It should also be noted that for the operations of UAS in non-segregated airspace there must be a licensed pilot responsible for the operation of the UA.

The primary role of the ICAO with respect to UAS can be summarised as (ICAO, 2011):

- serve as the focal point for global interoperability and harmonisation,
- develop a regulatory concept,
- coordinate the development of UAS SARPs,
- contribute to the development of technical specification by other bodies,
- identify communication requirements for UAS activity, and
- harmonisation of notions, concepts and terms.

### 1.3.2 Civil Aviation Safety Authority

CASA is Australia's aviation regulatory body, was quick to notice the growing commercial interest in UAS. As a result they have established rules and regulations regarding UAS in Australia. For example, CASA released the Advisory Circular (AC 101-1(0)) as guidance for the manufacture and operations of UAS in Australia and CASR subpart 101.G, supported by guidelines within AC 101-3 for the safe operation of model aircrafts. UAS operators in Australia must adhere to these rules and regulations. This includes that the operator of a UAS weighing more than 2kg must hold a RP certificate. Other operating standards that should be noted include:

- Visual Line of Sight (VLOS) - direct visual contact of the UA by the remote crew without the aid of spectacles.
- Operational altitude below 400 ft above ground or water.
- No flights within populated areas, including a 30 m separation between any bystander not involved in the operation and the UAS.
- Following Day Visual Meteorological Conditions (VMC) guidelines.
- Minimum of 3 nautical mile separation from aerodromes.
- Operate outside of controlled airspace.
- Operate outside of prohibited, restricted and dangerous areas.

## 1.4 Problem Statement

A bushfire emergency management team requires fire intelligence for effective and efficient bushfire response. This includes information on fire behaviour, such as the fire condition, location, size, direction and speed of distribution, and vegetation composition. Currently firefighters collect information on the state of a fire through a combination of satellite, aerial and ground observation. While each source has its own advantages, they also are faced with some limitations.

Satellite imagery are vital during bushfire situations as they provide essential information on the scope of the fire, including the direction of fire movement, size and location of the blaze,

etc. Since the year 2000 several high resolution satellite data have been launched such as BIRD (Bispectral InfraRed Detection), an experimental fire detection satellite. Although BIRD had higher spatial resolution compared to MODIS it lacked in temporal resolution compared to MODIS. While there are many satellite sensors that are widely used in fire detection and monitoring, they face different limitations (Altan et al., 2013).

The problem with satellite imagery is the cost, lack of spatial resolution and timely availability of data due to orbit restrictions, hence they are unable to supply (near-)real-time images (Fransaer et al., 2004). To address spatial-temporal demands, emergency services seek to use airborne remote sensing techniques to complement data from satellites.

Though aerial reconnaissance along with ground observations can provide critical information to emergency services, this is also somewhat limited. Aerial imaging is an alternative to satellite imagery, and when equipped with appropriate sensors they are able to supply emergency services with (near-)real-time data on fire behaviour. Flying manned aircraft during bushfires poses a risk to the aircraft. Hazards include low visibility due to smoke and haze, turbulence due to rising columns of hot air, and lack of view during night operations (Merlin, 2009; (Xu et al., 2014, Grenzdörffer et al., 2008) . Other downsides to flying manned aircraft are their cost and their limited flight time ranging between 4-10 hours (Merlin, 2009, Ambrosia et al., 2011).

The high degree of flexibility, safety, high image resolution and adaptability to fly in different weather conditions and environments, has driven greater use of UAS technology as remote sensing and photogrammetry platforms (Adams and Friedland, 2011, Xu et al., 2014, Ezequiel et al., 2014). Though there have been some efforts to utilise UAS technology during wildfires not all have been successful, with the Predator B Ikhana UAS being one exception (Ambrosia et al., 2011, Ambrosia and Wegener, 2009, Ambrosia et al., 2003). Furthermore investigations into the application of multiple UAS have not been very successful (Casbeer et al., 2005, Ameri et al., 2009, Zajkowski et al., 2016a). This is perhaps due to a limited understanding of bushfire behaviour, as well as a mismatch with UAS categories that could satisfy the data collection requirements.

### 1.5 Research Objectives

The primary objective in exploring other technologies for bushfire monitoring is to address limitations of current methods of data acquisition. UAS are well suited for the 'dull, dirty and dangerous' tasks associated with many surveillance applications (Meyer et al., 2009). They are a suitable platform for applications in bushfire monitoring, and are a potential option to replace some of the traditional methods for bushfire surveillance. However the application of UAS for bushfire missions requires the selection of the appropriate type of UAS. This involves, amongst other requirements, understanding critical UAS characteristics such as endurance, sensor payload (navigational and imaging), communication system (data link), weight, resistance to wind effects, and others.

The objectives of this study are the following:

- To identify appropriate categories of UAS for bushfire missions. This includes the most suitable category of UAS for hot-spot detection and low altitude site assessment.
- To propose a multiple UAS application in such a way that they can be utilised simultaneously in a complementary fashion (Figure1.3).
- To investigate the use of UAS for hot-spot detection using two sets of Predator B Ikhana UAS data collected between 2007-2009 of wildfires in the western U.S.
- To investigate how the use of low altitude UAS can assist bushfire site assessment and assist first responders with video data collected by commercial grade Vertical Take-off and Landing (VTOL) UAS.

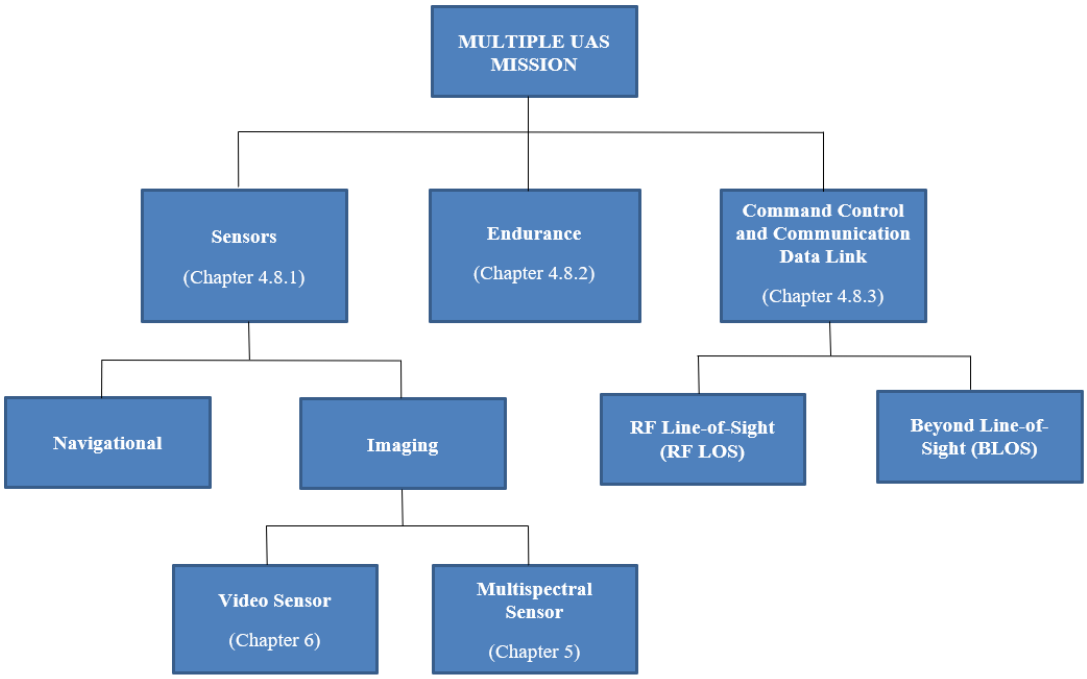


Figure 1.1 – A flowchart of how this research is divided and the topics that will be explored during this thesis

## 1.6 Proposed Methodology

The concept of simultaneous use of two different types of UAS, in different airspaces, for collecting different but complementary imagery to support bushfire emergency missions is introduced. The high altitude UAS is utilised for hot-spot analysis, while the lower altitude UAS fitted with a video sensor can be utilised for object tracking, site surveillance, identifying access routes, and close-up view of areas of interest to emergency services.

To explore how a multiple UAS bushfire applications can be beneficial compared to traditional methods of image data acquisition, two investigations were carried out. For the first two sets of National Aeronautics and Space Administration (NASA) Predator B Ikhana UAS data from the Western United States were analysed and compared with MODIS satellite data of the same area and the same bushfire events.

The second UAS investigation used video data collected by commercial VTOL UAS. Two different software packages were compared to study how video data can be best utilised for bushfire missions, and to identify advantages they may have for emergency services.

## 1.7 Thesis Structure

This thesis consists of a further five chapters:

Chapter 2 – outlines the influencing factors such as fuel load, weather and terrain and how they impact fire behaviour such as the shape, size, position of the fire front, its rate of spread and the maximum height of the flames. Furthermore the different categorised of fire are described along with the fire danger rating.

Chapter 3 – describes the different categories of UAS, their variation in size, endurance, flight altitude, and other capabilities. The advantages and limitations of the different categories are considered in the context of the requirements of bushfire missions.

Chapter 4 - describes a concept in flying multiple UAS in different airspaces for the acquisition of different types of image data. This chapter also briefly describes the traditional methods of collecting bushfire data.

Chapter 5 - is focused on the use of medium or high altitude UAS for hot-spot detection during bushfires. This chapter begins by discussing the spectral regions for hot-spot detection, followed by a description of MODIS satellite data. The Level 1 wildfire data collected by the Ikhana UAS during the period 2007-2009 were processed, analysed and compared against MODIS satellite data from the same area and time span. The algorithms for hot-spot analysis are described.

Chapter 6 – explores the advantages of video imagery, and how the application of spatial video, as a visually enriched GIS data source, can be useful during bushfire emergencies. This study is motivated by Australia's plans to use the Heron MALE (Medium Altitude Long Endurance) category UAS for such purposes. A description of the Heron UAS characteristics is given, followed by an overview of spatial video, a discussion of the appropriate format for video geo-referencing, how spatial video is fused with a spatial database, and the methods of converting video streams to image mosaics. An exercise utilising a commercial VTOL UAS fitted with a video sensor is described. A number of video streams collected by a UAS

platform are processed in two commercial software packages. The results are compared and discussed.

Chapter 7 – the research conclusions are drawn, the research outcomes described and recommendations for future research are presented.

# CHAPTER 2: BUSHFIRES IN AUSTRALIA

## 2.1 Introduction

In order to understand how UAS can be applied during bushfires it is important to have an understanding of the phenomenon of bushfires and the factors that control its behaviour. In Australia the term ‘bushfire’ is used to describe fires burning in the landscape, and includes forest, scrub or grass fires (Cheney and Sullivan, 2008). Bushfires are an inevitable natural disaster in Australia, posing serious threat to lives, properties, communities, as well as placing a considerable economic burden on the economy. Fire emission can be categorised as ‘natural or ‘anthropogenic’. There are three factors that impact the occurrence of a fire, they are: oxygen, fuels and ignition source.

Bushfires and grassfires are common in Australia because many Australian plants are fire prone and very combustible. Grassfires are fast moving, travelling across a field within five to ten seconds and smouldering for minutes (Geoscience Australia, 2016). They have a low to medium intensity and primarily damage crops, livestock, properties such as fences, sheds, and farming machinery. Compared to grassfires, bushfires travel slower but produce a higher heat output. This type of fire can pass in two to five minutes, but can smoulder for days (Geoscience Australia, 2016).

Bushfires can be categorised into three classes based on the main fuel layers involved in the combustion process: surface fires, crown fires and ground fires.

### 2.1.1 Surface Fires

Surface fires, which can be low to high intensity, are the most common propagation regime, in which a wide class of vegetation litter on the ground are consumed as flaming combustion. During such fires the tree canopies may be scorched but the fire does not travel through the tree crowns.

### 2.1.2 Crown Fire

This class of fires consumes the crown of trees and propagates with very high speed because the tree canopies are exposed to higher wind velocities than on the ground. As a general rule flame height is three to five times greater than the fuel height, and in such fires the height of the flame may be so great that a substantial part of the atmospheric boundary layer will be affected by flames (CFS, 2010). Under very strong winds these intense fires will experience high rates of spread, have the capacity to destroy large areas of forest land, and are very difficult to suppress. Crown fires tend to form a heterogeneous pattern due to the complex interaction of the convective flow and the tree canopies. This class of fire is almost certainly accompanied by spotting.

### 2.1.3 Ground Fire

Ground fires burn usually without flame in the organic layer above the mineral soil, their propagation is very slow and although they do not pose a great threat to the upper layers of the vegetation cover, they can produce considerable damage to the soil. In some particular conditions these ground fires can become flaming surface fires. This is quite common in the decaying phase of fires that are not completely extinguished; i.e. they may rekindle and start another loop in the fire development process.

## 2.2 Fire Danger

Weather information can be used in conjunction with fuel information to generate indices of fire hazard or danger rating (Tropical Savannas CRC and Bushfire CRC, 2017). Fire danger refers to the potential for a bushfire to start and spread, causing damage and posing a danger to lives. Fire danger rating (FDR) is set as a warning system for triggering necessary fire actions. Different ratings define the consequence of a fire if started, and how difficult it would be to supress the fire. The higher the FDR the more dangerous the fire conditions (Figure 2.1).

Fire danger is influenced by factors such as the temperature (C°), wind speed (m/s), relative humidity (%), content and fuel availability (%). The Fire Danger Index (FDI) is a calculation based on all of these values, and the higher the FDI the higher the fire danger, refer to table 3.1. There are two FDR systems used in Australia. Both were developed by A.G. McArthur (Luke and McArthur, 1986): the Forest Fire Danger Index (FFDI) for forest country; and the

Grassland Fire Danger Index (GFDI) for grassland and pastoral areas. These two systems are used because the burning characteristics of forest and grassland fuels differ.


Figure 2.1- Fire Danger Rating (CFA, 2012)

Table 2.1 - Categories of FDI can be assigned to a descriptive FDR according to this table (Tropical Savannas CRC and Bushfire CRC, 2017)

| **FDI** | **FDR** | **Definition and difficulty of suppression** |
|---|---|---|
| 0-11 | Low - Moderate | • High humidity, rainfall, little wind and bush is damp<br>• fires can be easily controlled<br>• head attack easy with water |
| 11-24 | High | • High humidity, rainfall, little wind and bush is damp<br>• head attack easy with water |
| 25 – 49 | Very High | • Hot, windy conditions and the bush is dry.<br>• The use of open fires is prohibited<br>• Fires can be difficult to control<br>• Head attack will generally succeed for FDI up to approximately 40. For FDI greater than 40, head |

| | | |
|---|---|---|
| | | attack may fail except in favourable circumstances and close back burning to the head may be necessary |
| 50 – 74 | Severe | • Very hot, windy and the bush is very dry<br>• Fires will be difficult to control and fast moving<br>• Direct attack generally fail. Back burn from a good secure line with adequate manpower and equipment. Flanks must be held at all costs. |
| 75 – 99 | Extreme | • Very hot, windy and bush is very dry.<br>• Fires will be very difficult to control and fast moving |
| 100 + | Catastrophic | • Fires will be unpredictable and very fast moving with highly aggressive flames<br>• Fires will likely be uncontrollable |

**2.3 How a Bushfire Spreads**

When bushfires develop they can spread along the ground rapidly through direct flame contact, radiant heat or burning embers. Direct contact mode is one where unburnt fuel is in contact with flames raising the temperature of the fuel load to ignition. Radiant heat mode refers to radiation of heat (in straight lines) by electro-magnetic waves, without direct contact between the source of radiation and the target fuel load. The heat radiated from the fire front is six times hotter compared to the back of the fire, with bushfires radiating greater heat compared to grassfires. Radiant heat is considered the major cause of death of humans and animals during a bushfire. Fires can also spread through the effect of embers. When embers land on fuels they can start small fires. If left unchecked these fires smoulder, grow and

spread. Embers are carried by winds ahead of the actual fire, sometimes several hundred meters.

## 2.4 Fire Behaviour

Fire behaviour refers to the manner in which fuel ignites, flames develop and fire spreads (Luke and McArthur, 1986). Important aspects of fire behaviour that are critical for bushfire response missions include: rate of fireline forward progress, fire perimeter spread and area spread, combustion rate, fireline intensity, fire burn out time, flame dimensions, scorch height, radiant heat output, convection column characteristics, fire whirlwinds, and spotting potential and distance. Once a fire has developed, its behaviour is influenced by three main factors (Figure 2.2):

- Fuel characteristics– availability and type, particle size, moisture content, quantity, arrangement and distribution.
- Weather – air temperature, relative humidity, wind speed and direction, and atmospheric stability.
- Topography – slope, aspect, effect on wind, and elevation.

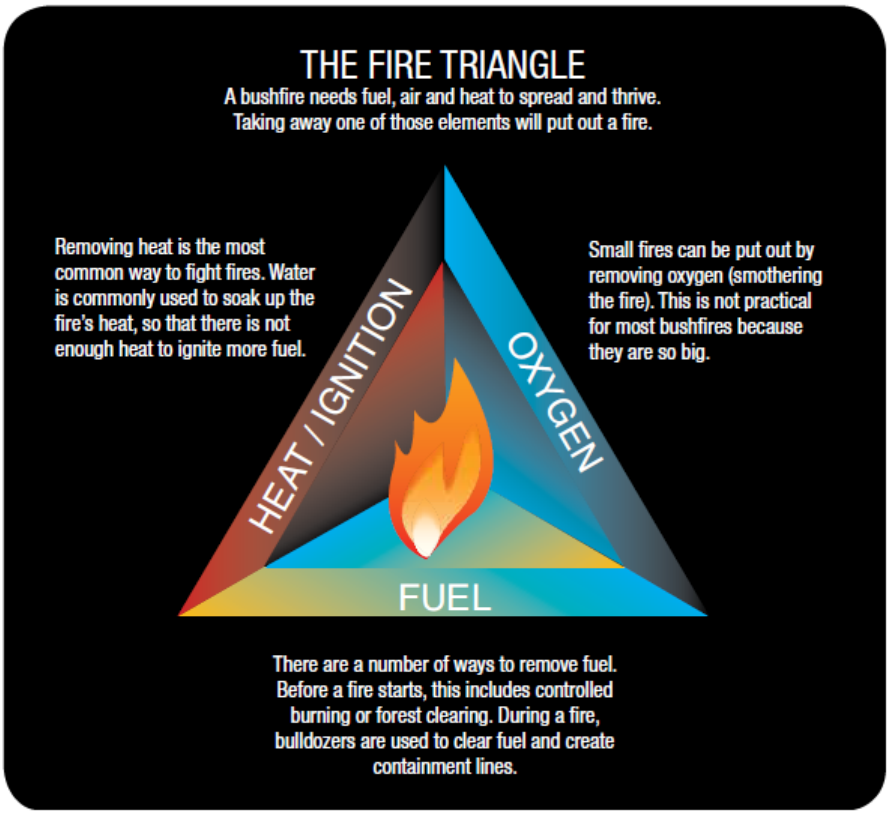


Figure 3.2

Figure 2.2 - The fire triangle (Department of Fire and Emergency Services, 2017)

### 2.4.1 Fuel

Fuel is one of the most important factors influencing fire behaviour and the fire spread. Fuelbed characteristics are temporally and spatially complex and can vary widely across the landscape of a bushland (Gould et al., 2011, Riccardi et al., 2007). In a bushfire, fuel is generally vegetation, grass (usually after it is drying out, or dead), leaves, bark, twigs, branches, trees and any other available product that combusts (Booth, 2009). Given the right conditions, most of these fuels will ignite and burn with different degrees of intensity. Fuel is the common environmental factor which can be manipulated to modify fire behaviour. Examples are back burning and trimming tree branches in remote regions near power lines. These steps are important controls set for reducing the risk and the likelihood of the ignition of a bushfires (Australia Attorney General's Department, 2010).

There are four variables of fuel that influence its contribution to fire behaviour: type of fuel, size and quantity of fuel, the arrangement of fuel, and the moisture content of the fuel load.

These fuel characteristics can affect the fire spread, flame structure, duration, and intensity of bushfires differently (Gould et al., 2011, Burrows, 1994). Fuel along with weather and topography will determine fire behaviour, severity of the fire in terms of suppression difficulty, and its physical impact on the forest that's is why it is important to know as much as possible about fuel characteristics (Burrows, 1994). For example, long dry grass, twigs and leaves will burn very quickly, while heavy forest and scrub will burn slowly, but at a much higher temperature and at a greater intensity. High intensity fires will consume larger and taller fuel compared to low intensity fires.

### 2.4.2 Weather

The key influencing weather elements are: rainfall, air temperature and relative humidity, wind and atmospheric stability, solar radiation and upper wind strength.

#### 2.4.2.1 Rainfall

The amount and duration of rain not only determines the immediate moisture content of the fuel load but also over a longer period determines the amount and type of available fuel (McCaw et al., 2009). The level of drought determines the seasonal severity of fire and the potential of the type of bushfire, whether forest or grassland. Fires can burn in dry forest early in the season before the grass has fully cured and is capable of carrying a moving fire. After a prolonged period of drought all surface fuels in forests may become available for burning including those in tall wet forests and forests in mountainous areas.

#### 2.4.2.2 Air Temperature and Relative Humidity

The moisture content of dead fuel can impact fire behaviour. Air temperature and relative humidity generally follow diurnal cycles, with air temperature increasing during the day, peaking in mid-afternoon and then decreasing while relative humidity decreases through the day, typically reaching a minimum in mid-afternoon and then increases during the night. This causes the moisture content in the dead fuel to lag behind changing temperature with fuel more moist at night and drier during the afternoon. Relative humidity in the atmosphere has more influence than temperature on moisture content. It follows that, given equal wind

conditions, the combination of dry air and low temperature may cause fires to spread faster than when the air is both hot and moist (Luke and McArthur, 1986).

#### 2.4.2.3 Effect of Wind on Fire Behaviour

Fire danger and difficulty of suppression are exponentially related to wind speed (Booth, 2009). Wind speed is the dynamic force behind the movement and spread of fires because it can rapidly change in strength and direction of the fire. As wind speed increases the rate of spread of the fire increases and it becomes much more difficult for firefighters to control. This applies to both grassland and forest fires. Wind acts on a fire in the following ways (NSW Rural Fire Service, 2015):

- Tilts the flames forward and provides more effective radiation and pre-heating of the unburnt fuels.
- Increases the chances of direct flame contact with fuels ahead of the fire.
- Maintains the oxygen supply to the combustion zone.
- Shifts the convection column ahead of the fire so that the convective energy of the fire reinforces and increases the wind speed in the flame zone, providing additional momentum to fire spread.
- Creates spotting by blowing burning embers ahead of the fireline.

### 2.4.3 Topography

The topography of the landscape can have a complex effect on the spread of fire, since influences the speed at which a bushfire will spread. Gullies and valleys can channel wind flow, establishing local wind directions and conditions. Mountain ranges will lift surface winds to higher altitudes, changing the temperature and moisture profiles of the air. Wind speed will be accelerated in windward slopes so that ridge-top winds will be stronger than winds in free air at the same level. Separation of wind flow across hills and ridges can generate turbulence and flow contrary to prevailing synoptic winds on leeward slopes. Under strong winds it is very difficult to predict the direction and strength of winds in valleys and lee slopes of rugged terrain. The two features of the topography that most influence fire behaviour are aspect and slope.

#### 2.4.3.1 Aspect

In countries such as Australia located in the southern hemisphere, north facing aspects receive more solar radiation than south facing aspects. This dictates the amount of solar radiation received by surface fuels and the moisture content of forest fuel with southerly and easterly aspects drying slower than northerly and westerly aspects. This means that bushfires are more manageable if they occur during mild fire seasons on southerly facing aspects because higher moisture content causes the fire to burn more slowly. However, this is irrelevant during moderate drought periods because fuels become uniformly dry so that the main influence of fire behaviour is the orientation of the aspect to the prevailing wind.

#### 2.4.3.2 Slope

Slope like wind speed has a considerable influence on rate of spread, especially when the slope of the ground is aligned with the direction of the prevailing wind. Both wind and slope increase the propagating heat flux by exposing the fuel ahead of the fire to additional convective and radiant heat (Luke and McArthur, 1986). Fire will travel faster up-slope than down-slope and with greater intensity because vegetation in front of the fire is pre-heated and will therefore be more readily ignited. The rate of spread of the fire up a slope of 10 degrees will generally be double the rate of spread of the fire on level ground, and up a slope of 20 degrees will generally be four times the rate of the fire on level ground (McCaw et al., 2009, Geoscience Australia, 2016) (Figure 2.3).

The interaction between wind and terrain, and the convection from fire is complex. When the wind speed is low the direction of the fire movement and spread is largely dominated by the slope angle in such a way that fire can be spread rapidly up-slope in the opposite direction of the prevailing wind, while under high wind speed the direction of fire spread is dominated by the wind direction. When considering the behaviour of large fires , the effect of slope can be virtually disregarded as far as rate of spread is concerned, since the process of spotting increases the rapid spread of fire across the topography, while slopes continue to have a significant influence on suppression difficulty (Luke and McArthur, 1986).

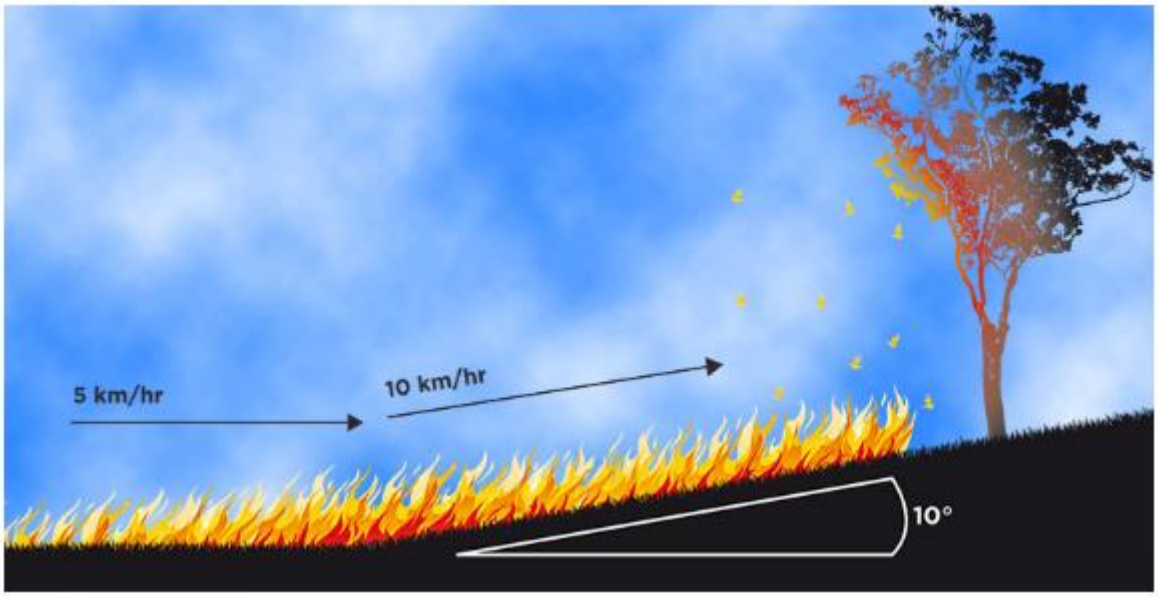


Figure 2.3 - the impact of slope on bushfire behaviour (The Government of South Australia, 2017)

Fire behaviour is the reaction of fire to the environment and variation in environmental conditions such as fuel load, weather and terrain. These environmental factors result in complex fire patterns. Understanding fire behaviour and how different influencing factors impact the physical attributes of a fire such as the fire height and depth of the fire flame, the speed, size and the shape of a fire are all of importance for the fire management team. The ability to predict reasonably accurate fire behaviour is essential for a number of purposes. Fire behaviour is important for fire danger rating, it is also used for predicting the rate of spread of a fire and finally it is important for prescribed burning operations that are done deliberately by setting fire under carefully defined fuel, weather and fire behaviour conditions.

Due to the rapid changing behaviour of bushfires (near) real-time information on the shape, size, position of the fire front, its rate of spread and the maximum height of the flames are required along with meteorological, topographic information along with details of fuel composition. These area valuable information and when obtained in (near) real-time they can assist the bushfire emergency management team in in a well throughout fire mitigation plan.

# CHAPTER 3 - CLASSIFICATION OF UAS

## 3.1 Introduction

There is no single standard when it comes to the classification of UAS. National and international UAS classifications are still immature and being regularly revised. UAS vary considerably in their size, flight endurance and other capabilities, and thus can be categorised into a number of different classes (Ameri et al., 2009; Everaerts, 2008; Watts et al., 2012). UAS categorisation requires continuous revisits due to persistent technological improvements. Over the years the classifications have altered due to improvements in flight endurance, payload capabilities and size reduction, resulting in the need to define new UAS categories with different flight endurance levels, size and capabilities. UAS come in a variety of shapes and sizes and are classified based on their physical properties such as their specific applications, size, mass and performance, or based on the airspace they fly in, such as flight altitude, location, etc. (Colomina and Molina, 2014, Everaerts, 2009, Watts et al., 2012). UAS have the capabilities to fly in a variety of airspaces such as in segregated air space, below 400 ft (~121m) and in the stratosphere and in non- segregated airspace. UAS that operate in the stratosphere are capable to operate during diverse weather conditions with zero impact on the UAS airframe. Depending on their sensor payload, the quality of the imagery could be impacted by cloud coverage. UAS of smaller frame size that operate below 400ft, due to their light weight are impacted by strong winds and rains. Due to safety rules and regulations, during such weather conditions they are not suitable for operations. While UAS that operate in non-segregated airspace require to meet and comply by civil airspace rules and regulations for safety purposes.

Each country has a different UAS classification but across Europe, the U.S.A and Australia a weight category of 150kg has been selected to differentiate between small (and comparatively simple) systems and the larger (and more sophisticated) systems that require special airworthiness approvals (Svensen, 2014). Although all systems can have the same safety impacts larger UAS require more regulations.

The definition of UAS encompasses fixed wing and rotary UAS, lighter-than-air UAS, lethal aerial vehicles, aerial decoys, aerial targets, alternatively piloted aircraft and uninhabited

combat aerial vehicles (Van Blyenburgh, 1999) with their primary airframe type , fixed-wing or rotary, explored in this thesis.

## 3.2 Components of an UAS

A UAS can be considered a 'system-of-systems', being effectively a set of discrete technologies integrated to fulfil a specific task (Colomina and Molina, 2014). The UAS made up of three main components: the UA, the Ground Control Station (GCS or C3) and the required Command and Control data link (C2). Depending on the application there are other critical components, such as the navigational and imaging sensors, the autopilot, the wireless system and the mechanical servos.

### 3.2.1 Unmanned Aircraft

An UA is recognised as an aircraft and major portions of the regulatory framework that applies to manned aircraft also apply to an UA. UA come in different airframes and they can be categorised based on their airframes. Each category varies considerably in size, flight endurance and other capabilities that characterise the different classes (Everaerts, 2008, Watts et al., 2012, Ameri et al., 2009) and they will be discussed in detail in Chapter three. An UA can be operated in semi-autonomous or autonomous mode, or a combination of both by an appropriately licensed RP at the GCS. For the safe operation and navigation of the UA two navigational technologies are typically fitted on the UA: a Global Navigational Satellite System (GNSS) receiver and an Inertial Navigational System (INS). The GNSS most used is the US's GPS (Global Positioning System), and is used to determine the position and velocity of the UA. This is especially important when operated in autonomous flight mode. In addition, the GPS/INS ensures that each image taken by the imaging sensor is geo-referenced.

Figure 3.1- From left to right, top to bottom: MAVinci SIRIUS, AscTec Falcon 8, Boeing Insitu ScanEagle, NASA Ikhana Preditor B, IAI Heron (Machatz-1) courtesy of Royal Australian Air Force (RAAF), Northrop Grumman RQ-4 Global Hawk

### 3.2.2 Ground Control Station

The GCS, sometimes also referred to as the Remote Pilot Station (RPS), is a fundamental component of a UAS, being used by the RP to communicate with and control the flight and image acquisition of the UA. The GCS may consist of nothing more than a handheld controller, or can be an elaborate fully-equipped cockpit. The licensed RP is at the GCS where he or she controls and monitors the UA, and in a more sophisticated UAS design responds to Air Traffic Control (ATC) commands and instructions, as well as communicating with them.

Figure 3.2- GCS of the Heron MALE category UAS and DJI phantom Advance UAS remote control

### 3.2.3 Command and Control Data Link

The communication uplink and downlink are essential for operating a UA. The C2 channel is the data link between the UA and the GCS. The communications uplink is essentially the commands sent by the RP used to control and manoeuvre the UA. The C2 downlink includes the data from the following sources (Barnard, 2007) :

- Header
- Inertial Measurement Unit (IMU)
- Flight Control Unit
- power
- warnings
- communications
- payload

- GPS
- sense (as in “sense and avoid”)

The telemetry and command bandwidth are considered separate from the payload bandwidth (Barnard, 2007). The command bandwidth is critical for the safe operation of the UAS while the payload bandwidth must be adequate for the transmission of the imagery collected by the UAS. Loss of payload bandwidth will not impact the safety of the mission, whereas the loss of the telemetry and command bandwidth will hinder the mission when the UAS is not being operated in autonomous mode.

### 3.2.4 Advantages of UAS

Imagery obtained through satellite, aerial or ground observation can be used in many applications, but are especially vital for disaster management. Satellite platforms offer global/ continental coverage while manned aircraft offer great flexibility, short response time and high resolution data (Everaerts et al., 2004). Although each has advantages they also suffer from limitations. UAS can overcome many of the limitations of traditional methods of obtaining geospatial imagery because of their capability to fly in diverse weather conditions while collecting valuable disaster related data, their unique characteristics of flight performance due to their ability to fly in different airspaces such as in segregated airspace (below 400 ft and in the stratosphere) and in non-segregated airspace, high image resolution during visually obscured missions, adaptability to flying at different altitudes, and their ability to operate in remote and dangerous environments. This will be further explored in this chapter.

The need for (near) real-time, high resolution and high accuracy data is increasing (Mondello et al., 2004). Satellite data are disadvantaged with respect to the available spatial resolution and the run cycle (Xu et al., 2014, Merion et al., 2010, Adams et al., 2010). Although more high resolution satellite data have become available recently at a reasonable cost, they are still limited by latency with respect to availability of data, and in the event of frequent cloud cover more satellite cycles are required before the area is completely imaged (Fransaer et al., 2004, Everaerts et al., 2004). Collection of remotely sensed aerial and metadata is perhaps the most important function of commercial UAS that can be utilised for a variety of applications

including disaster relief missions. Long endurance UAS with a high maximum take-off weight (MTOW), fitted with satellite-like imaging sensors can overcome such limitations. They have the flexibility to fly either in controlled airspace, or above it, making them an ideal alternative to satellite-imaged data.

During disaster relief missions such as bushfire mitigations, manned aircraft are limited with respect to flight operations due to the safety of the pilot and crew. Hazards include obscured visibility due to smoke, night operations, and turbulence from rising columns of hot air (Merlin, 2009). UAS applied in bushfire mitigations and data collection can provide imagery during night-time and smoky operations that currently prevent operations of piloted aircraft (Zajkowski et al., 2016b). Long endurance UAS are well suitable for dull, dirty and dangerous missions, such as missions that are of a monotonous nature, or entail hazards for the pilot of the manned aircraft (Meyer et al., 2009). Dull, dirty and dangerous refers to missions which would generally be long and tiring for the aircraft pilot and which will present a high risk factor to the pilot (Van Blyenburgh, 1999). While categories of small UAS are low-cost systems can be utilised for relatively small scale missions. Due to their light weight this category of UAS can be easily transported to any location and hand-launched. Other advantages of small UAS include low flying height and rapid acquisition of high resolution and (near) real-time spatial data (Choi and Lee 2011), making them very cost effective.

Of the many advantages of UAS, they can be used in high risk missions without endangering the lives of the RP and the RP crew. However, there is a broader potential scope for UAS including, inter alia, commercial, scientific, and security applications. Such uses mainly involve monitoring, communications and imaging (ICAO, 2011).

### 3.2.5 Limitations of UAS

Currently UAS face two types of limitations, technical and regulatory. Technical limitations, such as immature such as see and avoid technology, may ultimately be addressed through rapid technological development. These limitations can impact on the response time and the activity, but can be partially overcome by selecting alternative UAS replacements for the application in mind such as selecting low altitude UAS that can fly below 400ft for missions or high altitude UAS that can fly in the stratosphere. Regulatory limitations refer to the rules

and regulations set by local aviation authorities such as CASA or international entities such as the ICAO. The principle objective of the regulatory framework is to ensure safety of civilian aircraft.

For UAS to be integrated into non-segregated airspace consideration is required for regulation, airworthiness, C2, Detect and Avoid (DAA), RP licensing, RPAS operation and ATM (Air Traffic Management) integrations. Manned aircraft and their pilots are subject to many regulations, with most of these regulations focused on safety (Everaerts, 2008). Aircraft operating without a pilot on board present a wide array of hazards to civil aviation. The development of a complete regulatory framework for UAS is ongoing, until hazards generated by the operation of UAS are identified and the safety risks mitigated (ICAO, 2011). Until such time UAS cannot operate in civil international airspace. Hence an alternative is to operate UAS in segregated airspaces, such as below 400ft (121m) and above 39370ft (12km) (in the stratosphere). Although this is only a short term solution with the rules and regulations looked to be set for the operation of UAS in segregated airspaces, such as below 400 ft and in the stratosphere, in countries such as the U.S to avoid future air traffic in these airspaces (Kopardekar, 2015).

The communication data link between the UA and the GCS are important especially when operating a UAS BLOS (Beyond Line-of-Sight) mode. Communication between aircraft and the GCS requires radio spectrum with sufficient bandwidth, however currently there is no frequency band allocated to UAS by the International Telecommunications Union (ITU) (Everaerts, 2008). This means that the UAS will require use of available radio frequency in the operating country. As a result this can impact the speed of uplink and downlink transmission.

As UA do not have a pilot on board, the biggest obstacle to the integration of UAS in non-segregated airspace is the inability of UAS to satisfy see and avoid requirements, such as detecting other aircraft, providing right of way along with other visual applications that apply to manned aircraft (Stephenson, 2015). The solution to such obstacles is the design of DAA technology such as GBSAA (Ground Based Sense and Avoid) systems and ABSAA (Airborne Sense and Avoid) radar. GBSAA is a ground-based system for detecting airborne traffic and providing the necessary intelligence to the UAS. The ABSAA system is used for real-time detection, tracking and collision avoidance serving as the UAS pilot's "eyes" to

avoid mid-air collisions. DAA capabilities are important for the integration of UAS into non-segregated airspace and for BLOS operations, as they will allow the UAS to detect aircraft posing a risk to the UAS, assess that risk, and, if required, manoeuvre the UAS to maintain the required separation between aircraft and UAS.

Despite these limitations, developments in UAS technology continue, with predictions that the Small category of UAS will be the fastest growing category of UAS for civilian and commercial operations. This is due to their great versatility and relatively low capital and operating costs.

### 3.3 CASA Classification of UAS

CASA has classified UAS into the following categories based on their size (CASA, 2002):

- Micro - UAS with gross weight of 100 grams or less
- Small - UAS with a gross weight of 2kg and below
- Medium - UAS with a gross weight greater than 2kg and less than or equal to 150kg
- Large - UAS with a gross weight greater than 150kg

Most CASA regulations are concerned with safety. CASA rules and regulations specify that operators of UAS that weigh over 2kg require a RP Certificate or an Unmanned Aircraft System Operator's Certificate (UOC). Small category of UAS that are operated below 400ft AGL are not restricted in operations as long as they comply with CASA standard RPA operating conditions. For operations of UAS above 400ft AGL an approval needs to be issued by CASA prior to the UAS operation.

#### 3.3.1 UVS (Unmanned Vehicle Systems) International

UVS International is a non-profit organisation dedicated to the promotion of UAS, with a strong interest in non-military UAS operations (commercial & non-commercial) and the associated rules, regulations & standards. UVS International has classified UAS based on a number of features, such as flight altitude, flight endurance, speed, MTOW, size, and so forth (Bento, 2014). Tables 1 and 2 are based on (Blyenburgh, 2016) that differentiate UAS and UAS sub-systems into currently existing categories. Table 3.1 categorises UAS based on

MTOW, flight altitude, endurance, C2 range while Table 3.2 categorises UAS according to airframe types. Furthermore, UAS can be categorised based on the forms of propulsion they use.

Table 3.1 – UAS categorises based on MTOW, flight altitude, endurance, C2 range (Blyenburgh, 2016)

| | category | MTOW (kg) | Flight altitude range (m) | Endurance (hours) | C2 range (km) | Examples |
|---|---|---|---|---|---|---|
| **Tactical** | Nano | <0.025 | 100 | <1 | <1 | |
| | Micro (MAV) | <5 | 250 | 1 | <10 | Epsom & Sony Japan, Carolo C40 Mavionics & Rheinmetall, Germany |
| | Mini | <30 | 150-300 | <2 | <10 | M60 TAG USA, Colugo Kawada & Hitachi Japan |
| | Close Range (CR) | 150 | 3.000 | 2-4 | 10-30 | X-Vision SCR Spain, LUNA EMT Germany |
| | Short Range (SR) | 200 | 3.000 | 3-6 | 30-70 | Phoenix BAE Systems UK, Sniper Elbit Systems Israel |
| | Medium Range (MR) | 1.250 | 5.000 | 6-10 | 70-200 | Shadow 400 AAI Corp. USA, Fire Scout Northrop Grumman USA |

| | | | | | | |
|---|---|---|---|---|---|---|
| | Medium Range Endurance (MRE) | 1.250 | 8.000 | 10-18 | >500 | Shadow 600 AAI Corp.USA, SNARK TRG Helicorp, N. Zealand |
| | Low Altitude Deep Penetration (LADP) | 350 | 50-9.000 | 0.5-1 | >250 | CL289 EADS France & Germany, Mirach 150 Galileo Avionica Italy |
| | Low Altitude Long Endurance (LALE) | <30 | 3.000 | >24 | >500 | ScanEagle Boein & InSitu Group USA, Aerosonde Mk II Aerosonde Australia |
| | Medium Altitude Long Endurance (MALE) | 1.500 | 14.000 | 24-48 | >500 | Heron IAI-Malat Div. Israel, Predator General Atomics AS USA |
| **Strategic** | High Altitude Long Endurance (HALE) | 12.000 | 20.000 | 24-48 | >2.000 | Global Hawk Northrop Grumman USA, Helios AeroVironment & NASA Dryden USA |
| **Special Purpose** | Unmanned Combat | 10.000 | 10.000 | Approx. 2 | Approx. 1500 | Sharc Saab Sweden, |

| | | | | | |
|---|---|---|---|---|---|
| Aerial Vehicle (UCAV) | | | | | Barrakuda EADS Germany |
| Offensive (OFF) | 250 | 4.000 | 3-4 | 300 | Harpy IAI-MBT Israel, LOCAAS Lockheed Martin USA |
| Decoys (DEC) | 250 | 5.000 | <4 | 0-500 | Chukar Northrop Grumman USA, Flyrt Naval Research Lab. USA |
| Stratospheric (STRATO) | TBD | 20.000-30.000 | >48 | >2.000 | Currently not flying |
| Exo-strato-spheric (EXO) | TBD | >30.000 | TBD | TBD | Currently not flying |
| Space (SPACE) | TBD | TBD | TBD | TBD | |

TBD= to be defined

Table 3.2- UAS categorises according to airframe types (Blyenburgh, 2016)

| | **category** | **Rotary Wing** | **Fixed Wing** | **Others** | **Lighter-than-air** |
|---|---|---|---|---|---|
| **Tactical** | Nano | ✓ | | D,E | |
| | Micro (MAV) | ✓ | ✓ | D,E | |
| | Mini | ✓ | ✓ | D,K | ✓ |
| | Close Range (CR) | ✓ | ✓ | D,F,K | ✓ |

| | | | | | |
|---|---|---|---|---|---|
| | Short Range (SR) | ✓ | ✓ | G,K | ✓ |
| | Medium Range (MR) | ✓ | ✓ | H,T | |
| | Medium Range Endurance (MRE) | ✓ | ✓ | | |
| | Low Altitude Deep Penetration (LADP) | | ✓ | | |
| | Low Altitude Long Endurance (LALE) | | ✓ | | |
| | Medium Altitude Long Endurance (MALE) | ✓ | ✓ | | |
| **Strategic** | High Altitude Long Endurance (HALE) | | ✓ | | ✓ |
| **Special Purpose** | Unmanned Combat Aerial Vehicle (UCAV) | ✓ | ✓ | | |
| | Offensive (OFF) | | ✓ | | |
| | Decoys (DEC) | ✓ | ✓ | | |

| | | | | |
|---|---|---|---|---|
| Stratospheric (STRATO) | | ✓ | | ✓ |
| Exo-strato-spheric (EXO) | | ✓ | | |
| Space (SPACE) | TBD | TBD | TBD | TBD |

D= shrouded Fan

E= Flapping Wing

F= Gyroplane

G=Tilt Rotor

H= Rotor Wing

K= Motorised Parafoil

T= Tilt Body

TBD= To be defined

### 3.3.2 Other UAS Categories

Although no recognised international UAS category system exists, there are several recognised agencies and organisations that have published UAS categories. NATO (North Atlantic Treaty Organization) classifies UAS based on MTOW. This classification is utilised as the baseline for categorisation by organisations such as the Military Aviation Authority (MAA) (Table 2.3).

Table 2.3- UAS Classification Guide based on MTOW, NATO class, Common Taxonomy and CASA categorisation

| **MTOW** | **NATO Class** | **Common Taxonomy** | **CASA Category** |
|---|---|---|---|
| < 200g | Class I < 150 kg | Nano | Micro |
| 200g to 2kg | | Micro < 2kg | Small |
| 2kg – 20kg | | Mini 2 - 20kg | Medium |

| | | | |
|---|---|---|---|
| 20kg – 150kg | | Small > 20kg | |
| > 150kg | Class II 150 – 600kg | Tactical > 150kg | Large |
| > 600kg | Class III > 600kg | MALE / HALE / Strike | |

A general UAS classification in the civilian realm based on military descriptions in terms of size, flight endurance and capabilities, is provided by Watts et al. (2012):

- MAV/ NAV (Micro-UAS/ Nano-UAS)
- VTOL (Vertical Take-Off and Landing)
- LASE (Low Altitude, Short Endurance)
- LALE (Low Altitude, Long Endurance)
- MALE (Medium Altitude Long Endurance)
- HALE (High Altitude Long Endurance)

#### 3.3.2.1 MAV/ NAV (Micro-UAS/ Nano-UAS)

These categories of UAS are small in size and operate at very low altitudes, typically below 300 m. They are limited in flight time, generally operating for between 5-30 min, limited sensor payload, and selected applications. They evolved as a result of the US military's interest in developing miniature spy devices that could be used for situational awareness in areas where they cannot be observed. Examples such as Zano's Micro-Drone were initially designed for military applications and for the law enforcement market, are now available in the civilian sector (Paz-Frankel and NoCamels, 2014).

#### 3.3.2.2 VTOL (Vertical Take-Off and Landing) UAS

As fixed-wing UAS become larger in size, they can no longer be launched by hand and require a runway for take-off and landing. VTOL UAS have the advantage of hovering capabilities and manoeuvrability, and are an obvious alternative to fixed-wing UAS. They do not require a runway for take-off or landing, and therefore are of particular utility in remote areas or in disaster regions. This category of UAS comes in a variety of sizes, weight and

configuration, and can be found in the mini, CR, SR, MR and MALE categories (Bento, 2014). They generally operate at lower altitudes, for shorter time periods, and at lower speed compared to fixed-wing UAS (Watts et al., 2012).

Currently the smaller sized VTOL UAS are the most common. They have a limited payload, use rechargeable batteries and carry miniaturised sensors. The small-scale VTOL UAS are suitable for applications which require manoeuvring in tight spaces, such as transmission powerline inspections (Hrabar et al., 2010), site inspection, object tracking, CR photogrammetry, and building inspection and analysis. Small-scale VTOL UAS such as the AscTec Falcon 8 can operate for up to 12-22min depending on its payload, while larger sized VTOL UAS are utilised for military applications such as surveillance and reconnaissance. The Northrop Grumman's MQ-8C Fire Scout is a long endurance large scale VTOL UAS that has a flight endurance of up to 12 hours at a maximum speed of 135 knots, flying at an altitude of up to 16,000 ft (~ 5,000m) while carrying an array of sensors, making it useful for a diverse range of applications (Northrop Grumman Corporation, 2015).

#### 3.3.2.3 LASE (Low Altitude, Short Endurance)UAS

As the name implies this category of UAS is low endurance, relatively low in cost and can fly within VLOS for between 45 minutes and 2 hours, at altitudes up to 450 m. Advantages of such UAS are that they are light weight, making it easy to transport to any location, they can be easily launched and are ideal for small scale, high resolution imaging applications. Certificates are not required when operating such UAS outside of restricted flight zones and if complying with CASA rules and regulations. Due to their low cost they can be purchased by a wide range of users and used in diverse applications.

The limitations faced with such UAS include, their instability due to their light weight, especially in windy weather. Hence a number of considerations must be addressed when using such UAS including the weather conditions, camera angle, flight location, and the ground sampling distance (GSD). Prior to each mission the weather forecast must be checked and if there are predictions of heavy winds a reflight may be necessary. Flight plans for aerial photography are designed to run in the direction of the wind with larger forward (80%) and side (60%) overlaps. Such systems are generally capable of collecting and storing all the data on board, for example on a SD card. An example of this category is the MAVinci SIRIUS

UAS (Figure 1). Sensor limitations, short flight endurance, relatively low weight and their inability to provide real-time bushfire data make this category of UAS impractical for many bushfire services.

#### 3.3.2.4 LALE (Low Altitude, Long Endurance) UAS

LALE can carry larger payloads, of the order of a few kg to altitudes of up to 5000 m. As their name implies, this category of UAS can fly for extended periods, of 20 hours or longer, many kilometres from the GCS making it capable of operating BLOS. Some of the UAS in this category have limitations such as a limited imaging sensor payload and weak communication data link, but they also have many advantages, such as their long endurance. They typically acquire georeferenced colour, black and white imagery, or black and white infrared videos. This is particularly useful for firefighters as it can aid bushfire response management. Other applications of this category of UAS include missions of a scientific, emergency, surveillance, communications and industrial nature.

One example is the Boeing Insitu ScanEagle. Australian firefighters have seen the ScanEagle UAS used in the Wollemi National Park fires in early 2013 (Tomkins, 2013). The imagery from the ScanEagle was used to assess the movement of the fire front and to identify the locations of high-risk spot fires ahead of the front itself with Insitu Pacific Managing Director Andrew Duggan calling it a “game changer for emergency services and first responders”, showcasing its capabilities while also enhancing the safety of emergency services (Tomkins, 2013; Insitu, 2014).

#### 3.3.2.5 MALE (Medium Altitude, Long Endurance) UAS

This category of UAS is much larger than the previous categories, and is predominantly intended for military applications. They have more advanced aerodynamic design and control systems, and can operate to altitudes of 9000 m and above. Such UAS can be sent on flights hundreds of kilometres from their GCS, on missions lasting many hours (Watts et al., 2012). Examples of this category of UAS are the NASA Ikhana Predator-B, IAI Heron (Machatz-1) and REAPER UAS.

MALE UAS can be deployed in a short time and are capable of supplying (near) real-time geo-rectified, multi-spectral imagery to firefighters. Their high payload capability permits them to carry a variety of sensors including electro-optical (EO), infrared (IR) and synthetic aperture radar (SAR). They can also be fitted with SATCOM technology which can significantly enhance its capability by being able to send images to the GCS for near real-time analysis.

An example of the MALE category UAS that was successfully used in forest fire missions is the Ikhana UAS, used in the western United States between 2007-2009. It was the first civilian UAS to receive a Certificate of Airworthiness to operate in the U.S. National Airspace System (NAS), over the densely populated region of South California, to support imaging over firefighting efforts in October 2007 (Watts et al., 2012). The Ikhana flew at an altitude of 7000 m under the control of a NASA remote pilot. During its campaign the UAS carried out remote sensing data collection. In total it flew 20 missions over 60 fires, testing and developing imaging capabilities for forest fire monitoring (Watts et al., 2012). The UAS was able to provide near real-time, geo-rectified imagery to incident management teams within 10–15 min of data acquisition, resulting in an improved monitoring of fire conditions.

The REAPER UAS is another MALE category UAS that has been referred to as the most sophisticated and capable UAS that was deployed by the UK defence (Cross, 2010). It was used by the UK defence team in Afghanistan to gather intelligence and support for protection of forces. The REAPER UAS fitted with SATCOM technology that allowed the mission to spreads across 3 continents, with its headquarters situated in Qatar, the UA mission and operations in Afghanistan, the GCS where the RP and RP crew where located in Nevada USA while the product was analysed in UK through German satellite links.

#### 3.3.2.6 HALE (High Altitude, Long Endurance) UAS

With a growing demand for high resolution and accuracy geospatial data, the HALE category of UAS are a promising alternative to “satellite-like” imaging. HALE UAS are large and complex, and are capable of operating as a “very low-orbit” satellite by remaining in free airspace above 14 km (46000 ft) for days, weeks or even months (Fransaer et al., 2004). Anywhere between 12 and 25 km altitude falls within the stratospheric region. The advantage of the stratospheric region is that air traffic is controlled up to 14 km altitude, and above that

an aircraft is not limited in its movements, and in fact there is virtually no air traffic, allowing for more efficient mission planning (Everaerts et al., 2004). Due to their long endurance HALE UAS platforms are particularly valuable for strategic observation of large-scale (global/continental) phenomena (Watts et al., 2012).

This category of UAS is also capable of resolving the inherent drawbacks of both aerial and satellite platforms when equipped with appropriate sensors, for significant periods of time (Everaerts et al., 2004; Fransaer et al., 2004). Other advantages of the HALE UAS are significant cost advantages over satellite platforms, allowing a HALE UAS to be repeatedly returned to base for sensor modifications/upgrades or the addition of new payloads. Examples of this category are the Northrop Grumman RQ-4 Global Hawk (Figure 1) and the Zephyr QinetiQ.

The Zephyr QinetiQ is a light weight solar-electric HALE UAS designed to fly at altitudes up to 70000 ft for months at time to collect an supply (near) real-time remotely sensed imagery with high spatial, spectral and temporal resolution (Everaerts et al., 2004, Rapinett, 2009). The Zephyr is designed to be utilised for a variety of military and civil applications including surveillance, communications relay, remote sensing, mapping, atmospheric sensing missions, pipeline and crop inspection, forest fire monitoring, fisheries protection and border control (Kable Intelligence Limited, 2014).

With a diverse variety of UAS categories, it is important to explore bushfire behaviour along with influencing factors that impact that behaviour. Based on a review of bushfire behaviours recommendations will be made on the most suitable categories of UAS for successful bushfire survey and reconnaissance.

# CHAPTER 4: UNMANNED AIRCRAFT SYSTEMS (UAS) FOR BUSHFIRE DETECTION

## 4.1 Introduction

As there are many factors impacting on fire behaviour, firefighters and emergency services require continuous and timely 'intelligence' on fire conditions, location, speed, maximum height of the flame, vegetation type and volume, including unburned vegetation in the fire path, access routes, along with other information for a well-planned fire response. If this information is provided frequently it allows the fire response management team to act appropriately, saving resources, time and possibly lives (Ambrosia and Wegener, 2009). Once this information is collected and integrated into a GIS it can be used by the emergency services and firefighters. For this purpose fire monitoring can be defined as the determination in real-time of the evolution of the fire parameters (Merino et al., 2012).

Currently emergency services require access to satellite and airborne fire intelligence derived from imagery at appropriate temporal and spatial scales. The MODIS satellite provides images that can be used for a synoptic view of the fire location and extent. Identifying fires at their early stage is critical as they can be more easily controlled than when they have increased in size and ferocity. The spatial resolution of the MODIS satellite sensor is comparatively low, and therefore cannot detect smaller sized fires (Ambrosia and Wegener, 2009). A number of different manned aircraft are used in NSW for collecting fire intelligence, however they are unable to supply real-time data because the images cannot be transmitted directly from the aircraft to the firefighters or emergency services. The aircraft is required to land before the fire intelligence derived from image processing can be made available.

Because of their flight performance, high image resolution, adaptability to flying at different altitudes, and ability to access remote and dangerous environments, UAS can overcome most limitations of traditional methods of obtaining aerial and remotely sensed imagery (Ambrosia et al., 2011). If the appropriate UAS category was selected for each method of data acquisition not only can current limitations of traditional methods of data acquisition be

resolved but a safer working environment for fire fighters can be ensured because a number of risk factors for firefighters and emergency services can be reduced.

This chapter describes suitable UAS substitutes for traditional methods of data acquisition based on the detailed review of UAS categories in Chapter three.

### 4.2 Fire Detection Sensors

The electromagnetic (EM) spectrum describes the range of all types of EM radiation in terms of their frequencies and corresponding wavelengths (NASA, 2013) (Figure 4.1). The radiation reflected by different earth materials or objects at specific wavelengths is measured by a detectors that are sensitive to those wavelengths. The two most distinguishing features of a natural fire, particularly a luminous one, are its apparent source temperature and the power spectral density of its emitted radiation intensities (Sivathanu and Tseng, 1997). Whilst aerial reconnaissance based on the visible wavelength (wavelengths 0.4μm – 0.7μm) can be used during day time for viewing smoke during, the IR portion of the EM spectrum is the most useful range of wavelengths for day and night bushfire reconnaissance. The mid-infrared (wavelengths 3μm - 5.5μm) region is sensitive to radiation emitted from objects of high temperature, of the order of 800 to 1000 degrees Kelvin (°C + 273), and is used to detect strong radiation emissions from fire fronts. On the other hand, the far-infrared (wavelengths 8μm - 14μm) region is used to detect the naturally emitted radiation due to the Earth's temperature. These two bands are used together because the hypersensitivity of the mid-infrared band on its own can cause channel saturation (Dionizio and Trinder, 2012). Furthermore, the near-infrared spectral band (wavelengths 0.75μm – 2.5μm) (Figure 4.1) can be used to provide accurate data by elimination of false positives, caused by spectrally bright objects detected during the day.

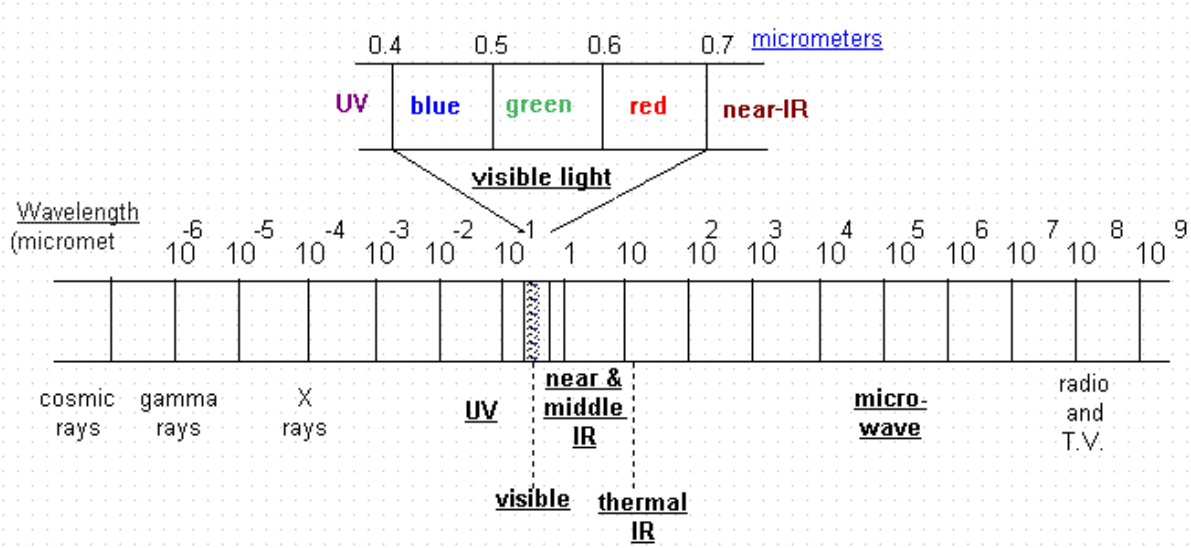


Figure4.1

Figure 4.1 - The electromagnetic spectrum (Crum, 1995)

### 4.3 Wien's Displacement Law

Wien's Displacement Law states that there is an inverse relationship between the temperature of a black body and the wavelength of its peak emission. This means the peak of the temperature curve of hotter surfaces shifts to the shorter wavelengths while cooler objects emit most of their radiation in the longer wavelength region (Figure 4.2). Wein's Displacement Law is expressed as:

(4.1) Wein's Displacement Law:

$$\lambda_{\max} = \frac{2898}{T}$$

Where $\lambda_{\max}$ is the wavelength at which the radiation is a maximum expressed in μm, $T$ is the absolute temperature in degrees Kelvin, and 2898 is the Wien's displacement constant expressed in K μm. For example, at 750 K (fire temperature condition) the wavelength at which the radiation is a maximum is 3.9 μm, while at 300 K (normal non-fire condition) the wavelength at which the radiation is a maximum is 9.7 μm (Philip, 2007). Examples of other sources, their maximum temperature and their peak wavelength are listed in Table 4.1.

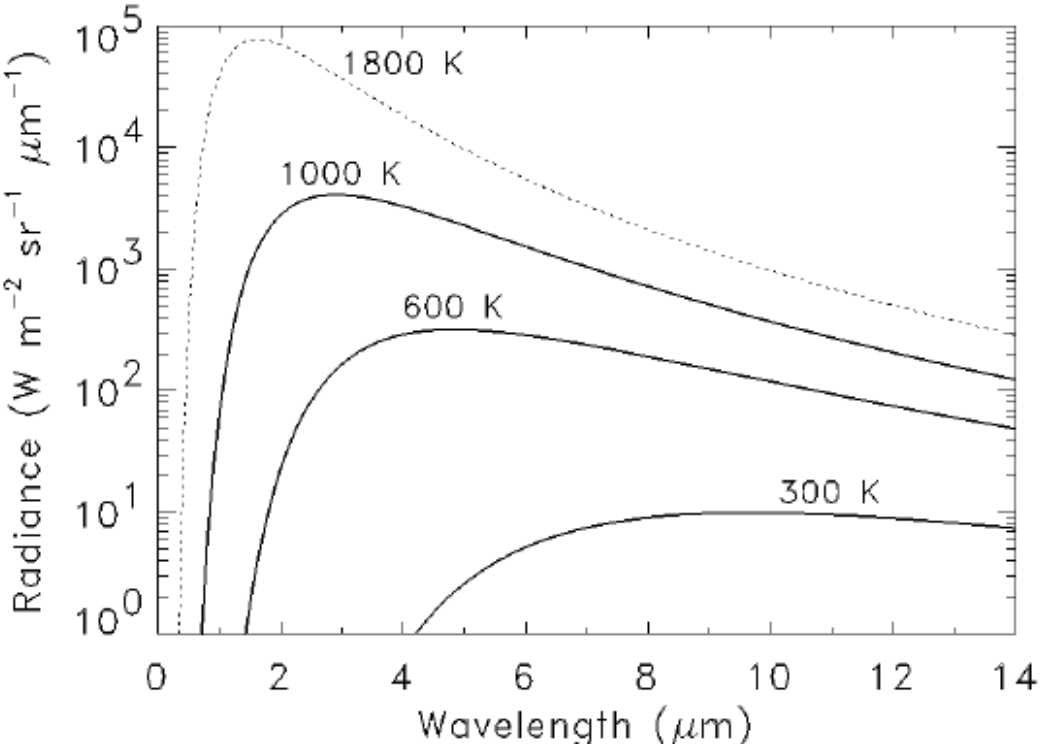


Figure 4.2 – Blackbody radiation curves (Ambrosia, 2012)

Table 4.1 - Spectrum of electromagnetic waves emitted from an ideal radiator at different temperatures along with their nominal wavelength ($\mu m$ ) (Ambrosia, 2012)

| Source | Temperature (C°) | Nominal Wavelength ($\mu m$) |
|---|---|---|
| Background | 25° | 10.0 $\mu m$ |
| Fuel Ignition | 275° | 5.0 $\mu m$ |
| Glowing | 550° | 4.0 $\mu m$ |
| Cool Fire | 725° | 3.0 $\mu m$ |
| Hot Fire | 1200° | 2.0 $\mu m$ |

### 4.4 Solar Zenith Angle and Scan Angle

The Solar Zenith Angle is the angle between the local zenith (i.e. directly above the point on the ground) and the line of sight from that point to the sun (Support to Aviation Control Service, 2011). This angle varies in such a way that the higher the elevation of the sun, the

smaller the solar zenith angle. The scan angle is the angle between the optical axis of a sensor and the earth's surface and the recording reflected radiation from the sun. The solar zenith angle and the scan angle are two important properties influencing thermal anomalies detected by sensors. The solar zenith angle influences the measured level of reflected sunlight in different ways. When the sun is at its highest point with a small solar zenith angle, such as noon time, sunlight passes through relatively less atmosphere which minimises scattering of the sunlight and any effects of pollution, haze or water vapour (Philip, 2007). Conversely, at a high solar zenith angle the atmospheric scattering is increased, reducing the amount of incident sunlight at shorter wavelengths. Therefore surfaces reflect light differently at high solar zenith angles than at low ones. Terrain slope and aspect along with the nature of the reflecting surface in the field of view of the sensing device will also influence the level of radiation recorded by a sensor.

### 4.5 Bushfire Detection Satellites

There are many satellites that are widely used to derive bushfire remote sensing data.

- Advanced Spaceborne Thermal Emission and Reflection Radiometer (ASTER)
- Advanced Land Imager (ALI) on EO-1 satellite
- Advanced Very High Resolution Radiometer (AVHRR)
- Moderate Resolution Imaging Spectroradiometer (MODIS)
- Landsat 5 TM (Thematic Mapper, no longer operational but historical data available)
- Landsat 7 ETM+ (Enhanced Thematic Mapper Plus)
- Landsat 8 Operational Land Imager (OLI)
- Spot 4 and 5
- Quickbird-2
- TET-1 (TechnologieErprobungsträger-1 or Technology Testing Device-1)
- BIROS (Berlin InfraRed Optical System).

Each sensor holds advantages and disadvantages such as spatial temporal resolutions, cost, and acquisition time (Table 4.2). High spatial resolution sensors have low temporal resolution (or there is no past data because data were only acquired on demand); additionally, the cost of data from these sensors ranges from $ 80 to thousands of dollars, depending on the sensor.

Consequently it is unfeasible to use this kind of product for monitoring active fires and burned areas and to establish an early-warning system.

MODIS fire products are considered among the most used reliable low cost products to monitor and detect hotspots and burned areas worldwide (John's book). Currently, the thermal IR channels band 22 (wavelength 3.929–3.989 μm) and band 31 (10.780–11.280 μm) on the MODIS instrument on board the NASA Terra and Aqua satellites are used by Geoscience Australia for hotspot detection of fires in the Australian region. These satellites orbit the Earth twice daily and image a given point at least four times a day, two in the morning and two at night. The spatial resolution of the thermal bands of MODIS is relatively low, being about 1000 metres, and the images are used to derive regional estimates of fire distribution (Ambrosia and Wegener, 2009). Multiple daily observations allow some estimation of fire movement at a large scale. Although the temporal frequency of the MODIS data is adequate for fire behaviour monitoring at a coarse scale, the spatial resolution is insufficient for identifying small fires.

Table 4.2 - Launch date, status, and spatial and temporal resolutions of major satellite sensors used for fire detection purposes (Altan et al., 2013)

| | **Landsat 5 TM/ 7 ETM+** | **Landsat 8** | **ASTER** | **Spot 4** | **Spot 5** | **AVHRR** |
|---|---|---|---|---|---|---|
| **Owner** | NASA | NASA | NASA | Space Imaging (France) | Space Imaging (France) | NOAA |
| **Launch Date** | March 1984/ April 1999 | | December 1999 | March 1998 | May 2002 | Since June 11, 1978, several satellite sensors have been launched |
| **Status** | Landsat 7 ETM+: the Scan Line Corrector abroad malfunctioned on May 31, 2003. Data only in the middle part of the images can be used. | | Working | Working | Recently launched sensors (2000, 2002, 2005) still work well. Continuous historical data from 1978 to present are available. | Working |
| **Spatial Resolution (m)** | 15-120 | 30-100 | 15 - 90 | 20 (10m monochromatic) | 10 (2.5 m panchromatic) | 1100 |
| **Temporal Resolution (day)** | 16 | 16 | 16 | 3 | 3 | 1 |

| | | | | | | |
|---|---|---|---|---|---|---|
| **Scene Size (km x km)** | 185 x 185 | 185 x 185 | 60 x 60 | 56 x 56 | 56 x 56 | 2400 x 6400 |

| | **IKONOS-2** | **MODIS** | **ALI** | **Quickbird-2** | **TET-1** | **BIROS** |
|---|---|---|---|---|---|---|
| **Owner** | Space Imaging (France) | NASA | NASA | Digital Globe (USA) | German Aerospace Center (Germany | German Aerospace Center (Germany) |
| **Launch Date** | September, 1999 | December 1999, Terra satellite; April 2002, Aqua satellite. | November, 2000 | October, 2001 | July, 2012 | June 2016 |
| **Status** | Terra MODIS band 5 and Aqua MODIS band 6 have erroneous data | Working | Working | Working | Working | Working |
| **Spatial Resolution (m)** | 1 - 4 | 250 - 1000 | 30 (10 m panchromatic) | 0.6-2.44 | 350 | 42.4 - 356 |
| **Temporal Resolution (day)** | 1-3 | 1-2 | 16 | 1-3.5 | Experimental | Experimental |
| **Scene Size (km x km)** | 11.3 x 11.3 | 2300 x 2300 | 37 x 185 | 16.5 x 16.5 | 178 x 178 | 178 x 178 |

### 4.6 Watch Towers and Manned Aircraft for Bushfire Detection

Fires can almost always be detected visually, during the day by observation of smoke and during the night by sighting flames (Luke and McArthur, 1986). Fire towers are used for ground visual observation, while manned aircraft are also used for fire detection. As the hire of manned aircraft is expensive they are typically used for confirming the fire results obtained by other means. Aircraft enable a unique perspective of a bushfire, since a larger ground area can be viewed with less obstruction compared to viewing the terrain on the ground from a watch tower at an oblique angle. Aircraft are also vital for a variety of additional firefighting purposes, including, reconnaissance of ongoing fires or new outbreaks, dropping water or retardant onto fires, and transport of firefighters and firefighting equipment (Luke and McArthur, 1986). In summary, their role is to collect (near) real-time fire intelligence and supply it to the emergency services.

### 4.7 Research and Development on the Application of UAS for Bushfire Missions

Casbeer et al. (2005) described the use of multiple LASE UAS for bushfire missions. An effective UAS path planning algorithm utilising infrared images collected on-board in real-time while flying along the boundary of the fire was developed. While promising it did have some limitations, such as initial rendezvous time, dealing with fuel contingencies and refuelling, and operations during irregular and growing fire shapes.

In 2013 the ScanEagle UAS – which was originally designed for military applications – was used by Australian firefighters in the Wollemi National Park fires. This long endurance UAS provided day and night surveillance and reconnaissance capability to the firefighters. The imagery from the ScanEagle was used to assess the movement of the fire front and to identify the locations of high-risk spot fires. This flight trial showcased to Australian firefighters how the application of a military grade UAS could be utilised by emergency services. The application of such UASs for disaster relief and response will continue to evolve in Australia, with the RAAF announcing that they have entered a Memorandum of Agreement (MoA) with Airservices Australia, for operating the Heron UAS in Australian civil airspace (Defence, 2015).

The NASA Ikhana a Predator-B UAS was used during 2007-2009 for wildfire surveillance in the western United States. It was the first civilian UAS to receive a Certificate of Airworthiness from the Federal Aviation Authority to be able to operate in U.S National Airspace System for disaster support and wildfire event imaging (Watts et al., 2012). The Ikhana is a sophisticated UAS equipped with multiple sensors, some similar to those carried on orbiting satellites, including electro optical (EO) sensors to provide colour video and IR images for night vision (Merlin, 2009). It could also carry a SAR payload plus laser designations, spotting and range-finding systems, and was successfully used in 20 missions involving surveillance of 60 fires (Merlin, 2009). The versatility of the sensors makes it a multi-purpose UAS capable of being used in different mission scenarios. The satellite communications system on the Ikhana UAS allows the RP to operate and steer the UAS. It also allows the UAS to provide geo-rectified imagery to incident management teams within 10 minutes of acquisition.

### 4.8 Mission Planning for the Application of Multiple UAS in Different Airspaces

Continuously changing fire behaviour makes ground-based reconnaissance difficult and dangerous. Although satellite and manned aircraft have advantages for aerial reconnaissance, they also have many limitations. To overcome these limitations and to exploit UAS capabilities it is suggested that different categories of UAS, operating in different airspaces, could substitute satellite and manned aircrafts for reconnaissance tasks during bushfires (Figure 4.3).

To undertake productive and safe missions a well-designed UAS flight plan is essential, which includes careful design of aircraft trajectory, and real-time mission management of the UAS. This is significant, especially when organising multiple UAS missions. MALE or HALE UAS categories can be used as alternate sources of satellite-like data as they are capable of flying at higher altitudes compared to manned aircraft, and can carry larger sensor payloads. These UAS are not only able to supply remotely sensed data but they are capable of providing (near-) real-time geo-referenced data to firefighters and other emergency responders when fitted with satellite like sensors. When close to airports or populated areas HALE UAS may be a preferred option compared to MALE UAS, as they can avoid disruption to air traffic movements in non-segregated airspace. LALE (Low Altitude, Long Endurance) UAS or larger categories of the VTOL (Vertical Take- off and Landing) UAS that are more stable and are long endurance can be used at a lower altitude concurrently with MALE or HALE UAS. By flying at lower altitudes LALE or VTOL UAS are capable of providing a close-up view of an area of interest. For example, such UAS can be used for aerial survey of escape routes, checking on properties, object tracking, or used for locating fire spotting. Firefighters can use this data for ground mission planning.

A HALE or MALE UAS could be flown with a LALE or VTOL UAS, and the two categories can follow a similar flight plan, with the lower altitude UAS over-flying an area a few minutes behind the higher altitude UAS. This will allow the two UAS to supply different types of data over the same region. Another approach is to have the LALE or VTOL UAS flying along the fire boundary, supplying firefighters with critical aerial survey data to prevent firefighters from placing their lives in danger. The data collected can be uploaded to, for example, Google Earth to provide firefighters with a “global” perspective of the fire, and can be used with recent satellite data for further analyses. The different types of data can be used to derive different levels of information across the area of interest, with the higher

altitude data used for hotspot analysis while the lower altitude data used for aerial survey and reconnaissance of properties, escape routes, etc.

As these categories of UAS are large they require meeting national and international rules and regulations during flight operations. A key factor in a successful UAS mission plan that includes integration of UAS in non-segregated airspace would include their ability to act and respond as manned aircraft. Much of this is subjected to technology development such as the ability of the aircraft to be controlled by the remote pilot, for the UA to act as a communications relay between the RP and ATC, the performance (e.g. transaction time and continuity of the communications link) as well as the timeliness of the aircraft's response to ATC instructions (ICAO, 2011). The following criteria are important for a safe and reliable ground mission plan (Willis et al., 2015):

- Airworthiness of the UAS
- Command and Control (C2)
- Detect and Avoid (DAA)
- RP licensing
- UAS operations
- ATM integration

The operation of an UAS is more difficult compared to the operation of a conventional aircraft. The lack of an on-board pilot introduces new considerations with regard to fulfilling safety-related responsibilities such as incorporation of technologies (ICAO, 2011). The RP will require completing licensing and training requirements developed similar to those for manned aviation that will include both aeronautical knowledge and operational components. The licensing may include specific adjustments considering the particular and unique nature and characteristics of the RP station environment and UA applications (from both a technical and flight operations perspective, e.g. VLOS or beyond VLOS) as well as aircraft type (e.g. aeroplane, helicopter) (ICAO, 2011).

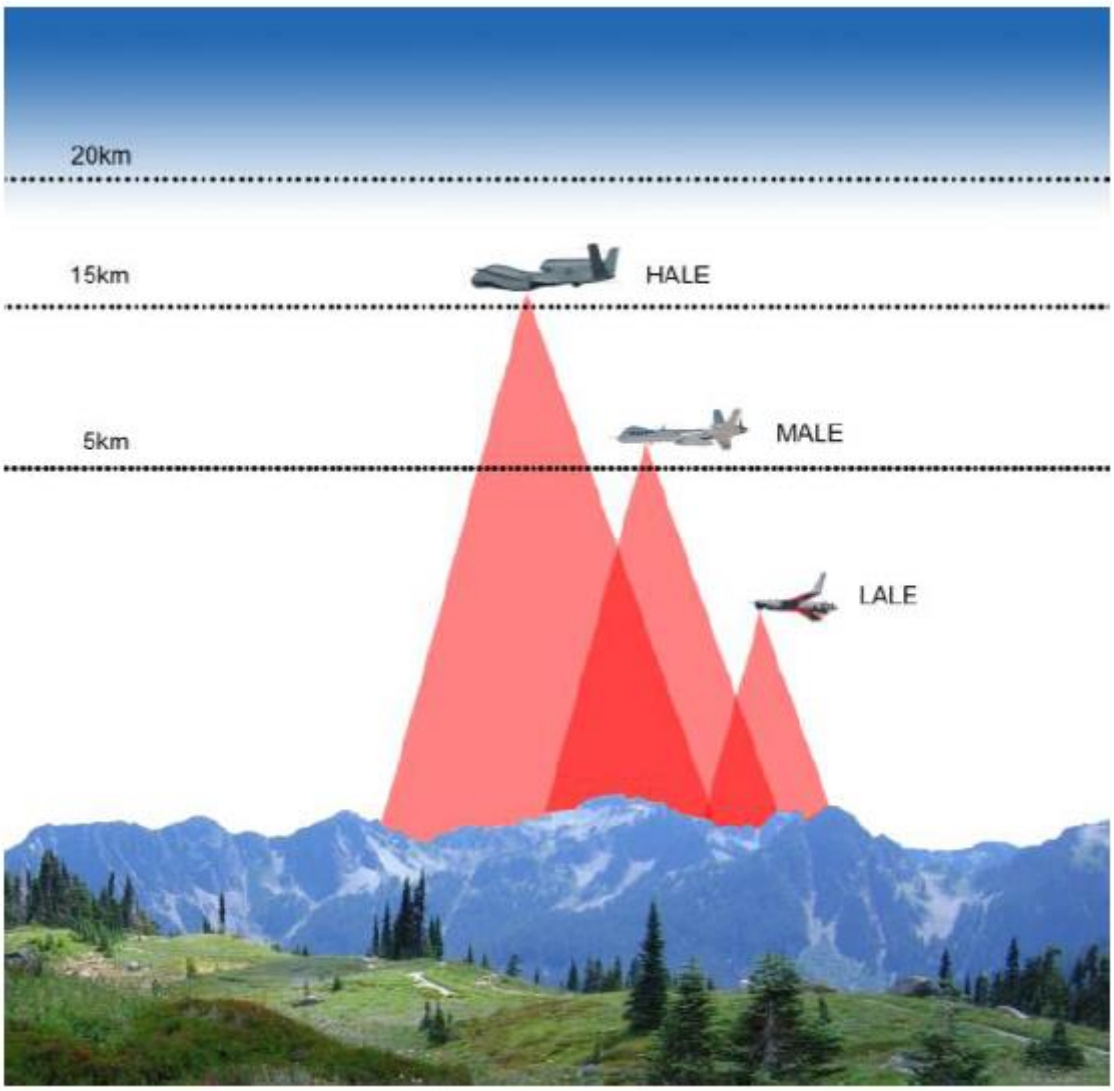


Figure 4.3 – Application of multiple UAS for bushfire data acquisition

### 4.8.1 UAS Bushfire Sensors

The most significant sensors for bushfire image and data acquisition are EO, near infrared, Mid-infrared and Thermal sensors. Smoke can be visually identified using EO imaging or video sensors while IR sensors are used to identify the fire location. The near infrared, mid infrared and thermal infrared sensors provide accurate fire location when applied simultaneously in collecting fire imagery. Smaller low altitude categories of UAS can carry a single imaging sensor for image acquisition due to their payload capacity while MALE and HALE category UAS can carry sophisticated satellite like multispectral sensors.

A key challenge in the operation of UAS for bushfire missions is to convert the remotely sensed data collected into meaningful information; hence the choice of sensor and the sensor resolution is very important. Medium (altitudes of up to 14km) and higher (altitudes of up to 20km) altitude UAS can be fitted with sophisticated sensors due to their long endurance and ability to carry a heavier payload, while lower altitude categories of UAS can only be fitted with video sensor or an imaging sensor. It is proposed that the sensor payload of the medium and high altitude UAS should be multispectral sensor sensitive from visible to the far-infrared end of the spectrum this will allow the UAS to collectively acquire a range of images in different bands. Lower altitude UAS can carry single imaging sensors due to their payload capacity and can be fitted with colour, or black or white thermal, or colour video sensors. The sensor requirement for lower altitude UAS is further explained in chapter 6.

The higher altitude UAS can carry satellite-like sensors such as the Autonomous Modular Scanner (AMS) sensor, on board the Ikhana UAS. This sensor is further described in chapter 5. This will enable the UAS to collect valuable bushfire information that is currently collected by satellites such as the MODIS satellite, but at a lower altitude and with better resolution.

It is proposed that lower altitude UAS can be fitted with an appropriate sensor for site assessment and object tracking. This UAS may serve as an ‘eye in the sky’ for firefighters, and could play the role of currently manned aircraft during bushfire missions. For such missions this UAS should be fitted with video sensors allowing firefighters and emergency services to view and track changes on the ground in (near) real-time and in their correct spatial location.

### 4.8.2 Endurance of UAS for Bushfire Monitoring

Fire-rate and fire intensity can change within a short period of time, with a number of factors influencing the acceleration of fires. Frequent, high quality and (near-) real-time fire intelligence concerning the shape, pattern, size, direction and intensity of a bushfire are essential (Cheney and Sullivan, 2008). Long endurance UAS are safer to operate compared to short endurance UAS. The RP and crew are able to operate the UAS from a safe location. UAS that fall within this category are VTOL, LALE, MALE and HALE categories. An

example is the REAPER UAS as mentioned in chapter three. If fitted with appropriate sensors they are also capable of day and night missions.

### 4.8.3 UAS bushfire Communication Systems

UAS datalink is critical in terms of mission requirements as well as safety, especially if the UAS is integrated into non-segregated airspace (Colomina and Molina, 2014). Some of the pressing matters regarding communication technologies are datalink availability to GCS, flexibility, adaptability, bandwidth, frequency, security and interoperability (van Blyenburgh, 2000). Security issues that are of concern include data link spoofing, hijacking, and jamming of UAS C2 and ATC communication (Gupta et al., 2013). Any form of data link loss can be a safety and security concern compromising the mission. This is a particular concern for larger UAS and their integration into non-segregated airspace.

Currently there is no defined bandwidth and frequency spectrum set for command and control of UAS. A safe, high frequency and high bandwidth datalink is important for C2 and ATC communication and for (near) real-time data downlink. Having a high bandwidth and high frequency C2 link can impact data efficacy such as the communication transaction time, continuity, availability and integrity (Willis et al., 2015).

UAS data links can be divided into two categories: Radio Frequency Line-of-Sight (RF LOS) and BLOS. They serve several important functions (Gupta et al., 2013):

1. Uplink of control data from the GCS and / or satellite-based communication (SATCOM) to UA
2. Downlink data from the on-board sensor and telemetry system to the GCS.
3. A means of making measurements of the azimuth and range from the ground station and satellite to the UAS to maintain good communications between them.

A UAS datalink consists of a radio frequency transmitter and receiver, an antenna and modem to link all these components with the UA sensors. The maximum achievable distance for RF-LOS operations are typically around 46–370 km (25–200 NM) depending on the operational altitude of the UAS. BLOS datalink includes RF-LOS technologies along with SATCOM. This operation not only involves the control of the UAS and transfer of sensor

outputs, but includes communications with ATC (Mitchell, 2009). ATC require a robust C2 link for operation of UAS in controlled airspace to monitor and control safe air traffic movements. It is critical to have reliable frequency bands to avoid loss of C2 link, (referred to as “lost link”) which can be a major concern for ATC. SATCOM is for long endurance UAS that fly well beyond LOS (e.g. 200-600 km). SATCOM is used for C2 of the UA and for communications (C3) with ATC. Different SATCOM frequency bands are possible, with the most common being Ku band, K band, S band, L band, and C band, with the X band mainly reserved for military use. As the distance between the GCS and the UA increases, the signal-to-noise ratios of the transmission link will fall. The signal loss may manifest as a lag in the UA command uplink and recovery of data downlink.

To explore how a multiple UAS mission can be carried out based on the recommendations made above, due to current limitations with the category of UAS that can be operated, only two sets of wildfire data collected by the AMS sensor on board the Ikhana UAS have been collected for analysis. The results of this work along with the sensor capabilities are reviewed and explained.

# CHAPTER 5 – AMS-WILDFIRE DATA ANALYSIS

## 5.1 Introduction

Given the dynamic nature of bushfires it is important to access forest fire intelligence at appropriate spatial and temporal scales (Ambrosia et al., 2011). As a result NASA decided to explore the application of UAS fitted with satellite-type imaging sensors during wildfires. Modifications were made to the Ikhana to make it applicable for a variety of civilian applications such as supporting Earth science missions, development of advanced aeronautical technology, and acting as a testbed to develop capabilities for improving the utility of unmanned aerial systems (Merlin, 2009). From 2006 till 2009 the Ikhana was primarily used in wildfire missions in the state of California, during which the Ikhana was deployed successfully in the U.S. National Air Space (NAS) for collecting fire intelligence (Merlin, 2009, Ambrosia et al., 2011). The multispectral channel sensor on board the Ikhana was capable of collecting and supplying (near) real-time fire data to emergency services.

To explore how UAS technology can be utilised during forest fire missions for collecting remote sensing data and the value of such intelligence, two sets of fire data collected by the Ikhana UAS have been obtained. From the list of missions in which the Ikhana was involved (Table 5.1), the Zaca and Witch/ Poomacha fires were selected. The two fires were in different terrain environments, the Zaca fire being a wildfire in the forest regions of California, while the Witch/ Poomacha fire impacted urban areas of California (Figure 5.1). Having two different sets of fire data made possible the exploration of the application of UAS data in different environments.

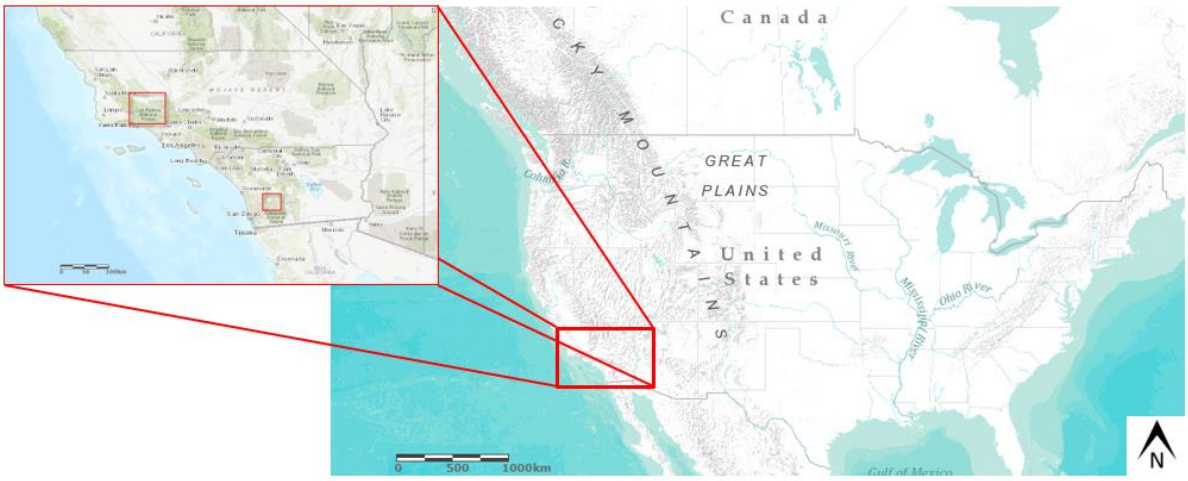


Figure 5.1- Locality map of the Zaca and Witch/ Poomacha fires

Table 5.1 - Missions from 2006-2009 (Ambrosia, 2012)

| Year | Aircraft | Flights | Hours | Fires Flown |
|---|---|---|---|---|
| 2006 | Altair | 4 | 68 | Mono Lake Prescribed Fire, Esperanza Fire (CA) |
| 2007 | Ikhana | 12 | 89 | Zaca, Tar, Colby, Babcock, Jackrabbit, Butler, North, Fairmont, Grouse, Lick, Bald, Moonlight, Zaca, SoCal Firestorm (CA); Trapper Ridge, Castle Rock (ID); WH (MT); Columbine, Hardscrabble, Granite Creek (WY); GW, Big Basin (OR); Domke Lake, South Omak (WA) |
| 2008 | Ikhana | 4 | 21 | Piute, Clover, Silver, North Mountain, American River, Cub Complex, Canyon Complex, Basin, Gap, Camp, Cascatel, Hidden (CA) |
| 2009 | Ikhana | 2 | 11 | Piute, Station Fire (CA; post burn assessment) |

CA: California; ID: Idaho; MT: Montana; WY: Wyoming; OR: Oregon; WA: Washington.

## 5.2 Ikhana Fire Data

The Witch/ Poomacha and Zaca fire data have been selected for this investigation. It was in Witch Creek area, east of Ramona in San Diego County, where a total of 197, 990 acres were burnt during the fire, 1125 residential structures and 509 outbuildings were destroyed,

together with damage to a further 77 residential structures and 25 outbuildings. 40 firefighters were injured, and there were 2 civilian fatalities (Figure 5.2). The Zaca fire at that time was the second largest fire in history to affect California, burning over 240,207 acres (972.083 km2). It began on private property near the forest and spread quickly to forest regions due to the extremely dry conditions (Figure 5.3).

Figure 5.2 - Witch fire destroyed neighbourhoods in Rancho Bernardo (San Diego State University, 2007a)

Figure 5.3 - Zaca fire (San Diego State University, 2007b)

### 5.3 NASA Predator- B Ikhana MALE Category UAS platform

The Ikhana UAS was 36 feet (11 m) long with a 66 feet (20 m) wingspan. It was able to carry 400 pounds (181 kg) of sensors internally and over 2,000 pounds (907 kg) in its external pods. The aircraft was powered by a Honeywell TPE 331-10T turbine engine and could remain airborne for more than 20 hours, reaching altitudes above 40,000 feet (12192 m) (but with limited endurance at such altitudes). Ikhana also had sense-and-avoid technology for communication between the UA, the GCS where the RP and the RP crew were located, and ATC. NASA purchased a GCS and satellite communication system for uplinking flight commands and downlinking aircraft and mission data. The RP was linked to the aircraft through a C-band line-of-sight (LOS) data link at ranges up to 150 NM (~92 km) and a Ku-band satellite link for over-the-horizon control, with a single camera on the UA providing the RP with forward visibility.

### 5.4 Autonomous Modular Scanner (AMS) Sensor

Ikhana was a versatile platform in that duplicate sensors such as those carried on orbiting satellites were installed to collect data (Ambrosia et al., 2011). The Ikhana UAS payload included the NASA Autonomous Modular Scanner (AMS) which was designed in such a way that made it useful for a variety of disaster relief mission applications. The sensor was refined for fire processing, but any algorithm or band combination could be derived, which would prove beneficial for other types of disasters, such as flood extent, oil slicks, etc (NASA, 2014).

The AMS multispectral line scanner was a complete re-build of the NASA Thematic Mapper Simulator with the same spectral characteristics as the Landsat Thematic Mapper (TM), but with additional channels, such as modifications to thermal channels to allow improved discrimination of a high range of temperature conditions (NASA, 2014, Ambrosia et al., 2011). It had 16 bands (Table 5.2) in which bands 2, 3, 5, 7, 9 and 10 are duplicates of Landsat TM 5, while the thermal channels spectral bandpass were configured to match those on the Visible Infrared Imaging Radiometer Suite (VIIRS) as they are closest to MODIS thermal channels. This was done to trial the capabilities of the VIIRS thermal channels so that when the time comes there can be a smooth transition from MODIS to VIIRS (NASA, 2014).

The spatial resolution of the data collected by the AMS sensor varied from 3 – 50 m depending on the altitude of the aircraft (Ambrosia and Wegener, 2009). The system operated with five to 24 scans per second with digitised swath width of 720 pixels in the cross-track direction as data is acquired continuously in the along-track direction (NASA, 2014). The scanning optics had a 108 degree field of view (FOV) in the cross-track direction and an instantaneous FOV (IFOV) of 2.62 milliradians that is further explained below. These operations provide a ground resolution of 8.0 m from an altitude of 10000 feet (3048 m) above the ground so that fires smaller than 8.0 m are detectable (Merlin, 2009).

Table 5.2 – AMS - wildfire band specifications

| Band | Wavelength, μm |
|---|---|
| 1 | 0.42–0.45 |
| 2 | 0.45–0.52 (TM1) |
| 3 | 0.52–0.60 (TM2) |
| 4 | 0.60–0.62 |
| 5 | 0.63–0.69 (TM3) |
| 6 | 0.69–0.75 |
| 7 | 0.75–0.90 (TM4) |
| 8 | 0.91–1.05 |
| 9 | 1.55–1.75 (TM5) (high gain) |
| 10 | 2.08–2.35 (TM7) (high gain) |
| 11 | 3.60–3.79 (VIIRS M12) (high gain) |
| 12 | 10.26–11.26 (VIIRS M15) (high gain) |
| 13 | 1.55–1.75 (TM5) (low gain) |
| 14 | 2.08–2.35 (TM7) (low gain) |
| 15 | 3.60–3.79 (VIIRS M12) (low gain) |
| 16 | 10.26–11.26 (VIIRS M15) (low gain) |
| FOV: 42.5 or 85.9 degrees (selectable) | |
| IFOV: 1.25 mrad or 2.5mrad (selectable) | |
| Spatial Resolution: 3-50 meters (variable based on altitude) | |

The key feature of the AMS was the real-time processor technology, which is the most critical element in disaster intelligence gathering. The AMS had an interface to a processor where all the data processing occurred in near-real-time. The on-board product generation, algorithm processes and geo-referencing processes took approximately 10 seconds per image. Digitised output from the detector with 716 16- bit cross-track pixels were combined with navigational and inertial sensor data to determine the location and orientation of the sensor. Finally, Level B (or Level II) products, autonomously geo- and terrain-corrected, were telemetered to the ground in real-time via the Ku-band satellite communications system. Once the data reached the GCS, quality assurance (QA) controls were applied on the data, after which the information was transferred to NASA Ames and later made available to remote users via the internet, allowing immediate integration into a GIS database system for visualisation, processing and analysis. The data transmission and QA control checks took a total of 10 minutes per image.

### 5.4.1 Instantaneous Field of View (IFOV)

The features discernible in an image depend primarily on the spatial resolution of the sensor and refer to the size of the smallest feature that can be detected (Canada Centre for Remote Sensing, 2015) (Figure 5.1). For passive sensors this depends on factors such as the Instantaneous Field of View (IFOV) of the sensor, which can be described as the area on the ground that is viewed by the sensor at a given time and represented by each pixel, the feature's contrast and colour with respect to its background as well as its shape.

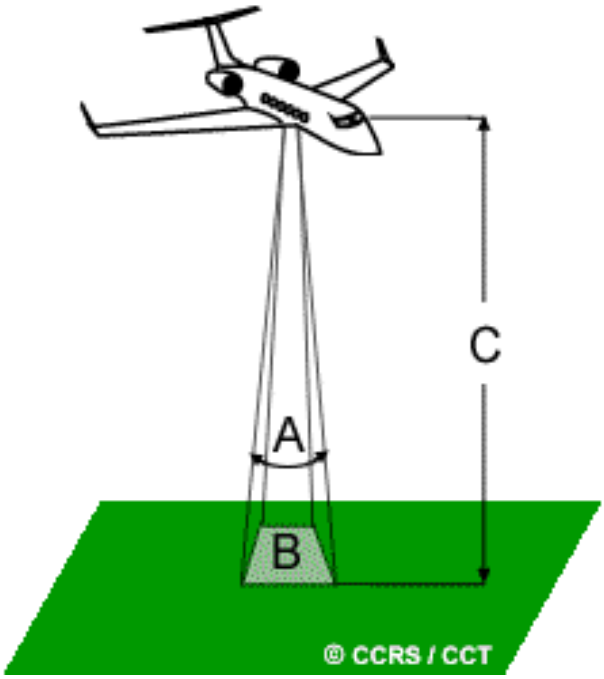


Figure 5.4 - IFOV of a passive sensor for flying height of the aircraft C, Angle A the instantaneously viewed by the sensor at a given time and B the corresponding area on the ground covered by the sensor (Canada Centre for Remote Sensing, 2015)

**5.5 Method for Processing and Analysing the Ikhana Data**

The AMS Ikhana data is in Level-1B HDF (Hierarchical Data Format) format, which contains the calibrated, georeferenced radiances for all AMS channels for one straight line flight track (Gumley et al., 1994a). To begin with each HDF file was initially opened in HDFView 2.11 (HDF Group, 2016) for analysis (Figure 5.4) . The file header included all the details of the flight mission, such as the name of the file, the date of flight, the time of flight, flight platform, latitude and longitude of the image edges, along with other relevant flight mission information. Once the file contents were viewed the HDF files were individually loaded into the Matlab software for processing (Appendix A). The steps employed for the processing of the AMS Ikhana data for this research are listed below and explained in this chapter:

1. Multiplying each calibrated band from the 'CalibratedData' file by their scale factor to obtain the true radiance ($W/m^2$-$sr$-$m$) value

2. Converting Bands 11 and 12 at-sensor spectral radiance ($L$) to effective at-sensor brightness temperature ($Tb$)
3. Converting band 7 at-sensor spectral radiance ($L$) to TOA reflectance ($\rho\lambda$)
4. Performing hotspot analysis and nearest neighbour interpolation to identify the fire pixels in each image strip

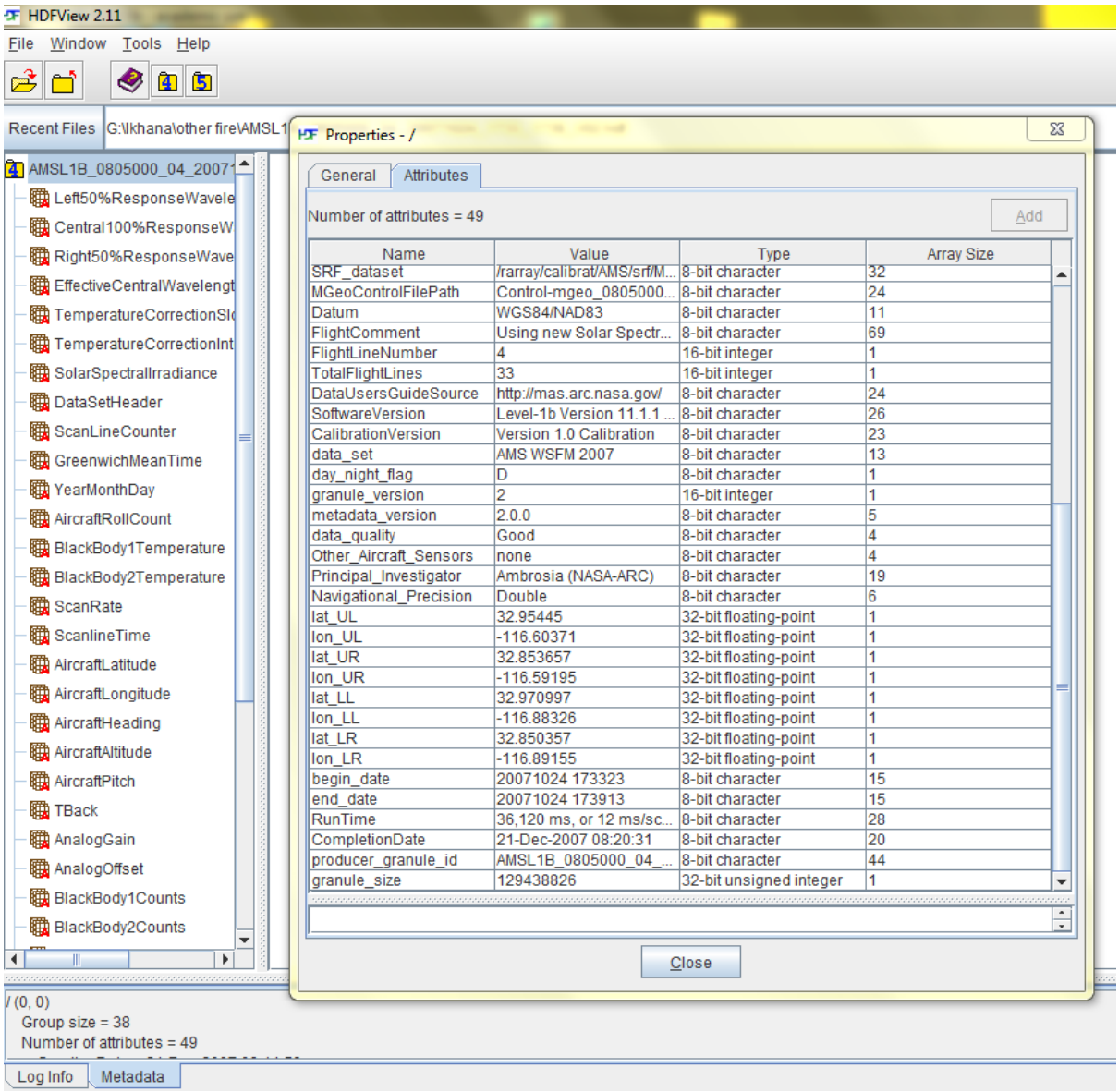


| Name | Value | Type | Array Size |
|---|---|---|---|
| SRF_dataset | /rarray/calibrat/AMS/srf/M... | 8-bit character | 32 |
| MGeoControlFilePath | Control-mgeo_0805000... | 8-bit character | 24 |
| Datum | WGS84/NAD83 | 8-bit character | 11 |
| FlightComment | Using new Solar Spectr... | 8-bit character | 69 |
| FlightLineNumber | 4 | 16-bit integer | 1 |
| TotalFlightLines | 33 | 16-bit integer | 1 |
| DataUsersGuideSource | http://mas.arc.nasa.gov/ | 8-bit character | 24 |
| SoftwareVersion | Level-1b Version 11.1.1 ... | 8-bit character | 26 |
| CalibrationVersion | Version 1.0 Calibration | 8-bit character | 23 |
| data_set | AMS WSFM 2007 | 8-bit character | 13 |
| day_night_flag | D | 8-bit character | 1 |
| granule_version | 2 | 16-bit integer | 1 |
| metadata_version | 2.0.0 | 8-bit character | 5 |
| data_quality | Good | 8-bit character | 4 |
| Other_Aircraft_Sensors | none | 8-bit character | 4 |
| Principal_Investigator | Ambrosia (NASA-ARC) | 8-bit character | 19 |
| Navigational_Precision | Double | 8-bit character | 6 |
| lat_UL | 32.95445 | 32-bit floating-point | 1 |
| lon_UL | -116.60371 | 32-bit floating-point | 1 |
| lat_UR | 32.853657 | 32-bit floating-point | 1 |
| lon_UR | -116.59195 | 32-bit floating-point | 1 |
| lat_LL | 32.970997 | 32-bit floating-point | 1 |
| lon_LL | -116.88326 | 32-bit floating-point | 1 |
| lat_LR | 32.850357 | 32-bit floating-point | 1 |
| lon_LR | -116.89155 | 32-bit floating-point | 1 |
| begin_date | 20071024 173323 | 8-bit character | 15 |
| end_date | 20071024 173913 | 8-bit character | 15 |
| RunTime | 36,120 ms, or 12 ms/sc... | 8-bit character | 28 |
| CompletionDate | 21-Dec-2007 08:20:31 | 8-bit character | 20 |
| producer_granule_id | AMSL1B_0805000_04_... | 8-bit character | 44 |
| granule_size | 129438826 | 32-bit unsigned integer | 1 |

Figure 5.5 - Ikhana HDF Level-1B file oped in HDFView 2.11

### 5.5.1 Obtaining the True Radiance (W/$m^2$-sr-m) Value for the Bands

For processing of the AMS data, the Level-1 B User Guide (Gumley et al., 1994b) was utilised. The first step for processing the data included importing the 'CalibratedData' into

the Matlab software and multiplying each calibrated band by their scale factor to obtain the true radiance ($W/m^2$-*sr-m*) value, Variable scaling factors are used for each band (Table 5.3). To retrieve the radiance values the integer radiance values are multiplied by the appropriate scaling factor as supplied in the metadata to convert the 16 bit integers to 32 bit floating point radiance values.

Table 5.3 - scale factor for the 12 different calibrated bands

| **Band** | **Scale Factor** |
|---|---|
| Bands 1 -10 | 0.1 |
| Bands 11-12 | 0.01 |

### 5.5.2 **Calculating Brightness Temperature (Tb)**

Once the true radiance values for each band are extracted the next step is to convert the at-sensor spectral radiance (*L*) to effective at-sensor brightness temperature (*Tb*) for channels 11 and 12 using the inverse Planck function (Equation 5.1). The at-sensor brightness temperature assumes that the Earth's surface is a Black Body, and includes atmospheric effects such as absorption and emissions along the path from the ground to the sensor. The conversion formula from the at-sensor's spectral radiance to at-sensor brightness temperature is:

(5.1) Planck function:

$$Tb = \frac{\frac{C_2}{\lambda}}{\ln(1 + \frac{C_1}{L * \lambda^5})}$$

where (NASA, 2016):

*L*= radiance ($W/m^2$-*sr-m*)

$C_1$= 1.1910439 x $10^{-16}$($W/m^2$)

$C_2$= 1.4387686 x$10^{-2}$ (*mK*)

$\lambda$ = band of detector centre wavelength (*m*)

*Tb* = brightness temperature (*K*)

### 5.5.3 **Calculating the TOA (top-of-atmosphere) Reflectance Value for Band 7**

Band 7 radiance values were converted from radiance to reflectance. As band 7 of the AMS sensor duplicates that of Landsat 5 TM band 4 the Landsat TM User Guide for converting radiance to reflectance is consulted (Gumley et al., 1994b). The TOA reflectance of the Earth is computed from (Equation 5.2):

(5.2) planetary TOA reflectance:

$$\rho\lambda = \frac{\pi * L\lambda * d^2}{E\ sun, \lambda * sin(\theta SE)}$$

where:

ρλ= planetary TOA reflectance [unitless]

π = mathematical constant equal to ~3.1415926 [unitless]

$L\lambda$= spectral radiance at the sensor's aperture [W/(m2 sr μm)]

ESUN λ = mean exoatmospheric solar irradiance [W/(m2 μm)]

d = Earth–Sun distance [astronomical units]

$d$= Earth–Sun distance [astronomical units]

$\theta SE$ = solar zenith angle [degrees]

The flight date and time is provided in the header of the HDF file. The TOA reflectance calculation requires the Earth–Sun distance ($d$), that is obtained from Jet Propulsion Laboratory (JPL) Ephemeris10 (DE405) data (JPL, 2017), with the value of $d$ for the Witch, Poomacha & Rice fires and Zaca fires are 0.98937 and 1.0126 [astronomical units] respectively. The solar exo-atmospheric spectral irradiances (ESUNλ) along with the solar zenith angle are supplied in the metadata, with the value of ESUNλ for the Witch, Poomacha & Rice fires and the Zaca fires are 1207.6049 and 1164.043 [W/(m2 μm] respectively.

There are three advantages to using TOA reflectance instead of at-sensor spectral radiance, which can vary significantly in space and time (Chander et al., 2009):

- It removes the cosine effect of different solar zenith angles due to the time difference between data acquisitions.
- TOA reflectance compensates for different values of the exo-atmospheric solar irradiance arising from spectral band differences.

- TOA reflectance corrects for the variation in the Earth–Sun distance between different data acquisition dates.

Each image strip is individually processed and the neighbouring image strips are compared. For rechecking purposes the value of the first pixel for each band is cross-checked manually. Once the images are processed they are imported into ENVI for geo-referencing. An image mosaic is built from the image strips that display the fire location. The size of the fire pixels are then compared with the size of the MODIS pixels, especially in the regions of smaller fire detection.

### 5.5.4 Fire Hotspot Detection Algorithm

Hotspot detection can identify the hot pixels from the relatively cold surrounding areas and is used to identify the fire pixels. This is an important function because even though a large region may be burned by a fire over its lifetime, only a portion of the burn area is actually in flames (fire front) at any given observation time (Kaufman et al., 1998, Lee and Tag, 1990). AMS used a multiband temperature threshold algorithm developed for use with the AVHRR satellite by the Canada Center of Remote Sensing (CCRS), referred to as the CCRS fire-detection algorithm (CFDA) (Ambrosia and Wegener, 2009, Ambrosia et al., 2011).

Band 11 (3.60–3.79 mm) and Band 12 (10.26–11.26mm) of the AMS sensor are used for fire detection along with Band 7 (0.76–0.90 mm). Band 7 is used for eliminating spectrally bright non-fire objects that cause false-positive detection during day missions (Peterson et al., 2013). The fire hotspot detection algorithm is (Ambrosia et al., 2011):

***If:***
Band 11 (3.60–3.79 mm) > Band 11 minimum temperature (e.g. 360° K) and
Band 12 (10.26–11.26mm) > Band 12 minimum temperature (e.g. 290° K) and
Band 11–Band 12 > Difference minimum (e.g. 14° K),
***And*** (if available),
Band 7(0.76–0.90 mm) < Reflectance maximum (e.g. 0.4) (to screen high-reflectance commission errors),
***Then,***
Pixel is classified as a fire hotspot

After the hotspot detection algorithm, to remove outlie pixels that are saturated and display as fire pixels but are non-fire pixels the nearest neighbour interpolation is applied. When the Nearest Neighbour interpolation is applied, single fire pixel outliers are removed and replaced by the mean value of the pixel and the adjacent pixel value which are closest to its current value.

### 5.6 Results and Discussion of the Ikhana Data

Initially the HDF files from the AMS data were loaded into ENVI software for mosaicking and analysis. During the mosaicking process differences in the overlapping areas were visible in locations where fires and smoke were observed. Although there is no change in terrain during such a short time span, given the dynamic nature of a fire the dimensions of a fire change rapidly due to the fire characteristics and behaviour. This does not impact georeferencing but is particularly noticeable around the smoke plume and fire front when the visible spectrum bands are displayed as RGB, Figures 5.5 and 5.6. Furthermore the time differences in Greenwich Mean Time (GMT) between the first scans of each image strip from the Witch, Poomacha & Rice fires were analysed, as shown in Table 5.4. The scanline time refers to the current scanline and is accurate to the nearest scanline (0.16 seconds) whereas GMT is represented only to the nearest whole second. Although all images were collected on the same day, they were not collected at the same time and such a small change between overlapping images can impact the image mosaicking. An alternative to overcome this was to classify each image individually to clearly view the fire pixels. Each Individual image strip prior to georefencing and rotating were opened and processed in Matlab.


Figure 5.6 - Witch Fire, image mosaic bands 6, 5, 4 are displayed as RGB. Overlap issues are noticeable where fire and smoke is visible.


Figure 5.7 - Zaca Fire image mosaic bands 6, 5, 4 are displayed as RGB. Overlap issues are noticeable where fire and smoke is visible.

Table 5.4 - GMT and scanline time (hours) for each image strip from the Witch, Poomacha & Rice Fires

| **Witch, Poomacha & Rice Fires, California, USA** | | |
|---|---|---|
| image | Greenwich Mean Time | scanline time (hours)- for first scanline |
| 4 | 17332274 | 17.556316 |
| 5 | 17422038 | 17.705662 |
| 6 | 17523878 | 17.87744 |
| 7 | 18034904 | 18.063622 |
| 8 | 18140119 | 18.233664 |
| 9 | 18324759 | 18.546553 |
| 10 | 18402323 | 18.673119 |
| 11 | 18475012 | 18.797256 |
| 12 | 18560489 | 18.934692 |
| 13 | 19111341 | 19.187057 |
| 14 | 19212181 | 19.356058 |
| 15 | 19300557 | 19.501547 |
| 16 | 19355771 | 19.599363 |

During processing of Band 11 of the HDF files of the AMS data by the Matlab software for the conversion pixel values from radiance to brightness temperature, some pixel values were displayed as complex values. Through analysis and manual checks it was identified that these values were falsely displaying and code was written to resolve this issue and to display the true values of these pixels.

While running of the hotspot detection algorithm from chapter 5.5.4 different threshold values for the algorithm were experimented with. The selection of the threshold values was based on assessing Band 7, Band 11 and Band 12 fire pixels values and non-fire pixels (surrounding pixels). Different fire locations were visually selected on the image strip and the values of these pixels were assessed. The best-fitting threshold values were selected for this research. The Matlab code is written in such a way that the threshold values can be changed at any time and as a result the number of identified hotspot pixels will change, impacting the final result. The threshold values set for the three bands applied in the hotspot detection

algorithm are listed below and the fire hotspots for image strips 4-16 of Witch, Poomacha & Rice Fires and the Zaca fire are displayed in Appendix B respectively.

***If:***

Band 11 (3.60–3.79 mm) > Band 11 minimum temperature (380° K) and
Band 12 (10.26–11.26mm) > Band 12 minimum temperature (240° K) and
Band 11–Band 12 > Difference minimum (14° K),

***And,***

Band 7(0.76–0.90 mm) < Reflectance maximum (0.2) (to screen high-reflectance commission errors),

***Then,***

Pixel is classified as a fire hotspot

During the ENVI and Matlab pixel analysis and comparison it was noticed that spectrally hot pixels (in magenta) in Figures 5.8, 5.9, 5.10 did not display as fire pixels. These pixels may be saturated due to a hot object being located at the centre of the pixels and as a result increasing the temperature brightness of the pixel and its neighbouring pixels. For example, sub-pixel fire hotspots near the edge of a pixel will likely result in an underestimated fire pixel temperature brightness, while fires near the centre of a pixel may overestimate the pixel's temperature brightness (Peterson et al., 2013). To remove these single pixel outlies, a code for nearest neighbour interpolation was written in the Matlab software after the hotspot detection algorithm code to remove these outlies as a result these pixels did not display as red fire pixels(fire pixels) in output and image mosaics (Figures 5.11 and 5.12).

As part of the AMS wildfire data comparison with MODIS it was noticed that there was a time lag between the two data acquisitions of one hour in the case of the Zaca Fire. Because of this time lag it is difficult to compare the two sets of fire data because of the dynamic nature of the fire. However it can be concluded that given the IFOV of the AMS scanner is 2.5 mrad, the equivalent GSD is 50 m from an altitude Above Ground Level (AGL) of 20000 m, and a cross-track scan width of 85.92 degrees. For an altitude of 7438 m (23,000 ft), which was the flying height for the Witch, Poomacha & Rice Fires, a spatial resolution of 19 m is provided. On the other hand the pixel resolution of MODIS is 1km.Unfortunately the pixel resolution of MODIS is too coarse to resolve the size of small fire hotspots that may be very intense but much smaller than large but low-intensity fires. Due to the small size of the

fires in comparison to the GSD of the MODIS pixels, there may be a greater error resulting from pixel saturation. It can be concluded that the smallest detectable fire in any given MODIS fire pixel was found to be ~100 $m^2$ (Giglio et al., 2003) in comparison to the data from the AMS wildfire sensor.

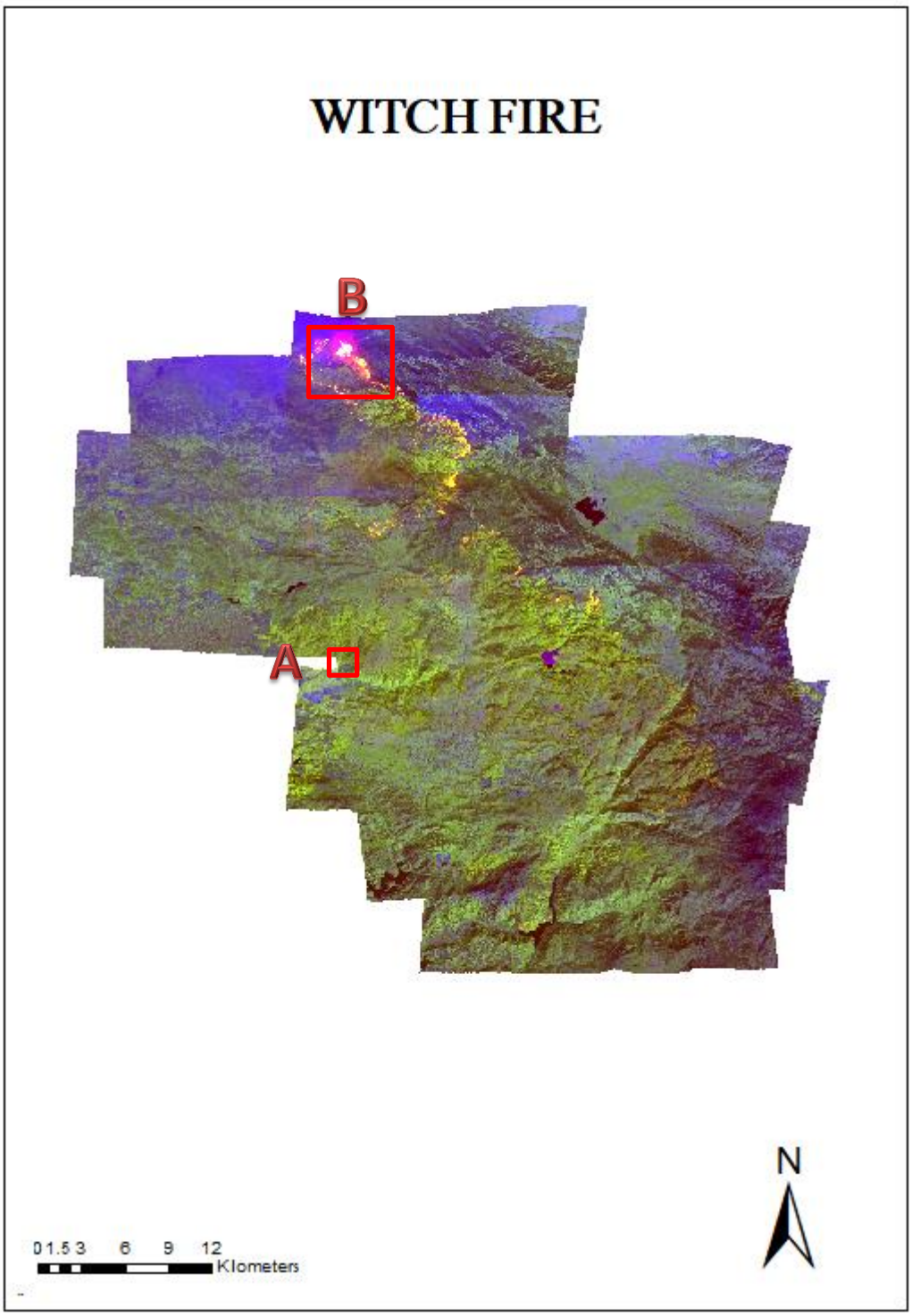


Figure 5.8 – Image mosaic of AMS wildfire sensor image strips of the Witch, Poomacha & Rice Fires, with a zoomed in view of areas A and B

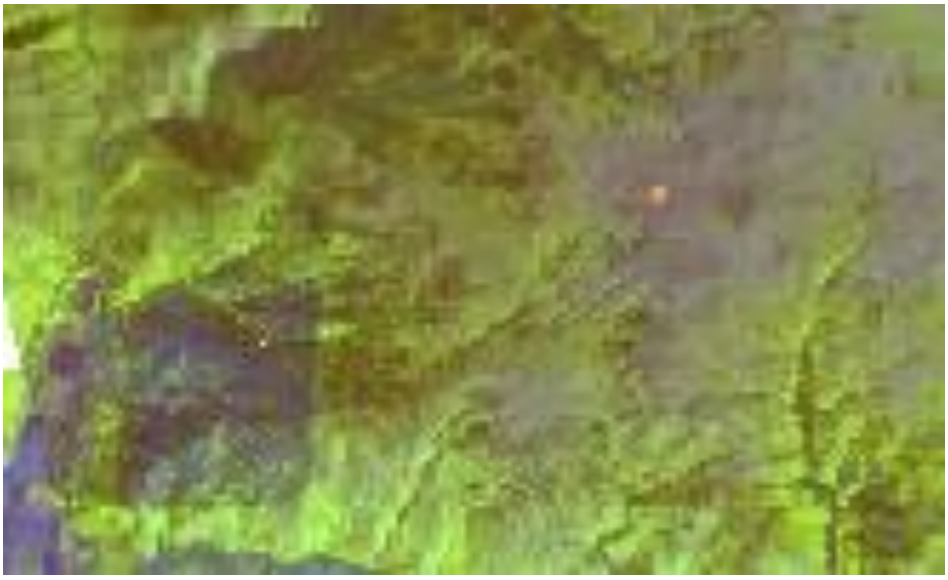

Figure 5.9 – Area A  of Image mosaic of AMS wildfire sensor image strips of the Witch, Poomacha & Rice Fires

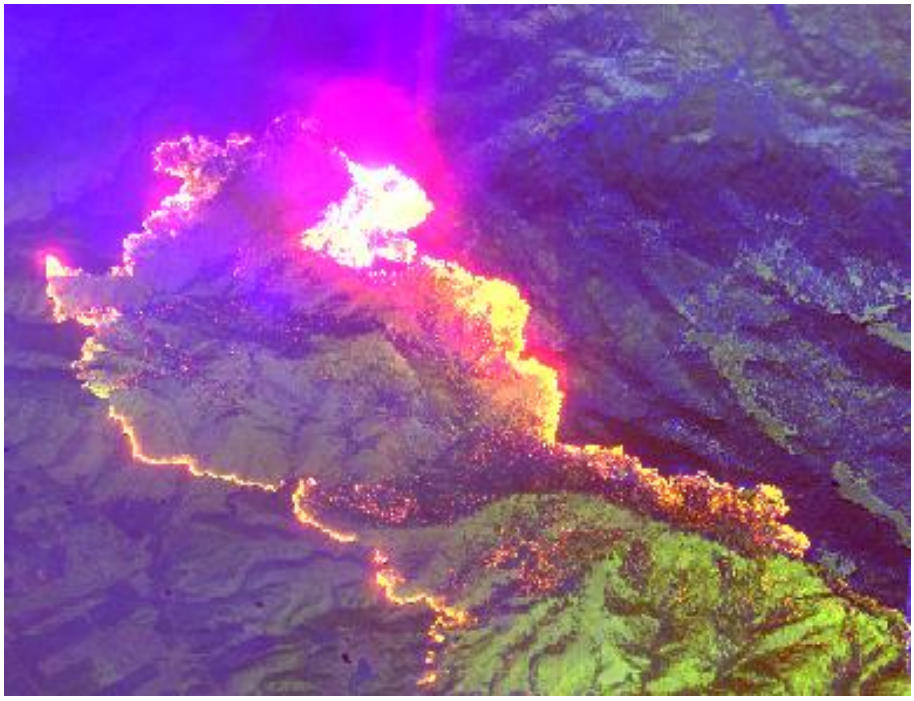

Figure 5.10 – Area B of Image mosaic of AMS wildfire sensor image strips of the Witch, Poomacha & Rice Fires


Figure 5.11 – Image mosaic of fire pixels of the Witch, Poomcha & Rice Fires


Figure 5.12 – Image mosaic of fire pixels of the Zaca Fires

## 5.7 Summary

The AMS wildfire sensor is a ‘satellite-like’ sensor capable of being used in a range of disaster relief missions. When such sensors are used on high altitude UAS (categories such as MALE category UAS or HALE category UAS) they are capable of providing a synoptic view of a fire affected region while collecting and providing high spatial and timely data to emergency services. The ability to fly other categories of UAS, such as LALE category UAS or long endurance VTOL UAS at lower altitudes of 400 ft (~121m), for collecting video data of fire borders can provide further high resolution intelligence to support firefighting activities. This information when collected at (near) real-time and integrated into a GIS

database, along with other layers of information such as terrain, meteorological, fuel characteristics and other levels of UAS data, can assist firefighters in a well-planned and rapid fire mitigation mission.

# CHAPTER 6 - APPLICATION OF LOW ALTITUDE UAS FOR BUSHFIRE MITIGATION

## 6.1 Introduction

During bushfires, manned rotary aircrafts (helicopters) (Figure 6.1) fitted with imaging and navigational sensors are applied for aerial surveying and reconnaissance such as identifying fire spotting and site analysis. These aircrafts operate at lower altitudes and limited flight time/ range. Applying such aircrafts in bushfire environments is dangerous as smoke and heat from the fire can increase risk factors in the mission. To generate a safe working environment such aircrafts can be substituted by low altitude categories of UAS such as LALE category UAS or long endurance VTOL category UAS.

Figure 6.1- Micro Flite helicopter applied in bushfires by CCF in Melbourne, Victoria, fitted with imaging and navigational sensors.

The focus of this study is based on Australia's plans in applying the Heron MALE category UAS in disaster relief and response mission including bushfires. During a bushfire, firefighters and emergency response teams are exposed to a high levels or risks that include chemical, environmental, electrical, and dangers caused by machinery to name a few. Many factors can accelerate of a bushfire such as, sparks from farm machinery and incinerators,

vehicle crashes, and electrical incidents such as fallen powerlines. So it is important for firefighters to perform a thorough risk assessment prior to entering a site. UAS fitted with video sensors can collect important information that shows dynamic changes in a geographic scene, and moving objects. Integration of such information into a GIS database can support a comprehensive site analysis.

To explore how the Heron UAS can be applied in disaster relief and rescue missions, including bushfire rescues, an exercise utilising a commercial VTOL UAS, DJI Phantom 3 Advance, fitted with an optical video sensor is performed. A number of video streams at three different altitudes, 50m, 80m and 100m above sea level are collected by the UAS platform, processed and analysed by two different commercial software packages, GeoMedia Motion Video Analyst Professional and Pix4D, to compare their outputs, along with the advantages of geo-registered video compared to still imagery. The results, advantages and limitations of the two different software packages are compared and discussed.

### 6.2 Research and Development on the Application of UAS in Australia

In recent years Australia has been considering adopting UAS technology in support of bushfire disaster missions (Sheridan, 2015). The Royal Australian Air Force (RAAF) operates two Heron UAS that are currently located at the RAAF base Woomera, in South Australia. The Heron, as shown in Figure 6.2, is suitable for a variety of disaster response missions including bushfire fighting operations. It can carry an array of sensors and its role during bushfires will be defined by the type of sensor it carries. One of the many advantages of the Heron is its ability to fly up to 24-25 hours within 250 km radius of the ground control station (GCS) at a maximum altitude of 30,000ft. It is fitted with an RF line-of-sight data link that permits it to supply (near-) real-time data to the GCS. Figures 6.3 and 6.4 are scenes from video streams collected by the Heron UAS in Afghanistan and at Woomera.

In 2015 RAAF announced that they had signed a Memorandum of Agreement with AirServices Australia, the Australian Government air navigation service provider, to operate the Heron UAS in Australian civil airspace (Department of Defence, 2015). This was a significant milestone that would allow a military-grade UAS to be operated for disaster response. Since then the Heron has been used during bushfires in the Shoalwater Bay area, north east of Australia, in the state of Queensland (Smart, 2016).


Figure 6.2- IAI Heron (Machatz-1) MALE category UAS


Figure 6.3- Video stream from IAI Heron (Machatz-1) in Afghanistan, courtesy of RAAF


Figure 6.4- Video stream from IAI Heron (Machatz-1) in Woomera, courtesy of RAAF

### 6.3 Orientation of camera axis for aerial data acquisition

Accurate measurements cannot be made from an image without rectification of tilt displacement and topographic relief displacements. In order to display an image in a GIS database geometric corrections or ortho-rectifications are required for the image or video to be georeferenced to a ground coordinate system. such that the scale of the photograph can be used to measure true distance of features within the photograph. Aerial imagery or video can be classified in the following categories based on their camera angle during image or video acquisition (Figure 6.5).

- True vertical camera angle – this is known as a camera faced vertically on the aircraft for image acquisition. An orthophoto is an accurate representation of the Earth' s surface. Orthophotos have the benefits of high detail, timely coverage combined with the benefits of a map including uniform scale and true geometry.

- Near vertical camera angle – a camera mounted in the aircraft at nearly vertical. The deviation is a result of camera tilt displacement on the aircraft during image and video acquisition. Generally the tilt should be less than 2 -3 degrees.

- Oblique camera angle – a camera that has been tilted intentionally. The total area photographed by oblique angled cameras is greater than vertical cameras with their application mainly for reconnaissance. There are two types of oblique angles, low oblique and high oblique. Low oblique is a tilt of up to 30 degrees while a high oblique is a camera tilt of greater than 30 degrees and less than 90 degrees.

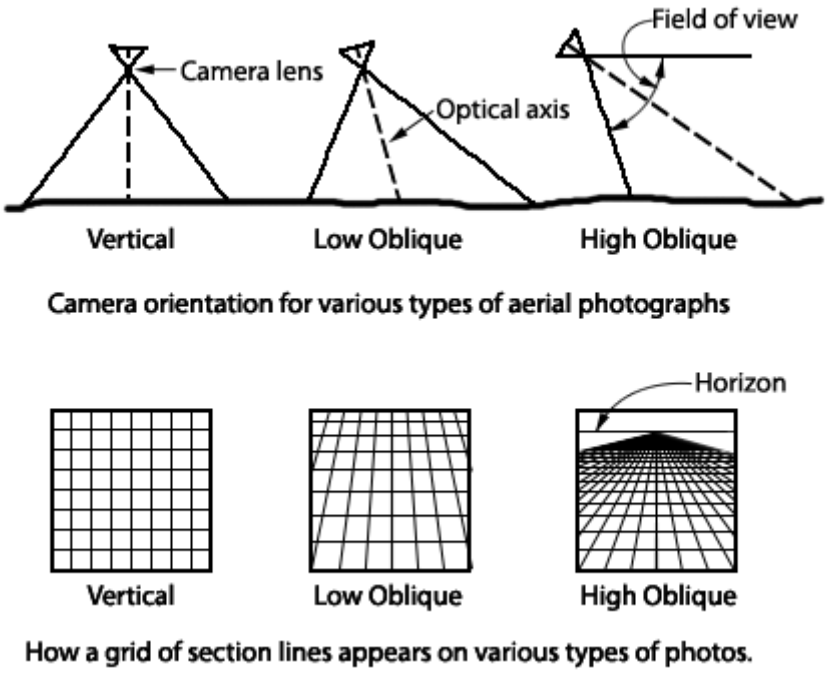


Figure 6.5 – Camera orientation for various aerial photographs

### 6.4 Video sensors

Video sensors are the most common sensor payload on UAS such as the Heron because of their relatively low-cost and light-weight (Se et al., 2010). Video streams alone are of limited use for bushfire disaster management because they provide little situational (i.e. geospatial) awareness to the viewer, and it is labour-intensive for firefighters to analyse the (often) many hours of data collected (Se et al., 2010, Ruano et al., 2014). Of benefit are video streams linked with location and orientation information in order to create geographically referenced data (Lewis et al., 2011). When video streams are 'geo-registered' and displayed or analysed within a GIS database, together with other data sources such as satellite and aerial imagery, they are capable of providing a different set of cues for scene segmentation, image analysis and object tracking (Kumar et al., 1998, Xiao et al., 2008). This information can be utilised to

assist in the rapid creation of imagery-derived maps that can aid in disaster response efforts (Bendea et al., 2008, Eisenbeiß, 2009).

### 6.4.1 Video Geo-referencing

Image processing for creating image mosaics from image sequences typically involves matching of corresponding features in overlapping image frames, and then geometrically modifying each frame so that the video stream is stitched together to form a mosaic with consistent geometry. Video processing is similar; however it exploits the temporal nature of the video stream. To be able to geo-reference individual video frames the UAS should be equipped with the appropriate navigational sensor payload in order to provide the desired metadata, which should include camera characteristics, the instantaneous Global Navigation Satellite System (GNSS) positions and the Inertial Navigation System (INS) attitudes of the aircraft, to determine the six exterior orientation parameters of each video frame. Geo-referencing accuracy is bounded by the level of accuracy of the acquired metadata (Taylor and Settergren, 2012). Some GIS software packages such as Hexagon's Geospatial GeoMedia Motion Video Analyst Professional and ArcGIS Full Motion Video Add-in (Kalinski and North Coast Media LLC, 2015) can perform geo-referencing of the video stream, by linking to information on aircraft coordinates, and in effect tagging the video pixels with geodetic coordinates (Wildes et al., 2001). Depending on the type of sensor used on the UAS the position and orientation of the sensor is collected and this information is used to determine the reference coordinate system, this is referred to as direct georeferencing. The accuracy of direct georeferencing procedures can be adjusted with GCP. The integration of live or recorded video streams from airborne platforms into a GIS database is essential for providing situational awareness for emergency services during bushfires. Figure 6.6 displays the process of video geo-referencing.

In order to relate the GNSS derived position and INS attitude components of the video and image point coordinates, a multi-sensor system calibration is required before undertaking the image acquisition, in order to resolve the misalignments between the GNSS/INS lever arms, the INS body frame and the imaging sensor frame (boresight transformation), with sufficient accuracy.

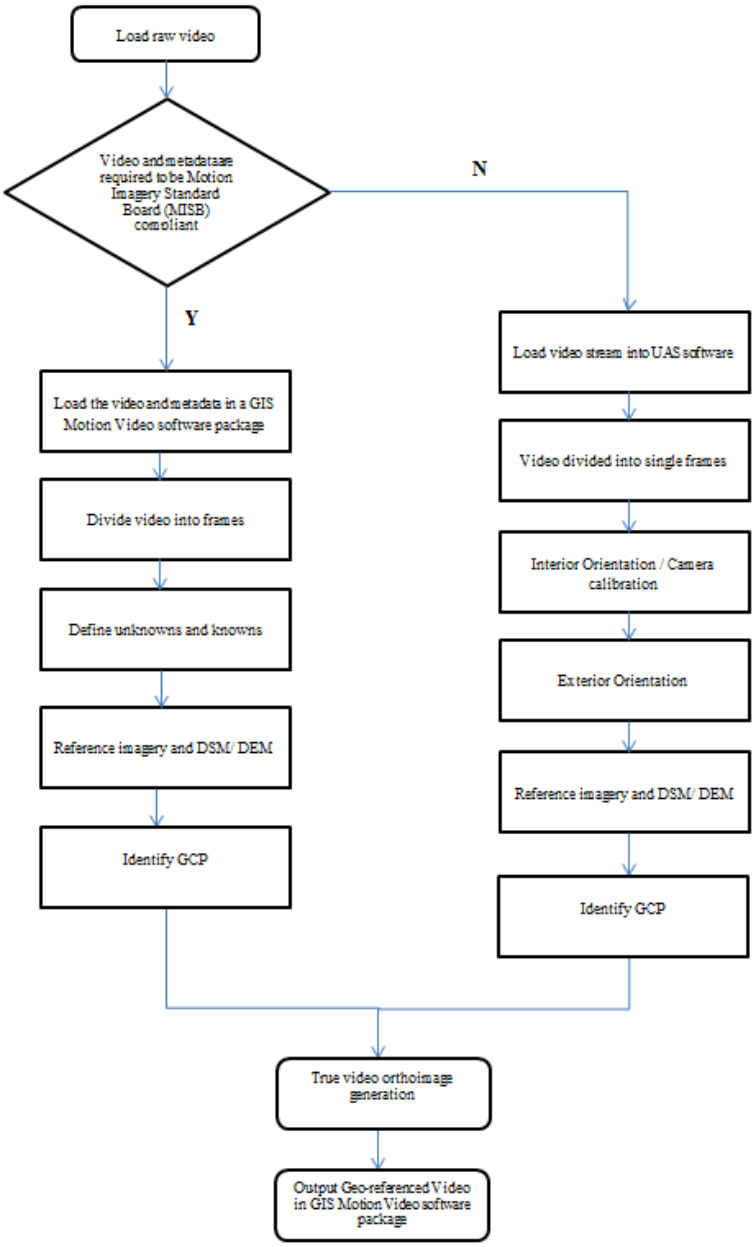


Figure 6.6 - Process of video Geo-referencing

### 6.4.2 GeoMedia Software

GeoMedia is a GIS database that offers tools to integrate video streams over other layers of geospatial data. The Motion Video Analyst Professional (MVAP) function integrates UAS video and imagery data into one seamless geospatial environment. For example, if operated in real-time, the telemetry data (includes camera coordinates, camera angle and camera frame coverage) are used to display the UAS flight line, camera angle, video frame, as vector layers of data in a map window while a separate window displays the video stream. Real-time

telemetry and video streams collected and downlinked to the GCS can also be post-processed and geo-fused with aerial and satellite imagery.

### 6.4.3 Pix4D Software

The Pix4D software is capable of UAS image and video processing. It can therefore be used to convert video streams (and metadata) into geo-referenced "orthomosaics". The process of image mosaicking using Pix4D is based on the application of the fundamental principles of photogrammetry combined with robust computer vision algorithms. Bundle adjustment algorithms take advantage of structure-from-motion principles are used to extract features on individual images that can be matched with features on multiple images. The image coordinate measurements and the interior orientation parameters define a bundle of light rays while the exterior orientation parameters define the position and the direction of the bundles in space. Using the collinearity equation, the bundles of light rays are rotated ($\omega$, $\phi$, $\kappa$) and shifted X, Y, Z until conjugate light rays are converged as well as possible at the locations of object space tie points and light rays corresponding to GCP pass as close as possible through their object points. The whole process is an incremental one in which the bundle adjustment is undertaken on an initial image pair and then further images are sequentially added in each iteration so as to produce a seamless "panorama".

### 6.4.4 Metadata format

For geo-referencing of UAS video streams the motion imagery system needs to be Motion Imagery Standard Board (MISB) compliant, which implies using MPEG-2 Transport Stream (TS), H.264/AVC compression and KLV metadata (MISB, 2016). The metadata and video streams are combined using a video multiplexer to create a single video file. Such a file is considered fully MISB compliant.

### 6.4.5 Interior and Exterior Orientation

A relationship between the camera or sensor, the image or images in a project, and the ground must be defined. This is done through interior and exterior orientation. The interior

orientation data describe the metric characteristics of the camera needed for photogrammetric processes. Two sets of parameters need to be considered, the camera geometric parameters such as the perspective centre, this is the theoretical point in the camera which the light rays forming the image pass through and the principal distance of the camera and the coordinates of the principal point, secondly, the parameters of systematic error arising from the use of incorrect constants, such as calibrated focal length and incorrectly located principal point. During the process of camera calibration, the interior orientation of the camera is determined. There are several ways to calibrate the camera. This can be done automatically during the processing stage where the radial and discentering distortion of the lens assembly can be determined as part of the camera calibration process.

Exterior orientation aims to define the position and rotation of the camera at the instant of exposure. The GNSS determines the UAS platform's instantaneous coordinates, while the INS measures the 3D accelerations and angular velocity components of the reference point of the inertial measurement unit (IMU) and hence the 3 instantaneous tilts of the camera. The exterior orientation is determined using a mathematical model referred to as the collinearity equations (6.1), which defines the transformation between image and object space –the relationship between the local image coordinates and the global mapping reference frame. The six parameters of the exterior orientation of each frame are the projection centre coordinates in the ground coordinate system $X^c$, $Y^c$, $Z^c$, and the 3 rotations axis ω, ϕ, κ around the X, Y and Z axis respectively.

Collinearity equations (6.1)

$$xj - x_0 + \Delta xj = -c\frac{[m11\ (Xj - X^c) + m12(Yj - Y^C) + m13(Zj - Z^C)]}{m31\ (Xj - X^c) + m32(Yj - Y^C) + m33(Zj - Z^C)]}$$

$$yj - y_0 + \Delta y = -c\frac{[m21\ (Xj - X^c) + m22(Yj - Y^C) + m23(Zj - Z^C)]}{m31\ (Xj - X^c) + m32(Yj - Y^C) + m33(Zj - Z^C)]}$$

Where:

c = principle distance often approximated to be the camera's focal length (*f*)

xj, yj = image coordinates of object j

$x_0$, $y_0$= are displacement coordinates between the actual origin of the image coordinates and the true origin defined by the principle point

Δxj, Δyj = corrections applied to the image coordinates for systematic errors

$X^c$ $Y^c$ $Z^c$ = camera coordinates in the object space

X, Y, Z = object coordinates of any point

*m* = elements of the *M* Matrix in which the rotation ω, ϕ, κ about the 3 axes X,Y,Z respectively

The image coordinates x, y are measured, and the principle distance of the camera c is assumed constant. Every measured point on the image results in two collinearity equations, (equation 6.1), but also adds three additional unknowns, namely the coordinates of the object point (Xj , Yj , Zj ). This process is carried out for the first video frame and then consecutively carried out for the other frames. Using the rotation matrix *M* rotations are made based on the rotation angles ω, ϕ, κ to create a true orthogonal image (equation 6.2). This means that the effects of tilt and elevation in buildings are eliminated using a Digital Surface Model (DSM) making the buildings look as if they are erected straight up.

Rotation Matrix (6.2)

$$M= M_{\kappa}M_{\phi}M_{\omega}$$

Where *M* is the rotation matrix describing the relationship between the orientation of the image and object system in terms of ω, $\phi$, κ. The definition of the rotations has to be respected; most often the successive rotations with the sequence ω, $\phi$, κ or $\phi$, ω, κ are used. A transformation from one rotation system to the other can be made. Through direct orientation the navigational sensor data are registered to each video frames to define the relationship between the image and object space. A minimum of two overlapping images are required to define object points with the accuracy of the output dependent on the accuracy of the GNSS and INS sensors. GCP can be applied as an option to increase the accuracy and position of the output. Once this is done the video stream can be integrated into the GIS database.

### 6.4.6 Ortho-imaging and Image Mosaics

A compact image mosaic provides a much larger image context than a single video frame (Kumar et al., 1998). The mosaicking process involves “stitching” together sequences of video streams into image mosaics so as to generate high-resolution 2D maps. The process involves ortho-rectifying the video frames using, the interior and exterior orientation of the video frames from the UAS metadata. The process of ortho-rectifying images involves reprocessing the raw images to correct scale variations and image displacement resulting from terrain relief and sensor and aircraft tilt. Once all images of video frames have been ortho-rectified, images mosaics can be build.

To build an image mosaic appropriate forward and side overlap are required. Forward overlap is the overlap between two images in the same flight line while side overlap is the overlap between adjacent flight lines. During digital image acquisition generally there is a forward overlap of minimum 60% and a recommended 85% and a side overlap of 30%-60%. Small overlaps reduce the capability of joining the multiple images to form the mosaic, while too much overlap may result in too many unnecessary images that may affect the project budget negatively. The accuracy of the image mosaic is influenced by the accuracy of the telemetry data and the quality of the DEM describing the terrain form. A single image mosaic can be generated from the multiple overlapping images using tie points to “stitch” the overlapping images (Figure 6.7). The final result is a synoptic view of the area of interest that can be used for further analysis and better geographical awareness for users. Furthermore, the geo-referenced image can be integrated with other layers of data, such as aerial photos, satellite imagery, or geospatial information within a GIS database.

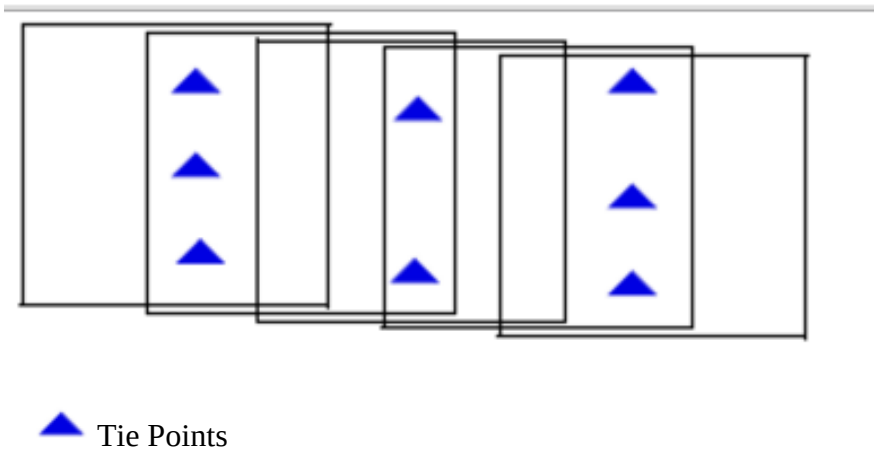


Figure 6.7 - image mosaic built from overlapping image strips (hexagonGeospatial, 2017)

### 6.5 Method of UAS Video Geo-referencing

It is recommended that the UAS equipped with video sensor to be flown at a lower altitude, below 400ft (~122m). Although flying the UAS at higher altitudes will result in larger terrain coverage by the cameras it comes at the detriment of the image resolution. This can be significant for some missions as small objects may be more difficult to identify in both the aerial videos and ortho-imagery, which can ultimately defeat the purpose of an aerial surveying and reconnaissance. Therefore, the altitude of the camera needs to be carefully selected in order to optimize the coverage by the camera.

1. Site selection

To comply with CASA rules and regulations the UAS mission was preformed outside of CASA restricted zones referred to in chapter 1.3.2. It was important that the location selected for the exercise had important features such as moving objects, buildings, tress, power poles and roads and access routes.

2. Flight time and weather consideration

For this exercise the Phantom 3 Advance UAS, a rotary UAS was fitted with a video sensor. Descriptions of this UAS are provided below. As the UAS platform is light weight, its flight can be impacted by rain and wind, causing substantial rotation of the camera also known as crabbing effects and could ultimately impact the output result, so special consideration must be given to the time and day of the exercise. Therefore, the exercise was conducted on a sunny day at a time when the wind velocity was low. However, for a bushfire mission long endurance military grade UAS that fly at lower altitudes are recommended as they are more durable for the intense bushfire environment. This is because at lower altitudes strong winds are produced in a bushfire environment that can cause drifting effects to the UA.

3. Ground Control Points (GCP)

Prior to the flight eight targeted Ground Control Points (GCP) were setup on the ground and their coordinates along with the coordinates of six additional non targeted GCP (fixed

structures) were determined using RTK-GNSS. The GCP are distributed in such a way that more than three GCPs are featured in each flight. The coordinates of the GCP have been collected in case the accuracy of the UAS flight is impacted by turbulence from the wind. The GCP can be optionally applied for rectification of the sensor accuracy or to increase the desired software output accuracy.

4. Flight mission planning

Flight planning is a fundamental part of aerial data acquisition. A flight plan must be prepared for data acquisition that includes additional consideration given to the flight time, weather conditions, UAS type, camera angle, flight location and the accuracy and ground sampling distance (GSD). UAS flight planning is different compared to traditional aerial photogrammetry flight planning with manufactures developing their own mission planning software. The commercial mission planning packages for aerial images allow, defining the geographical area for the aerial survey, flight height, the coordinate system and camera parameters, flight line, forward and side overlap, sensor selection. Additional information such as, start and home point have to be defined for autonomous flight planning.

Prior to the flight it is important to determine what GSD is required for the specific mission. The GSD is the projection of the pixel size onto the ground plane. It is determined by the camera internal geometry (focal length and the size of the CCD array) and the aircraft's flight altitude, as per below:

**GSD = (pixel size * flying height) / focal length**

For this exercise the UAS mission plan consisted of flying the UA manually in a single flight line at three different altitudes: 50 m, 80 m and 100 m. Flying the UAS at higher altitudes increases the area of coverage of the video frames which may be useful when converting the video frames to image mosaics. The basic geometry for collecting imagery is to have the aerial camera pointing downwards. Due to weather conditions and turbulence a true vertical image can never be obtained, however the tilts can be corrected for through exterior orientation.

5. Accuracy

The accuracy of the data acquisition is dependent of the type of data and its application. For bushfire mission's rapid and clear information is essential to quickly position the location for navigating firefighters and emergency services to get to the site.

6. Data acquisition and extraction

After the UAS video streams have been collected they are analysed in two different software packages: GeoMedia Motion Video Analyst Professional (MVAP) and Pix4D. The videos are used along with the ortho-rectified imagery to compare the advantages of geo-registered video and ortho-imagery. Moving objects and aircraft velocity are carefully analysed to study how they affect the display of these objects in the image mosaics especially at the beginning and the end of the videos.

### 6.5.1 Description of the Phantom 3 Advance UAS

The Phantom 3 Advance is a VTOL UAS (Figure 6.8) that is capable of flying for approximately 23 minutes at a maximum speed of 16 m/s (when there is no wind). It is fitted with a Sony EXMOR video sensor that can collect 2.7K video with 12 megapixel resolution. It is also equipped with a GPS receiver and an IMU. The video stream and metadata are collected and stored on the micro SD card. The remote pilot (RP) can control the UA using the remote controller while receiving a live view on their tablet computer using the DIJ Go app. In this UAS images are stored in JPEG or DNG format, and videos are recorded as MP4 or MOV (MPEG–4 AVC/H.264) files, while the metadata is stored in DAT format. The Phantom 3 UAS is capable of flying at a 3-5 km range of the RP, which means it is not suitable for use during critical bushfire fighting operations. For this exercise the video sensor was applied in collecting colour video streams during each flight along with necessary flight metadata. Some characteristics of the Phantom 3 Advance UAS are listed in Table 6.1.

Table 6.1 - Some Phantom 3 Advance UAS characteristics

| | |
|---|---|
| Aircraft Weight | 1280 g |

| | |
|---|---|
| Hover Accuracy | • Vertical: +/- 0.1 m (when Vision Positioning is active) or +/- 0.5 m<br>• Horizontal: +/- 1.5 m |
| Max Speed | 16 m/s |
| GNSS Mode | GPS/GLONASS |
| Controllable Range | Pitch -90° to +30° |
| Stabilisation | 3-axis (pitch, roll, yaw) |
| Max Flight Time | Approx 23 minutes |
| Sensor | Sony EXMOR 1/2.3" Effective pixels: 12.4 M (total pixels: 12.76 M) |
| Lens | FOV 94° 20 mm (35 mm format equivalent) f/2.8, focus at ∞ |
| Image Max Size | 4000 x 3000 |
| Supported File Format | • FAT32/exFAT<br>• Photo: JPEG, DNG<br>• Video: MP4, MOV (MPEG-4 AVC/H.264) |

Figure 6.8 - Phantom 3 Advance is a VTOL UAS

### 6.6 Results and Discussion of UAS Video Geo-referencing

Conventionally aircraft velocity is of importance in photogrammetry flight mission planning. A high velocity flight can result in less forward overlap while a low velocity flight can result in too much overlap. Both results can be harmful for the project output with. The camera shutter speed should also be set based on the aircraft velocity to eliminate the generation of blurred images. Although these are all limitations that impact traditional methods of collecting still imagery, they are not of a concern for this project as the type of data collected are video streams.

The video streams of the 6 different flights are processed in the two different software packages and compared. Although all flights run roughly along the same flight line, the terrain coverage for the flight at 100 m is greater than for the other two flights. An area of 9990 $m^2$ is covered during the 100m flight while and area of 5000 $m^2$ and 8000 $m^2$ are covered during the 50m and 80m flights .As the flight altitude increases, the map scale decreases with objects becoming smaller. Although objects are visible to the naked eye at 100 m flight altitude, the image resolution is sharper and smaller objects are more easily distinguishable at 50 m and 80 m flight altitude. The GCP positional accuracy is estimated to be 0.5 cm for the E, N coordinate components, and 1 cm for the height component. The GSD for the three different altitude flights are displayed in Table 6.2. The computed GSD represent the pixel size on the ground. From the table below it can be seen that as the GSD decreases the sampling rate increases to cover the same area on the ground, thereby increasing image resolution.

Table 6.2 - GSD for 50 m, 80 m and 100 m altitude UAS flight

| Flight Height | GSD |
|---|---|
| 50 m | 0.93 cm |
| 80 m | 1.48cm |
| 100 m | 1.85 cm |

During the flights prominent features extracted from the video were building, trees, the road, GCPs, electrical poles and wires, vehicles and pedestrian movement. Flying the UAS at low altitudes provides a detailed view of the region including the ability to survey a building and the site around the building along with identifying access routes. With a high resolution video sensor and a low altitude flight, detailed information such as powerlines information can be extracted (Figure 6.9) while it would be difficult to export this level of detail from the 100 m flight (Figure 6.10). This level of detail and intelligence can be applied by firefights for site risk assessment in identifying hazards and setting controls to reduce the likelihood of these risks.

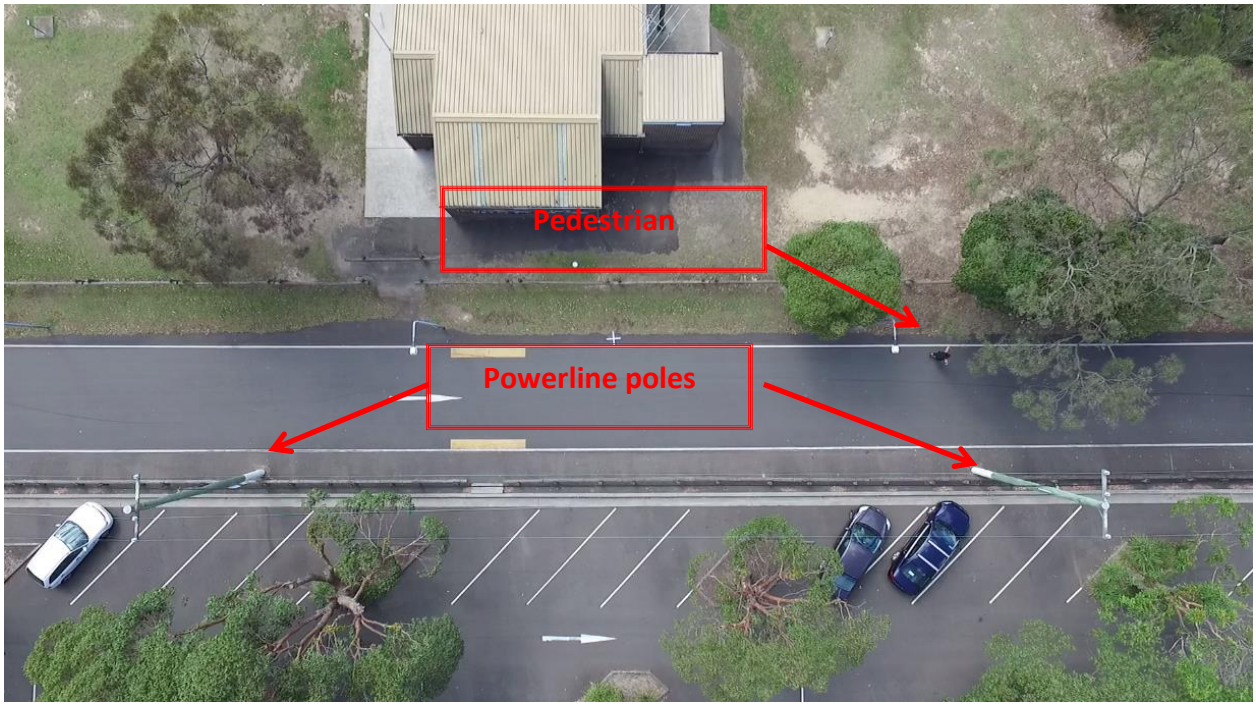


Figure 6.9 – Phantom 3 Advance flight at 50m altitude identifying prominent features (scale 1:282)


Figure 6.10 – Phantom 3 advance flight at 100 m altitude identifying prominent features (scale 1:564)

A video streams is built of 23 frames per second. A multiplexer or converter is used to ensure the video stream and metadata are MPEG Transport Streams (TS) compliant as required by GeoMedia. Pix4D supports MP4 video data and CSV metadata formats. The metadata collected by the UAS are first converted from DAT to the CSV format using the maps-made-easy website (MapsMadeEasy, 2016). Later, the video and metadata were combined into a single MPEG-TS file using the HandBrake converter (HandBrake, 2016). The output products produced by the two software packages are discussed below. The results produced by the two different software packages are further explored to assess the level of information that can be extracted from them.

### 6.6.1 Analysis of Output from GeoMedia

After loading the MISB compliant video stream into the GeoMedia Video Warehouse, it is displayed both in the map window and the video display window, with the metadata attributes displayed on the right hand side of the video display window as seen in Figures 6.11 and 6.12. During the field exercise the UAS was flown over a road with moving cars and pedestrians, which were tracked by the UAS. The purpose of detecting moving objects in the video stream is to obtain spatial temporal properties from moving objects and detailed information on attributes such as their speed, position, motion trajectory, and acceleration for tracking the objects over time and derive a set of properties, such as their behaviours, from their trajectories. The main advantage of GeoMedia is that it offers geo-referenced video over still imagery (ie: aerial imagery) offering the ability to observe spatial temporal variations on site. For example from the behavioural movement and direction of vehicle, possible pedestrian collisions can be determined in advance or it can be applied in identifying and tracking civilian movements during bushfire site evacuations and rescue. Other examples can be identifying and viewing the movements of objects such as trees falling on powerlines. Such information cannot be obtained from still imagery as moving objects cannot get detected.

Although the flight velocity is an important factor to take into consideration during a UAS mission, it does not hinder the results produced in GeoMedia. Displaying the video in GeoMedia offers effective decision making capabilities, while the analyst has the ability to

play the video back and forward or to replay the video context; this is particularly useful in the high velocity flights (Figure 6.12). Although the scale factor of the different altitude flights can impact the object visibility, ortho-images of selected areas can be generated instantly for further zooming and analysis, allowing an overall useful tool for remote visual inspection, object tracking and site assessment. With the added advantage of building image mosaics as the video stream runs in the Video Warehouse toolbar window.

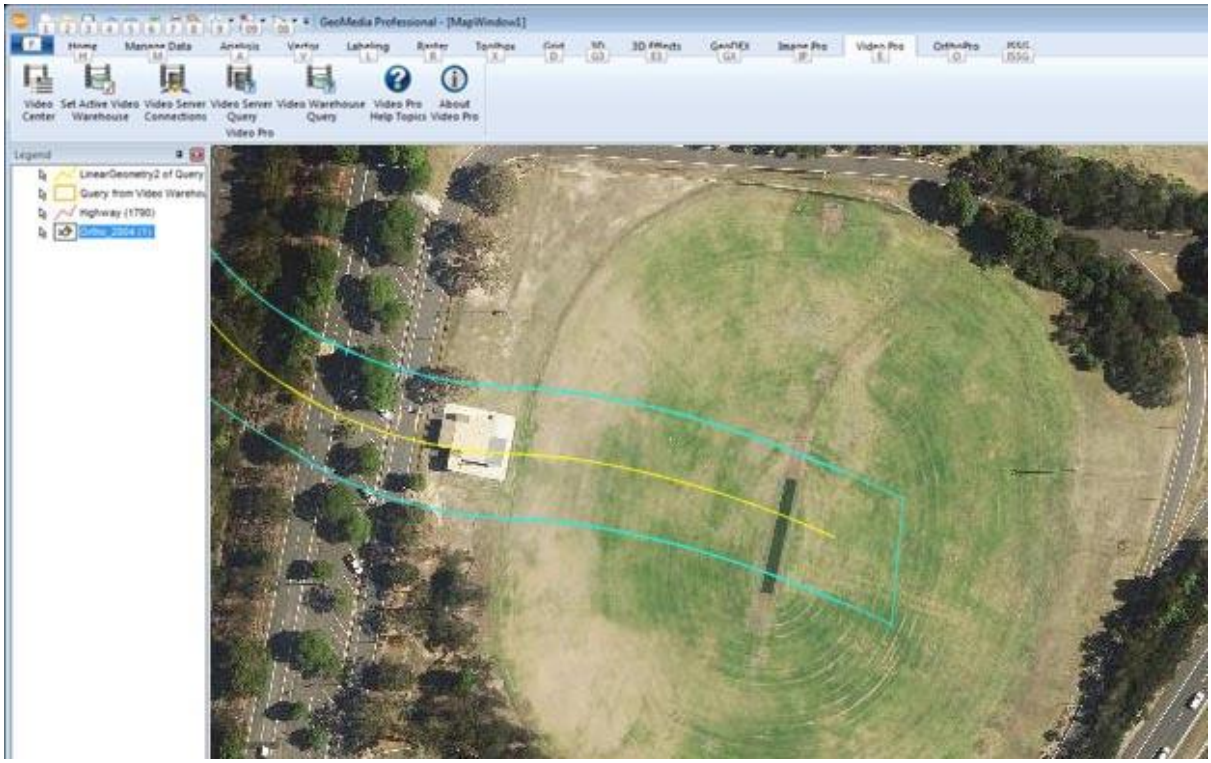


Figure 6.11 – GeoMedia geographic window displaying the flight line (in yellow) and the video footprint coverage (aqua lines) (scale 1:700)

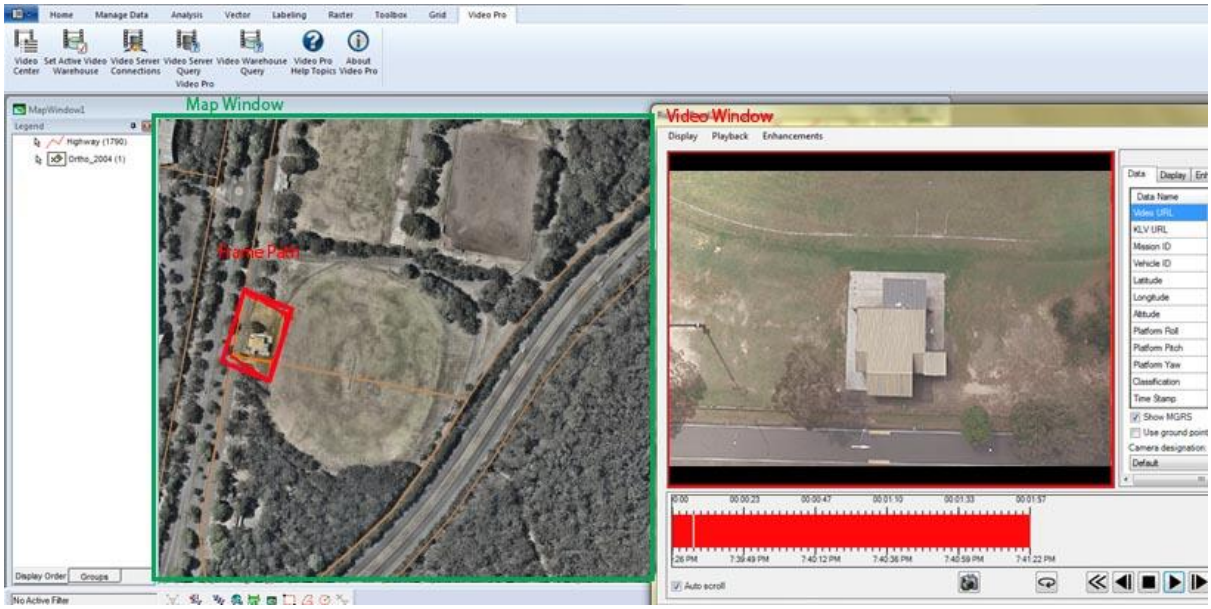


Figure 6.12 - GeoMedia Motion Video Analyst Professional (MVAP) video display window

### 6.6.2 Analysis of Output from Pix4D

The Pix4D software converts still imagery and video data into image mosaics as shown in Figure 6.13. The software allows the analyst to specify the internal and external camera parameters. This involves running Automatic Aerial Triangulation (AAT), Bundle Block Adjustment (BBA), and camera self-calibration steps multiple times until an optimal reconstruction is achieved (Pix4D, 2016). During this process the video stream is geometrically corrected and the coordinate system can be changed to the desired output. The maximum number of frame overlaps is user-specified. To remain consistent throughout the processing of the different video streams, a frame overlap of 10 frames is selected for all videos. The extracted frames are ortho-rectified and saved as images in the working folder. To improve the accuracy of the output product in Pix4D, the coordinates of the GCP were imported and marked on the overlapping images; Figure 6.15 displays the GCP, in blue.

Once the video streams are corrected the output result are 3D ‘point clouds’ as seen in Figure 6.16. A DEM and an image mosaic can be generated from the ortho-rectified images. For this exercise the image mosaics were saved as KML files and loaded into Google Earth Pro as shown in Figure 6.17. The image mosaic allows a holistic view of the imaged region but limits the analyst’s ability to perform (near-) real-time object tracking and site analysis.

Furthermore Pix4D does not offer a single database for processing, geo-registering and displaying the video file for subsequent visualisation and analysis.

The results of the Pix4D processing indicate the average residuals for the GCP and the root mean square errors (RMSE) for the observations to be extremely accurate. For our values below the largest residual is in the order of $3\mu m$ (Table 6.3). Relatively large residual values indicate error in the photogrammetric network of observations. Large error can be resulted due to mismeasured GCP, data entry error, and poor quality of GCP. The results also demonstrate that the flight altitude and UAS velocity are both important factors when converting video streams to image mosaics. A high velocity UAS flight can result in fewer video frames. Applying a consistent 10 frame overlap reduces the forward overlap between video frames in the high velocity flight, and the effects of this reduction are reflected in the image mosaic and image cloud points (Figure 6.13, 6.14). Lower video frame overlaps can impact the quality of the ortho-images in such a way that they cannot be used for stereo viewing and processing. At the same time a high velocity UAS flight can impact on how moving objects are displayed in the image mosaic. Although moving objects can be viewed and followed conveniently in a video, the result of converting video to image mosaic can reduce information content. Moving objects can either be concealed or displayed blurry in the image mosaic. Figure 6.15 are orthoimages created from the video stream of the 100 m UAS flight with a high velocity moving object marked red in them. This moving object was North West of the image mosaic (Figure 6.13) but was concealed. This is particularly observed at the beginning and end of the video frames where there are fewer overlapping frames and for fast moving objects such as cars. These moving objects are not displayed in the final image mosaic. On the other hand the results of a low velocity UAS flight can create too many image overlaps when converting the video to ortho-images which causes too many duplicated objects.

Table 6.3- Pix4D GCP error report

| GCP Name | Accuracy XY/Z[m] | Error X[m] | Error Y[m] | Error Z[m] | Projection Error [pixel] |
|---|---|---|---|---|---|
| Point 1 (Building corner A) | 0.05/ 0.05 | -0.010 | -0.013 | 0.000 | 0.644 |
| Point 2 (Building corner B) | 0.05/ 0.05 | 0.021 | -0.021 | 0.043 | 0.593 |
| Point 3 (GCP1) | 0.05/ 0.05 | 0.010 | 0.005 | 0.004 | 1.210 |
| Point 4 (GCP2) | 0.05/ 0.05 | -0.007 | -0.031 | -0.128 | 0.939 |
| Point 5 (GCP3) | 0.05/ 0.05 | -0.024 | 0.023 | -0.092 | 0.933 |
| Point 6 (GCP4) | 0.05/ 0.05 | 0.023 | -0.031 | 0.039 | 1.007 |
| Point 7 (GCP5) | 0.05/ 0.05 | -0.007 | -0.017 | 0.053 | 1.100 |
| Point 8 (GCP6) | 0.05/ 0.05 | 0.029 | 0.017 | -0.112 | 0.924 |
| Point 9 (Back of Building corner A) | 0.05/ 0.05 | 0.030 | 0.013 | 0.182 | 1.047 |
| **Mean [m]** | | 0.007222 | -0.006111 | -0.001222 | |
| **Sigma [m]** | | 0.019734 | 0.020907 | 0.097914 | |
| **RMS Error [m]** | | 0.019958 | 0.020637 | 0.092322 | |

Figure 6.13 -Pix4D image mosaic built from the video frames collected from the Phantom Advance UAS of Sutherland NSW (scale 1:564)

Figure 6.14 - zoomed in section of the image mosaic displaying distortions on the edge of the video frame

Figure 6.15 – Moving car (in red circle) at the edge of the 100 m UAS (Scale 1:564)

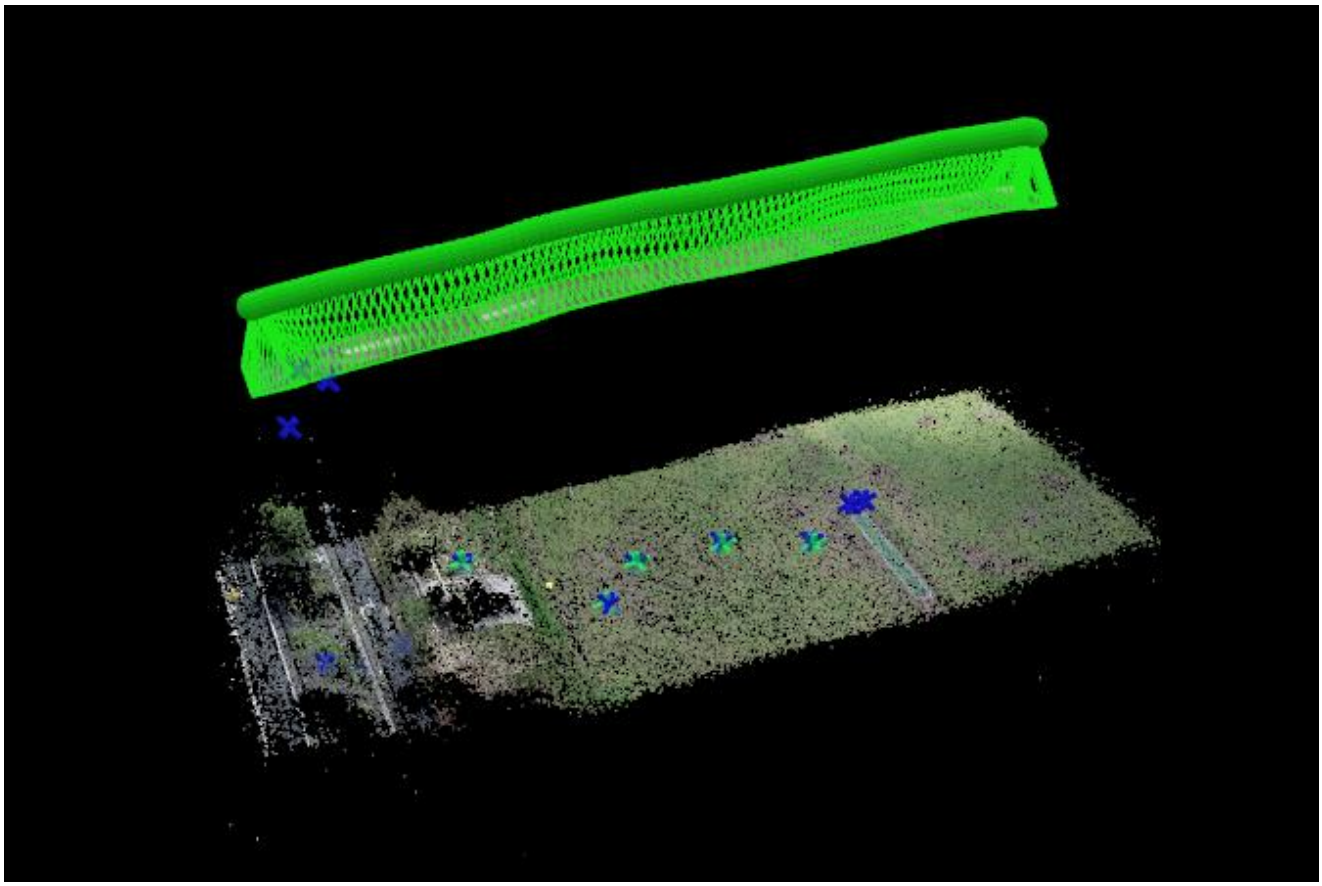

Figure 6.16 - Pix4D point cloud of Sutherland NSW, displaying the UAS flight line (in green) and the area mapped along with the marked GCP (in blue) and fixed structures used as GCP


Figure 6.17 -KML image mosaic (in red rectangle) generated in Pix4D on imported in Google Earth Pro

## 6.6 SUMMARY

Since the higher the flight altitude the greater the GSD, a to be able to successfully apply UAS equipped with a video sensor during a bushfire mission a maximum flight altitude of 400 ft (121m) is recommended. At altitudes above 400ft object sizes become smaller and analysis of object characteristics becomes difficult. This allows the UAS to collect high resolution video along the bushfire border without the UAS being impacted by heavy gusts and winds generated by the bushfire itself safer for other UAS to operate in other airspaces by mitigating the possibility of collisions.

The results of the output product of the two different software packages support the conclusion that flight velocity it does not impact the quality of the video data. Geo-referenced videos loaded in a GIS database offer a single, streamlined system to process, visualise and analyse the data, with the added advantage of (near-) real-time processing. The video stream can be geo-fused into a GIS database and displayed over other layers of geospatial data such as aerial imagery, road and cadastre boundaries, and when applied to bushfire emergency management situations it can aid rescue coordination efforts. This can provide spatial temporal context of attributes such the speed, position, motion trajectory, and acceleration of

moving objects when displayed in a GIS database. Such videos can be applied in site assessment, object tracking and risk assessments. While there is the added advantage of generating image mosaics loaded over aerial photos, satellite imagery can be used to provide a synoptic view of the area of interest.

Although it was preferred to apply this exercise during a controlled fire with a LALE category UAS or a long endurance VTOL UAS, due to limitation improvisations were made to display the advantages of such categories of UAS for site analysis and object tracking for firefighters and emergency services and the capability of viewing aerial photography along with video data integrated in a single GIS data base system. Not only will this offers the users the ability to select the type of data for analysis but also offers a diverse view of a location in 2D and 3D. When video streams are integrated into a single GIS database system along with other forms of geospatial intelligence such as satellite imagery and aerial photography, they can provide a richer and detailed view of an area.

# CHAPTER 7: CONCLUDING REMARKS AND RECOMMENDATIONS

## 7.1 An Overview of this Thesis

Influencing factors such as fuel composition, weather conditions and topography information that impact the physical attributes of a fire, such as the fire height and depth of the fire flame, the speed, size and the shape of a fire, are all of importance for firefighting. This drives the need for remotely sensed data. Emergency services and firefighters are not able to respond to a fire emergency without access to fire 'intelligence'. When such information is supplied to emergency responders in a timely manner it can assist in developing a plan of attack, thereby saving resources, time and possibly lives.

Unmanned Aerial Systems (UAS) can fly in a variety of airspaces, such as in segregated air space which includes below 400 ft, and in the stratosphere, and in non- segregated airspace. This research recommends a higher altitude UAS of the MALE or HALE category as an aerial platform for obtaining synoptic remotely sensed data of the bushfire region in tandem with a lower altitude UAS, such as the LALE category UAS or long endurance category of VTOL UAS, to provide a detailed view of specific regions across the fire boundary. With such a multiple UAS mission the possibility of the two UAS colliding is eliminated. These UAS must satisfy the appropriate criteria defined by ICAO and CASA, such as Airworthiness, Command and Control (C2), Detect and Avoid (DAA), remote pilot licensing, and UAS operations requirements. It is recommended that the UAS for bushfire missions be of the long endurance variety, fitted with appropriate imaging and navigational sensors based on its mission capabilities, with high bandwidth C2 data link and communication with ATC.

For the successful application of multiple UAS in different airspaces it is recommended that a higher altitude UAS be fitted with 'satellite-like' sensors such as the AMS wildfire sensor as was applied during the bushfires in California. Such a sensor is capable of supplying data that can be used for hotspot analysis and identifying fire location, shape and size in (near-) real-time. It is recommended that the lower altitude UAS be fitted with video sensors for collecting 3D data that can be used for site assessment, object tracking, and other local-level tasks.

## 7.2 Overall Results

The overall results of this study support the contention that UAS technology can be used for bushfire missions. Not only can the application of UAS create a safer working environment for the RP and the RP crew as they are located at a safe location while flying the aircraft, but it also provides valuable high spatial and temporal resolution imaging data. The conclusions of chapters five and six are summarised below:

**Specific Conclusion from Chapter 5**

- During AMS wildfire data comparison with MODIS it was noticed that there was a time lag between the two data acquisitions of one hour in the case of the Zaca Fire. Due to this time lag it can be difficult to compare the two sets of fire data because of the dynamic nature of a fire.

- The results from the AMS wildfire sensor and MODIS sensor outputs comparison highlighted the difference in the resolution of the two datasets. At an altitude of 7438.8586 m (23,000 ft), which was the flying height of the Predator – B Ikhana for the Witch, Poomacha & Rice Fires, the spatial resolution is 15m. On the other hand, the pixel resolution of the MODIS data is 1000m. The pixel resolution of MODIS is too coarse to resolve the size of small fire hotspots that may be very intense relative to large but low-intensity fires. Due to the small size of the fire in comparison to the pixel size, there may be greater error resulting from pixel saturation.

- Random pixel hotspots were detected in the AMS wildfire data that were not near the main fire. The number of pixels saturated were of the order of 2-4 pixels. These pixels may be saturated due to a hot objects located at the centre of the pixels, and as a result increasing the brightness temperature of the pixel and the neighbouring pixels. For example, sub-pixel fire hotspots near the edge of a pixel will likely result in an underestimated fire pixel brightness temperature, whereas for fires near the centre of a pixel the pixel's brightness temperature may be overestimated. During the image processing these pixels did not display as fire pixels. The hotspot detection algorithm code removed these random pixels.

- A long endurance UAS collected and supplied (near-) real-time, day and night, Level 1-B, georeferenced data to emergency services and firefighters that provided them with the ability to track fire movement and to develop a fire plan to address the fire danger.

**Specific Conclusion from Chapter 6**

- Video stream allowed spatial temporal properties to be measured from moving objects, and detailed information on attributes such as their speed, position, motion trajectory, etc, to be obtained. When such data is integrated into a GIS database such as GeoMedia it permits the viewing of georeferenced video overlain on road and cadastre boundaries and still aerial imagery, to observe spatial-temporal variations. Such information cannot be obtained from still imagery alone.

- The output products from GeoMedia and Pix4D indicated that flight velocity of video streams does not impact the quality of the video data conversion to georegistered video or ortho-imagery. Georeferenced videos loaded in a GIS database offer a single, streamlined system for the processing, visualisation and analysis of the data. When video stream are geo-fused into a GIS database and applied to bushfire emergency management situations it can aid rescue coordination efforts. This can provide spatial-temporal context of attributes such the speed, position, motion trajectory, and acceleration of moving objects when displayed in a GIS database. There is the added advantage of generating image mosaics overlain on aerial photos and satellite imagery to provide a synoptic view of the area of interest.

.

## 7.3 Research Limitations

- Limitation of this research was the fact that we were not able to demonstrate this concept of the simultaneous application of multiple UAS in different air spaces for the acquisition of different categories of data. A low altitude UAS could be used for the analysis of fire boundaries, risk assessment, object tracking and identifying fire

hotspots. A higher altitude UAS fitted with satellite-like sensors could be used for hotspot detection during a bushfire mission.

- For the exercise described in Chapter 6 the desired UAS category with the necessary imaging sensor payload was not used for data acquisition. It was hoped to use a military UAS category but due to certain factors beyond our control a commercial grade UAS was used instead. The exercise was to demonstrate how a low altitude UAS fitted with video sensors can be used for site assessment, identifying access routes and object tracking, and how such data i a GIS database could provide the video sensor with spatial context for subsequent analysis.

### 7.4 Recommendations for Future Work

The following recommendations are made:

- Demonstration of the simultaneous application of dual-UAS for the acquisition of different levels of data in one experiment.

- Integrating two levels of remotely sensed and low altitude video data of the same area into a single GIS database and investigating how the two different data sources can be used.

- Comparison of different software packages that can accommodate remotely sensed and video data.

- Investigate different hotspot detection algorithms.

- Investigate how changing the threshold levels of the CCRS hotspot detection algorithm affects the fidelity of fire hotspot pixel identification.

As concluding remark, it is clear that UAS can replace current traditional methods of bushfire data acquisition. Although two separate projects were used to discuss the many advantages of

UAS, a single dual-UAS mission has not been attempted due to a number of UAS technical and regulatory limitations.

# REFERENCE


ADAMS, S., FRIEDLAND, C. & LEVITAN, M. Unmanned Aerial Vehicle Data Acquisition for Damage Assessment in Hurricane Events. Proceedings of the 8th International Workshop on Remote Sensing for Disaster Management, Tokyo, Japan, 2010.

ADAMS, S. M. & FRIEDLAND, C. J. 2011. A Survey of Unmanned Aerial Vehicle (UAV) Usage for Imagery Collection in Disaster Research and Management. *9th International Workshop on Remote Sensing for Disaster Response.*

ALTAN, O., BACKHAUS, R., BOCCARDO, P., TONOLO, F., TRINDER, J., VAN MANEN, N. & ZLATANOVA, S. 2013. The Value of Geoinformation for Disaster and Risk Management (VALID): Benefit Analysis and Stakeholder Assessment. Published by the Joint Board of Geospatial Information Societies (JB GIS), Copenhagen.

AMBROSIA, V. 2012. UAS Remote Sensing Platforms for Emergency Response and Management. *In:* REGION, A. N. C. (ed.) *Remote Sensing of Fire and Ecosystem Impacts.* USDA-FS Wildland Fire Training Center, McClellan Park, CA.

AMBROSIA, V. G., WEGENER, S., ZAJKOWSKI, T., SULLIVAN, D. V., BUECHEL, S., ENOMOTO, F., LOBITZ, B., JOHAN, S., BRASS, J. & HINKLEY, E. 2011. The Ikhana unmanned airborne system (UAS) western states fire imaging missions: from concept to reality (2006–2010). *Geocarto International,* 26**,** 85-101.

AMBROSIA, V. G. & WEGENER, S. S. 2009. *Unmanned airborne platforms for disaster remote sensing support*, INTECH Open Access Publisher.

AMBROSIA, V. G., WEGENER, S. S., SULLIVAN, D. V., BUECHEL, S. W., DUNAGAN, S. E., BRASS, J. A., STONEBURNER, J. & SCHOENUNG, S. M. 2003. Demonstrating UAV-acquired real-time thermal data over fires. *Photogrammetric engineering & remote sensing,* 69**,** 391-402.

AMERI, B., MEGER, D., POWER, K. & GAO, Y. UAS Applications: Disaster & Emergency Management. 2009. American Society for Photogrammetry and Remote Sensing, 45-55.

AUSTRALIA ATTORNEY GENERAL'S DEPARTMENT 2010. Handbook 10 National Emergency Risk Assessment Guidelines. *In:* DEPARTMENT, A. G. S. (ed.). Australian Government Attorney-General's Department.

BARNARD, J. 2007. Small UAV (< 150 kg TOW) Command, Control and Communication Issues. The Institution of Engineering and Technology.

BENDEA, H., BOCCARDO, P., DEQUAL, S., GIULIO TONOLO, F., MARENCHINO, D. & PIRAS, M. Low cost UAV for post-disaster assessment. Proceedings of The XXI Congress of the International Society for Photogrammetry and Remote Sensing, Beijing (China), 3-11 July 2008, 2008.

BENTO, M. D. F. 2014. Unmanned Aerial Vehicles: An Overview. *Inside GNSS.* January/ Febuary 2008 ed.: Inside GNSS.

BLYENBURGH, P. V. 2016. Reference Section, RPAS & RPAS Sub- System. *RPAS Remotely Piloted Aircraft Systems The Global Perspective.* 14 ed. UVS-info.

BOOTH, T. H. 2009. Bushfires in Australia. *In:* CSIRO (ed.). CSIRO.

BURROWS, N. D. 1994. *Experimental development of a fire management model for Jarrah (Eucalyptus Marginata Donn ex Sm.) forest.* Doctor of Philosophy, Australian National University (ANU).

CANADA CENTRE FOR REMOTE SENSING. 2015. *Natural Resources Canada, Spatial Resolution, Pixel Size, and Scale* [Online]. Available: http://www.nrcan.gc.ca/node/9407 [Accessed 1 April 2017.

CASA 2002. Unmanned Aircraft and Rockets *Unmanned Aerial Vehicle (UAV) Operations, Design Specification, Maintenance and Training of Human Resources.* Australia: CASA.

CASA. 2013. *RPAs (Drones) in Civil Airspace and Challenges for CASA* [Online]. Canberra, Australia: Civil Aviation Safety Authority, Government of Australia. Available: http://www.casa.gov.au/scripts/nc.dll?WCMS:STANDARD:1001:pc=PC_101593 [Accessed 8 August 2014].

CASA 2014a. Notice of Proposed Rule Making, Remotely Piloted Aircraft Systems. *NPRM 1309OS – May 2014.* Canberra, Australia: CASA.

CASA 2014b. Annex C Draft Advisory Circulars:101-1, 101-4, 101-5. Australia: CASA.

CASBEER, D. W., BEARD, R. W., MCLAIN, T. W., SAI-MING, L. & MEHRA, R. K. Forest fire monitoring with multiple small UAVs. 2005 American Control Conference, ACC, June 8, 2005 - June 10, 2005, 2005 Portland, OR, United States. Institute of Electrical and Electronics Engineers Inc., 3530-3535.

CFA, C. F. A. 2012. *About Fire Danger Ratings, CFA - Country Fire Authority* [Online]. Country Fire Authority (CFA). Available: http://www.cfa.vic.gov.au/warnings-restrictions/about-fire-danger-ratings/ [Accessed 27 February 2017].

CFS, G. O. S. A. 2010. *CFS Fact Sheet - Bushfire Behaviour in Detail* [Online]. Available: http://www.agedcommunity.asn.au/wp-content/uploads/2014/10/cfs_fact_sheet_201_bushfire_behaviour.pdf [Accessed 27 February 2017].

CHANDER, G., MARKHAM, B. L. & HELDER, D. L. 2009. Summary of current radiometric calibration coefficients for Landsat MSS, TM, ETM+, and EO-1 ALI sensors. *Remote sensing of environment,* 113**,** 893-903.

CHENEY, P. & SULLIVAN, A. 2008. *Grassfires: Fuel, Weather and Fire Behaviour,* National Library of Australia Cataloguing-in-Publication entry, CSIRO Publishing.

CHOI, K. & LEE , I. 2011. A UAV BASED CLOSE-RANGE RAPID AERIAL MONITORING SYSTEM FOR EMERGENCY RESPONSES. *Conference on Unmanned Aerial Vehicle in Geomatics,.* Zurich, Switzerland.

COLOMINA, I. & MOLINA, P. 2014. Unmanned aerial systems for photogrammetry and remote sensing: A review. *ISPRS Journal of Photogrammetry and Remote Sensing,* 92**,** 79-97.

CRUM, S. 1995. *Aerial Photography and Remote Sensing* [Online]. Department of Geography, University of Texas at Austin,. Available: http://www.colorado.edu/geography/gcraft/notes/remote/remote.html [Accessed 27 February 2017].

DEPARTMENT OF DEFENCE. 2015. *Airservices Australia and Defence strengthen collaboration on Unmanned Aircraft Systems,* [Online]. http://news.defence.gov.au/2015/05/29/airservices-australia-and-defence-strengthen-collaboration-on-unmanned-aircraft-systems/ (01 Jun. 2015): Australian Government, Canberra, ACT. Available: http://news.defence.gov.au/2015/05/29/airservices-australia-and-defence-strengthen-collaboration-on-unmanned-aircraft-systems/ [Accessed 21/6/2015.

DEPARTMENT OF FIRE AND EMERGENCY SERVICES, D. 2017. *Factsheet Fire Behaviour* [Online]. Available: https://www.dfes.wa.gov.au/safetyinformation/fire/bushfire/BushfireFactsheets/DFES_Bushfire-Factsheet-How_bushfires_behave.pdf [Accessed 27 February 2017].

EISENBEIß, H. 2009. *UAV Photogrammetry.* Doctor of Sciences, University of Technology Dresden.

EVERAERTS, J. 2008. The use of unmanned aerial vehicles (UAVs) for remote sensing and mapping. *The International Archives of the Photogrammetry, Remote Sensing and Spatial Information Sciences*, 37**,** 1187-1192.

EVERAERTS, J. 2009. NEW PLATFORMS - Unconventional Platforms (Unmanned Aircraft Systems) for Remote Sensing. *In:* 56, T. R. (ed.) *European Spatial Data Research (EuroSDR).*

EVERAERTS, J., LEWYCKYJ, N. & FRANSAER, D. 2004. Pegasus: design of a stratospheric long endurance UAV system for remote sensing. *The International Archives of the Photogrammetry, Remote Sensing and Spatial Information Sciences,* 35.

EZEQUIEL, C. A. F., CUA, M., LIBATIQUE, N. C., TANGONAN, G. L., ALAMPAY, R., LABUGUEN, R. T., FAVILA, C. M., HONRADO, J. L. E., CANOS, V. & DEVANEY, C. UAV aerial imaging applications for post-disaster assessment, environmental management and infrastructure development. Unmanned Aircraft Systems (ICUAS), 2014 International Conference on, 2014. IEEE, 274-283.

FRANSAER, D., LEWYCKYJ, N., VANDERHAEGEHEN, F. & EVERAERTS, J. 2004. PEGASUS: Business model for a stratospheric long endurance UAV system for remote sensing. *The international archives of the photogrammetry, remote sensing and spatial information sciences, Istanbul, Turkey*.

GEOSCIENCE AUSTRALIA, C. O. A. 2016. Bushfire. *In:* AUSTRALIA, G. (ed.). CANBERRA ACT: Commonwealth of Australia (Geoscience Australia).

GOULD, J. S., MCCAW, W. L. & CHENEY, N. P. 2011. Quantifying fine fuel dynamics and structure in dry eucalypt forest (Eucalyptus marginata) in Western Australia for fire management. *Forest Ecology and Management,* 262**,** 531-546.

GRENZDÖRFFER, G. J., ENGEL, A. & TEICHERT, B. 2008. The photogrammetric potential of low-cost UAVs in forestry and agriculture. *The International Archives of the Photogrammetry, Remote Sensing and Spatial Information Sciences,* 31**,** 1207-1214.

GUMLEY, L., HUBANKS, P. & MASUOKA, E. 1994a. MODIS Airborne Simulator Level-1B Data User Guide, April 1994.

GUMLEY, L., HUBANKS, P. & MASUOKA, E. 1994b. *eMAS: Level-1B Data User's Guide* [Online]. Available: http://mas.arc.nasa.gov/reference/guide.html [Accessed 12 November 2014].

GUPTA, S. G., GHONGE, M. M. & JAWANDHIYA, P. 2013. Review of unmanned aircraft system (UAS). *technology*, 2.

HANDBRAKE. 2016. *HandBrake* [Online]. Available: https://handbrake.fr/downloads.php [Accessed 24 July 2016].

HARRIMAN L & J., M. 2013. A new eye in the sky: Eco-drones.

HDF GROUP. 2016. *The HDF Group* [Online]. Available: https://support.hdfgroup.org/products/java/hdfview/ [Accessed 1/1/2015 2015].

HEXAGONGEOSPATIAL. 2017. *Tie Points* [Online]. Available: https://hexagongeospatial.fluidtopics.net/search#!search;query=tie+points [Accessed 1 April 2017].

HRABAR, S., MERZ, T. & FROUSHEGER, D. Development of an autonomous helicopter for aerial powerline inspections. Applied Robotics for the Power Industry (CARPI), 2010 1st International Conference on, 2010. IEEE, 1-6.

ICAO 2005. Global Air Traffic Management Operational Concept. *Doc 9854 AN/458.* First Edition ed.: Secretary General.

ICAO 2011. Unmanned Aircraft Systems (UAS), ICAO Circular 328-AN/190. Quebec, Canada.

JPL, J. P. L. 2017. *Solar System Dynamics* [Online]. Available: https://ssd.jpl.nasa.gov/?ephemerides [Accessed 1 July 2015].

KABLE INTELLIGENCE LIMITED. 2014. *Zephyr Solar-Powered HALE UAV - Airforce Technology* [Online]. Available: http://www.airforce-technology.com/projects/zephyr/ [Accessed 21/08/2014 2014].

KALINSKI, A. & NORTH COAST MEDIA LLC. 2015. *Georeferenced Full Motion Video: Mitigating a Difficult a Big Data Problem : Geospatial Solutions* [Online]. Geospatial Solutions. Available: http://geospatial-solutions.com/georeferenced-full-motion-video-mitigating-a-difficult-big-data-problem/ [Accessed 23 March 2017].

KAUFMAN, Y. J., JUSTICE, C. O., FLYNN, L. P., KENDALL, J. D., PRINS, E. M., GIGLIO, L., WARD, D. E., MENZEL, W. P. & SETZER, A. W. 1998. Potential global fire monitoring from EOS-MODIS. *Journal of Geophysical Research: Atmospheres,* 103**,** 32215-32238.

KOPARDEKAR, P. H. 2015. *NASA Ames Research Center UAS Traffic Management Project Enaballing Civillian Low-Altitude Airspace and Unmanned Aeerial Systems Operations,* RPAS Yearbook.

KUMAR, R., SAWHNEY, H. S., ASMUTH, J. C., POPE, A. & HSU, S. Registration of video to geo-referenced imagery. 14th International Conference on Pattern Recognition, ICPR 1998, August 16, 1998 - August 20, 1998, 1998 Brisbane, QLD, Australia. Institute of Electrical and Electronics Engineers Inc., 1393-1400.

LEE, T. F. & TAG, P. M. 1990. Improved detection of hotspots using the AVHRR 3.7-um channel. *Bulletin of the American Meteorological Society,* 71**,** 1722-1730.

LEWIS, P., FOTHERINGHAM, S. & WINSTANLEY, A. 2011. Spatial video and GIS. *International Journal of Geographical Information Science,* 25**,** 697-716.

LIGHT, J. 2016. Drones to be Intergrated into Airspace by 2030. *Drone Magazine.*

LUKE, R. H. & MCARTHUR, A. G. 1986. *Bushfires in Australia,* Canberra, Canberra publishing and Printing Co.

MAPSMADEEASY. 2016. *Maps Made Easy* [Online]. Available: https://www.mapsmadeeasy.com/ [Accessed 24 July 2016].

MCCAW, L., MILLS, G., SULLIVAN, A., HURLEY, R., ELLIS, P., MATTHEWS, S., PLUCINSKI, M., PIPPEN, B. & BOURA, J. 2009. Victorian 2009 bushfire research response: Final Report. *In:* DEPARTMENT OF ENVIRONMENT & CONSERVATION WA, B. O. M., CSIRO, GREAT SOUTHERN PLANTATIONS, TERRAMATRIX (ed.) *Research Results from February 7th 2009 Victorian Fires Findings on: Fire Behaviour Investigation.*

MERINO, L., CABALLERO, F., MARTÍNEZ-DE-DIOS, J. R., MAZA, I. & OLLERO, A. 2012. An unmanned aircraft system for automatic forest fire monitoring and measurement. *Journal of Intelligent & Robotic Systems,* 65**,** 533-548.

MERION, L., CABALLERO, F., MARTÍNEZ-DE-DIOS, J. R., MAZA, I. & OLLERO, A. Automatic Forest Fire Monitoring and Measurement using Unmanned Aerial Vehicles. VI International Conference on Forest Fire Research, 15-18 November 2010 Coimbra, Portugal.

MERLIN, P. W. 2009. Ikhana: Unmanned Aircraft System Western States Fire Missions. Washington, D.C. USA: National Aeronautics and Space Administration, NASA History Office.

MEYER, J., DU PLESSIS, F. & CLARKE, W. 2009. *Design considerations for long endurance unmanned aerial vehicles,* INTECH Open Access Publisher.

MISB, M. I. S. B. 2016. *About the MISB* [Online]. Available: http://www.gwg.nga.mil/misb/faq.html#section1.1.

MITCHELL, B. 2009. Satellite Spectrum to Support Unmmanned Aircraft Systems (UAS) Control Links. *In:* ICAO (ed.) *Aeronautical Communications Panel (ACP) Working Group F Meeting, Agenda 4: Development of material for ITU-R meetings.* Bangkok, Thailand: ICAO.

MONDELLO, C., HEPNER, G. F. & WILLIAMSON, R. A. 2004. 10-year industry forecast. *Photogrammetric engineering and remote sensing,* 70**,** 5-58.

NASA. 2013. *National Aeronautics and Space Administration- Goddard Space Flight Center -Imagine the Universe* [Online]. Available: https://imagine.gsfc.nasa.gov/science/toolbox/emspectrum1.html [Accessed 15 March 2017].

NASA. 2014. *Wildfires Today - NASA Autonomous Modular Scanner (AMS) – WILDFIRE Airborne Instrument* [Online]. Available: wildfiretoday.com/documents/AMS_sensor_description.

NASA. 2016. *MODIS Characterization Support Team* [Online]. Available: http://mcst.gsfc.nasa.gov/forums/how-can-i-extract-temperature-l1b-data-product [Accessed 7 July 2015].

NORTHROP GRUMMAN CORPORATION. 2015. *MQ-8C Fire Scout Data Sheet* [Online]. San Diego. Available: http://www.northropgrumman.com/Capabilities/FireScout/Documents/pageDocuments/MQ-8C_Fire_Scout_Data_Sheet.pdf [Accessed 9 October 2016].

NOVA SCIENCE PROGRAMMING ON AIR AND ONLINE. 2002. *Spies That Fly -Time Line of UAVs* [Online]. Available: http://www.pbs.org/wgbh/nova/spiesfly/uavs.html [Accessed 19/8/14 2014].

NSW RURAL FIRE SERVICE, R. 2015. *Bush Fire Behaviour* [Online]. Available: http://www.rfs.nsw.gov.au/plan-and-prepare/building-in-a-bush-fire-area/bush-fire-protection-measures/bush-fire-behaviour [Accessed 27 February 2017].

PAZ-FRANKEL, E. & NOCAMELS. 2014. *Zano's Micro-Drone Follows You To Capture HD Selfies From The Sky* [Online]. NoCamels. Available: http://nocamels.com/2014/12/micro-drone-zano-selfies/ [Accessed 28 December 2016].

PETERSON, D., WANG, J., ICHOKU, C., HYER, E. & AMBROSIA, V. 2013. A sub-pixel-based calculation of fire radiative power from MODIS observations: 1: Algorithm development and initial assessment. *Remote Sensing of Environment,* 129**,** 262-279.

PHILIP, S. 2007. *Active Fire Detection Using Remote Sensing Based Polar-Orbiting and Geostationary Observations: An Approach Towards Near Real-Time Fire Monitoring.* Master of Science (M.Sc).

PIX4D. 2016. *Pix4D site support* [Online]. Available: https://support.pix4d.com/hc/en-us/articles/205327965-Menu-Process-Processing-Options-1-Initial-Processing-Calibration#gsc.tab=0 [Accessed 24 July 2016].

RAPINETT, A. 2009. *Zephyr: a high altitude long endurance unmanned air vehicle.* Masters in Physics, University of Surrey.

RICCARDI, C. L., OTTMAR, R. D., SANDBERG, D. V., ANDREU, A., ELMAN, E., KOPPER, K. & LONG, J. 2007. The fuelbed: a key element of the Fuel Characteristic Classification System This article is one of a selection of papers published in the Special Forum on the Fuel Characteristic Classification System. *Canadian Journal of Forest Research,* 37**,** 2394-2412.

RUANO, S., GALLEGO, G., CUEVAS, C. & GARCIA, N. Aerial video georegistration using terrain models from dense and coherent stereo matching. Geospatial InfoFusion and Video Analytics IV; and Motion Imagery for ISR and Situational Awareness II, May 5, 2014 - May 6, 2014, 2014 Baltimore, MD, United states. SPIE, The Society of Photo-Optical Instrumentation Engineers (SPIE).

SAN DIEGO STATE UNIVERSITY. 2007a. *The San Diego Wildfires Education Project, San Diego 2007 Wildfires - Witch Fire* [Online]. Available: https://interwork.sdsu.edu/fire/photo_gallery/2007_fires/witch.html [Accessed 1 April 2017].

SAN DIEGO STATE UNIVERSITY. 2007b. *Zaca Fire, 2007, Los Padres National Forest, Santa Barbara County* [Online]. San Diego, California: San Diego State University. Available: https://interwork.sdsu.edu/fire/resources/ZacaFire.htm [Accessed 2017 2017].

SE, S., FIROOZFAM, P., GOLDSTEIN, N., DUTKIEWICZ, M. & PACE, P. Automated UAV-based video exploitation for mapping and surveillance. Proceedings of the 2010 Canadian Geomatics Conference and Symposium of Commission I, 2010.

SHERIDAN, J. 2015. Application of the Heron MALE Category UAS for Disaster Relief and Response. *In:* HOMAINEJAD, N. (ed.). NSW.

SMART, P. 2016. Heron UAS to operate in civil airspace. *Australian Defence Magazine.*

STEPHENSON, C. 2015. *International Federation of Air Traffic Controllers Associations Views and Considerations Concerning RPAS,* RPAS Year Book, UVS International.

SUPPORT TO AVIATION CONTROL SERVICE. 2011. *Solar Zenith Angle (SZA)* [Online]. Available: http://sacs.aeronomie.be/info/sza.php [Accessed 27 February 2017].

SVENSEN, G. 2014. *Barriers to Commercial UAS Expansion in Australia.* Master of Science and Technology (Aviation), University of New South Wales.

TAYLOR, C. R. & SETTERGREN, R. J. Full-motion video georegistration for accuracy improvement, accuracy assessment, and robustness. SPIE Defense, Security, and Sensing, 2012. International Society for Optics and Photonics.

THE GOVERNMENT OF SOUTH AUSTRALIA, C. 2017. *Bushfire Behaviour* [Online]. The Government of South Australia. Available: http://www.cfs.sa.gov.au/site/prepare_for_bushfire/know_your_risk/bushfire_behaviour.jsp [Accessed 27 February 2017].

TROPICAL SAVANNAS CRC, C. R. C. F. T. S. M. & BUSHFIRE CRC. 2017. *Fire Ecology and Management in Northern Australia* [Online]. Available: http://learnline.cdu.edu.au/units/env207/fundamentals/weather.html [Accessed 14 January 2017].

VAN BLYENBURGH, P. 1999. UAVs: an overview. *Air & Space Europe,* 1**,** 43-47.

VAN BLYENBURGH, P. 2000. Uavs-current situation and considerations for the way forward. DTIC Document.

WANG, J., GARRATT, M., LAMBERT, A., WANG, J. J., HANA, S. & SINCLAIR, D. 2008. Integration of GPS/INS/Vision Sensors to Navigate Unmanned Aerial Vehicles. *The International Archives of the Photogrammetry, Remote Sensing and Spatial Information Sciences,* XXXVII**,** 863-970.

WATTS, A. C., AMBROSIA, V. G. & HINKLEY, E. A. 2012. Unmanned aircraft systems in remote sensing and scientific research: Classification and considerations of use. *Remote Sensing,* 4**,** 1671-1692.

WILDES, R. P., HIRVONEN, D. J., HSU, S. C., KUMAR, R., LEHMAN, W. B., MATEI, B. & ZHAO, W.-Y. Video georegistration: algorithm and quantitative evaluation. Computer Vision, 2001. ICCV 2001. Proceedings. Eighth IEEE International Conference on, 2001. IEEE, 343-350.

WILLIS, R., GADD, M. & CARY, L. 2015. International Civil Aviation Organization, The ICAO RPAS Panel. *RPAS Yearbook- RPAS: The Global Perspective.* 13 edition ed.

WONG, K. & BIL, C. Uavs over Australia. 21th International Council of the Aeronautical Sciences Conference (ICAS 98), Melbourne, Victoria, Australia, 1998. 13-18.

XIAO, J., CHENG, H., HAN, F. & SAWHNEY, H. Geo-spatial aerial video processing for scene understanding and object tracking. Computer Vision and Pattern Recognition, 2008. CVPR 2008. IEEE Conference on, 2008. IEEE, 1-8.

XU, Z., YANG, J., PENG, C., WU, Y., JIANG, X., LI, R., ZHENG, Y., GAO, Y., LIU, S. & TIAN, B. 2014. Development of an UAS for post-earthquake disaster surveying and its application in Ms7.0 Lushan Earthquake, Sichuan, China. *Computers and Geosciences,* 68**,** 22-30.

ZAJKOWSKI, T. J., DICKINSON, M. B., HIERS, J. K., HOLLEY, W., WILLIAMS, B. W., PAXTON, A., MARTINEZ, O. & WALKER, G. W. 2016a. Evaluation and use of remotely piloted aircraft systems for operations and research-RxCADRE 2012.

ZAJKOWSKI, T. J., DICKINSON, M. B., HIERS, J. K., HOLLEY, W., WILLIAMS, B. W., PAXTON, A., MARTINEZ, O. & WALKER, G. W. 2016b. Evaluation and use of remotely piloted aircraft systems for operations and research–RxCADRE 2012. *International Journal of Wildland Fire,* 25**,** 114-128.

# APPENDIX A - MATLAB SOFTWARE CODE FOR AMS DATA

```
% open relevant files from the metadata
% seperate each band from the calibrated data.
% then seperate the rows and columns for each band to build a complete
image
clc
clear
close all
[FileName,PathName,FilterIndex] = uigetfile('*.hdf', 'Select a HDF file');
CalibratedData = hdfread(FileName, '/CalibratedData', 'Index', {[1  1
1],[1  1  1],[2805    12   716]});
PixelLatitude = hdfread(FileName, '/PixelLatitude', 'Index', {[1  1],[1
1],[2805   716]});
PixelLongitude = hdfread(FileName, '/PixelLongitude', 'Index', {[1  1],[1
1],[2805   716]});
lat=PixelLatitude;
lon=PixelLongitude;
axesm eqdcylin
setm(gca,'maplatlimit',[min(min(lat)) max(max(lat))]);
setm(gca,'maplonlimit',[min(min(lon)) max(max(lon))]);
PixelElevation = hdfread(FileName, '/PixelElevation', 'Index', {[1  1],[1
1],[2805   716]});
SolarAzimuthAngle = hdfread(FileName, '/SolarAzimuthAngle', 'Index', {[1
1],[1  1],[2805   716]});
SolarZenithAngle = hdfread(FileName, '/SolarZenithAngle', 'Index', {[1
1],[1  1],[2805   716]});
SZ=double(SolarZenithAngle);
SA=double(SolarAzimuthAngle);
NoImageLayer=size(CalibratedData,2);
for i=1:NoImageLayer
    Temp=CalibratedData(:,i,:);
    W=size(Temp,1);
    H=size(Temp,3);
    ProcessedIm=zeros(H,W);
    for j=1:H
        for k=1:W
            ProcessedIm(j,k)=Temp(k,1,j);
        end
    end
    ProcessedIm=mat2gray(ProcessedIm);
    ProcessedIm=ProcessedIm';
    eval(['Im' num2str(i) '=ProcessedIm;'])
    figure
    imshow(ProcessedIm);
    title(['Image ' num2str(i) ]);
end
%% multiply each band by its scale factor. this information was supplied in
the metadata
band7=squeeze(CalibratedData(:,7,:));
B7=(double(band7))*0.1;
band9=squeeze(CalibratedData(:,9,:));
B9=(double(band9)).*0.1;
band10=squeeze(CalibratedData(:,10,:));
B10=(double(band10)).*0.1;
```

```
band11=squeeze(CalibratedData(:,11,:));
B11=(double(band11)).*0.01;
band12=squeeze(CalibratedData(:,12,:));
B12=(double(band12)).*0.01;

%% Compute Brightness Temperature

% Compute Brightness Temperature for Band 11

c1=0.014387686;
c2=1.1910439e-16;
L11=((3.60+3.79)/2)./1e6;
radiance11=double(B11).*1e6;

% identified complex values in band 11. these values were real values but
% were displaying as complex values in matlab. i identified the pixels and
fixed the
% values. these values were also cross checked manually

%
StoreIndex=[1767,463;1777,458;1838,406;1967,480;1970,476;1999,477;2007,481;
2066,407;2067,407;2068,407;2089,488;2090,488;2092,488;2097,488;2098,488;209
9,488;2120,440;2121,467;2122,467;2125,470;2130,471;2133,471;2134,471;2140,4
26;2141,426;2164,449;2165,449;2168,449;2169,449];
% radiance11=NaNR(StoreIndex,radiance11);
temp_Band11=(c2./(L11^5.*radiance11));
temp2_Band11=log(double(temp_Band11)+1);
BT_Band11=L11.*temp2_Band11;
BT_Band11=real(BT_Band11);
BT1_Band11=c1./BT_Band11;

% Comute Brightness Temperature of Band 12

c1=0.014387686;
c2=1.1910439e-16;
L12=((10.26+11.26)/2)./1e6;
radiance12=double(B12).*1e6;

temp_Band12=(c2./(L12^5.*radiance12));
temp2_Band12=log(double(temp_Band12)+1);
BT_Band12=L12.*temp2_Band12;
BT1_Band12=c1./BT_Band12;

% compute the reflectance value for band 7

top=(pi.*B7).*(0.98937^2);
a=cos((SZ.*pi)./180);
bottom=(1207.6049.*a);
BT1_Band7=top./bottom;

%% Hot spot detection using the ikhana hotspot detection algorithm

BT=BT1_Band11-BT1_Band12;
firetest1=(BT1_Band11>380);
firetest2=(BT1_Band12>240);
firetest3=(BT>14);
firetest4=(BT1_Band7<0.15);
fire=(firetest1&firetest2&firetest3&firetest4);
```

```
% display the figure
figure, imshow (fire, []);
colormap (jet);
[r,c]=find(fire==1);
FireNo=numel(r);
%colorbar;



%display the DEM
figure, imshow (PixelElevation, []);
colormap (jet);
%colorbar;

% %% knn nearest neighbors
%
% X is the data and Y its corresponding value
% Number of rows of X and Y are same
N = 2805;   % Vector dimension of X
Y = fire;
M = 100;    % Number of vectors used for training
train_y=Y(1901:2000,451:550);
X = fire;
test_x=X;
test_y=train_y;


X = X(1:M,1:100);
X = double(X);
Y = find(Y(1,1:5))-1;
for j=2:M;
    Y = [Y find(train_y(j,1:100))-1];
end
Y = Y';

% test data set : t_x, value corresponding to an entry in t_x : t_y
n = 100;    % No. of test cases : n
t_x = test_x(1:n,1:100);
t_x = double(t_x);
t_y = find(test_y(1,1:100))-1;
for j=2:n;
    t_y = [t_y find(test_y(j,1:100))-1];
end
t_y = t_y';

error_fraction = [];

K = 49;   % K is the no. of neighbours to be looked at
for k=1:K;
    count = 0;
    for i=1:n;
        IDX = knnsearch(X,t_x(i,1:100),'K',k);
        cmp = mode(Y(IDX));
        if cmp ~= t_y(i)
            count = count + 1;
        end
    end
    ef = count/n;
```

```
%    disp(['Fraction of estimates wrong while considering ' num2str(k) '
neighbours is ' num2str(ef)]);
    error_fraction = [error_fraction ef];
end
x = 1:1:K;
plot((1:K),error_fraction,'-*k');
xlabel('No. of neighbours')
ylabel('Error fraction')
```

# APPENDIX B- MATLAB HOTSPOT ANALYSIS RESULTS

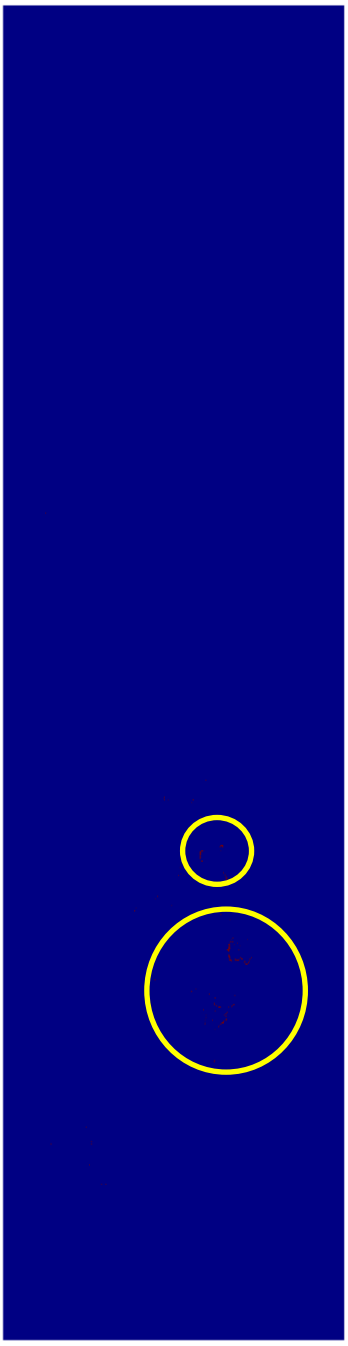

Figure B.1- Image strip 4 from the AMS wildfire sensor of the Witch, Poomacha & Rice Fires, with the fire pixels in red (yellow circle around them) and non-fire pixels in blue

Figure B.2 - Image strip 16 from the AMS wildfire sensor of the Witch, Poomacha & Rice Fires, with the fire pixels in red (yellow circle around them) and non-fire pixels in blue

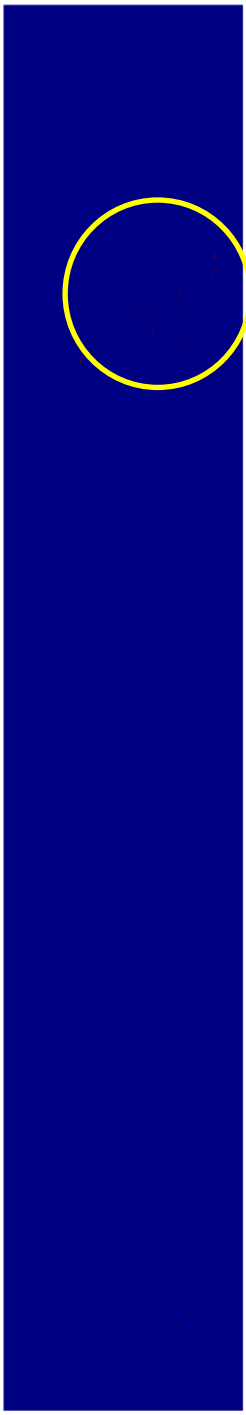

Figure B.3 - Image strip 6 from the AMS wildfire sensor of the Witch, Poomacha & Rice Fires, with the fire pixels in red (yellow circle around them) and non-fire pixels in blue

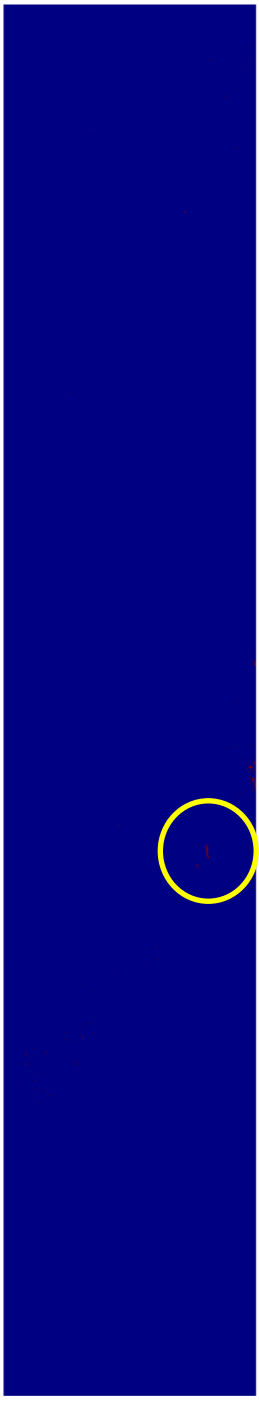

Figure B.4- Image strip 7 from the AMS wildfire sensor of the Witch, Poomacha & Rice Fires, with the fire pixels in red (yellow circle around them) and non-fire pixels in blue

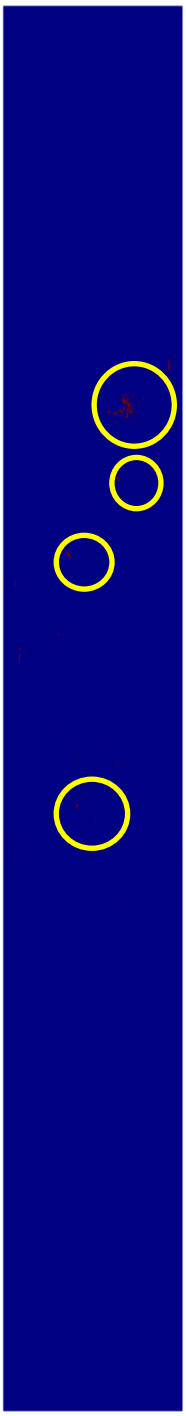

Figure B.5 - Image strip 8 from the AMS wildfire sensor of the Witch, Poomacha & Rice Fires, with the fire pixels in red (yellow circle around them) and non-fire pixels in blue

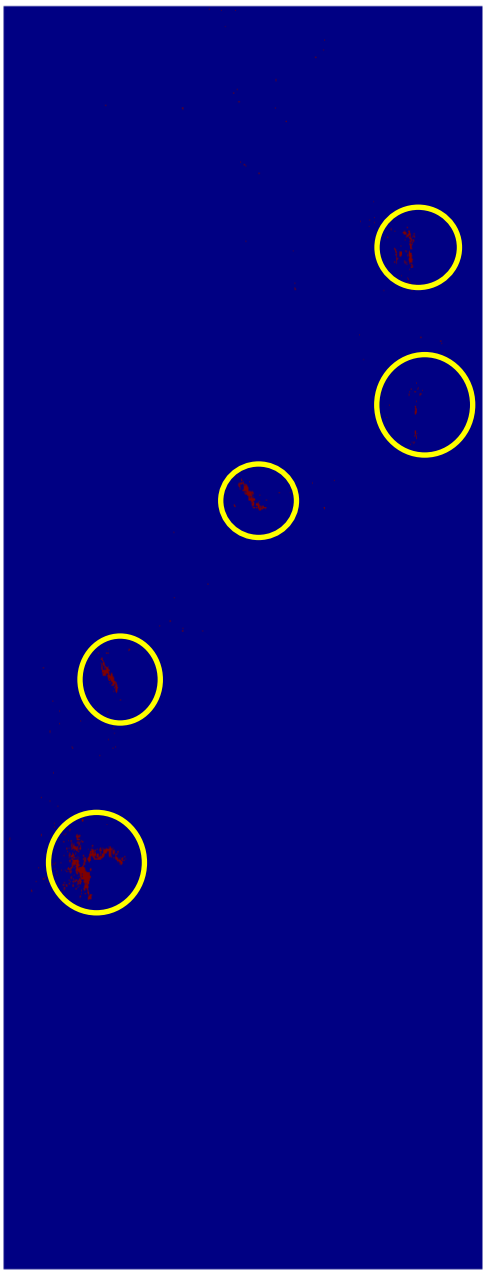

Figure B.6- Image strip 9 from the AMS wildfire sensor of the Witch, Poomacha & Rice Fires, with the fire pixels in red (yellow circle around them) and non-fire pixels in blue

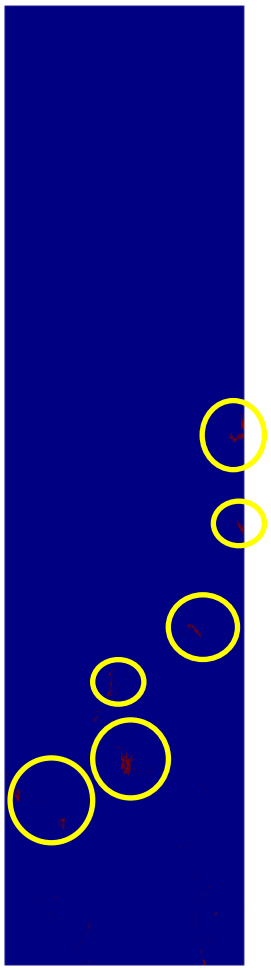

Figure B.7 - Image strip 10 from the AMS wildfire sensor of the Witch, Poomacha & Rice Fires, with the fire pixels in red (yellow circle around them) and non-fire pixels in blue

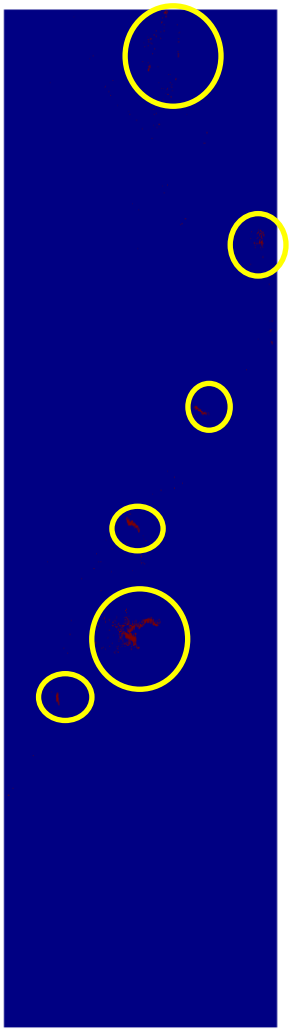

Figure B.8- Image strip 11 from the AMS wildfire sensor of the Witch, Poomacha & Rice Fires, with the fire pixels in red (yellow circle around them) and non-fire pixels in blue

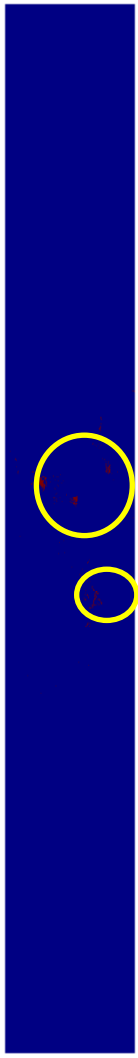

Figure B.9 - Image strip 12 from the AMS wildfire sensor of the Witch, Poomacha & Rice Fires, with the fire pixels in red (yellow circle around them) and non-fire pixels in blue

Figure B.10- Image strip 13 from the AMS wildfire sensor of the Witch, Poomacha & Rice Fires, with the fire pixels in red (yellow circle around them) and non-fire pixels in blue

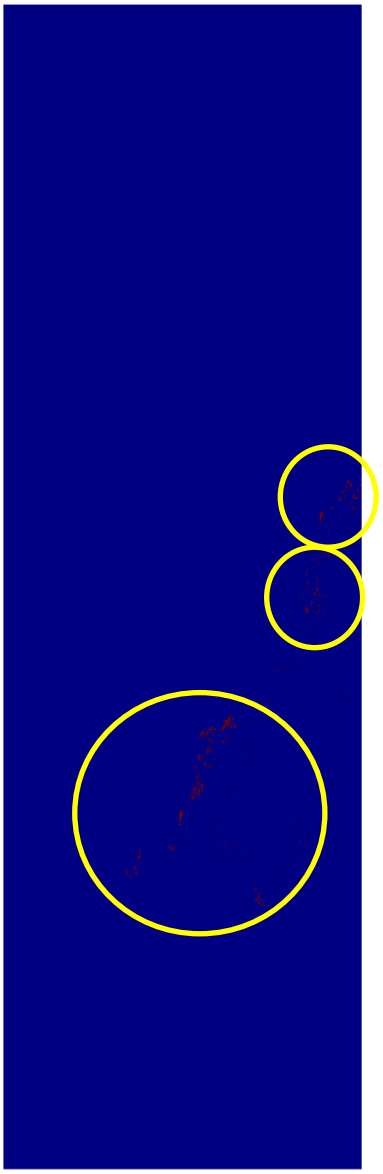

Figure B.11 - Image strip 14 from the AMS wildfire sensor of the Witch, Poomacha & Rice Fires, with the fire pixels in red (yellow circle around them) and non-fire pixels in blue

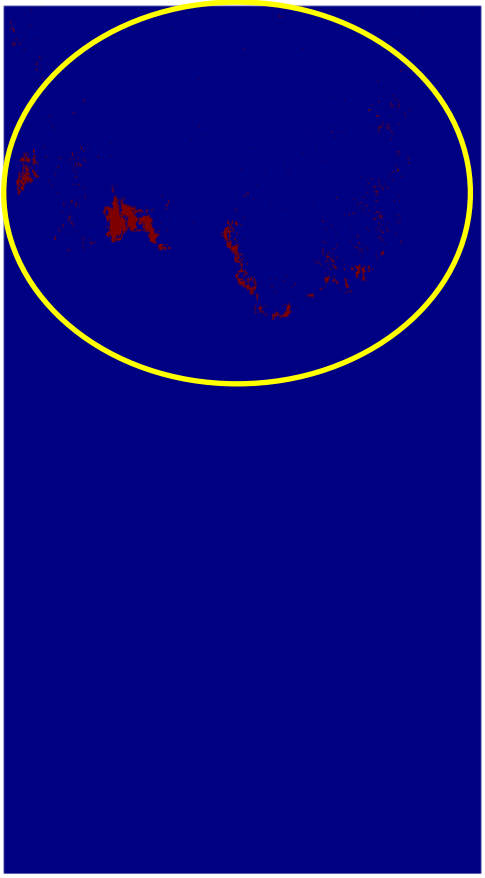

Figure B.12- Image strip 15 from the AMS wildfire sensor of the Witch, Poomacha & Rice Fires, with the fire pixels in red (yellow circle around them) and non-fire pixels in blue

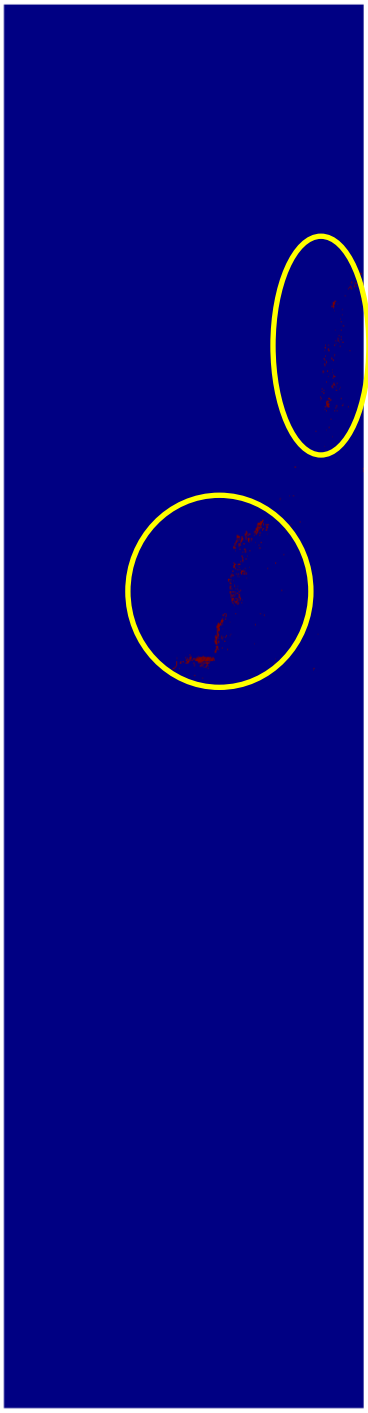

Figure B.13 - Image strip 16 from the AMS wildfire sensor of the Witch, Poomacha & Rice Fires, with the fire pixels in red (yellow circle around them) and non-fire pixels in blue

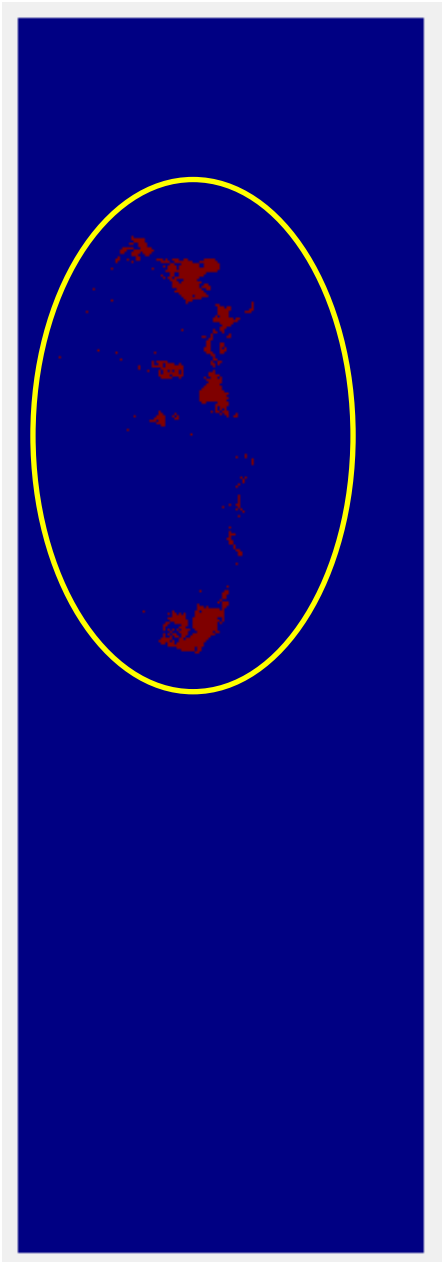

Figure B.14- Image strip 1 from the AMS wildfire sensor of the Zaca Fire, with the fire pixels in red (yellow circle around them) and non-fire pixels in blue

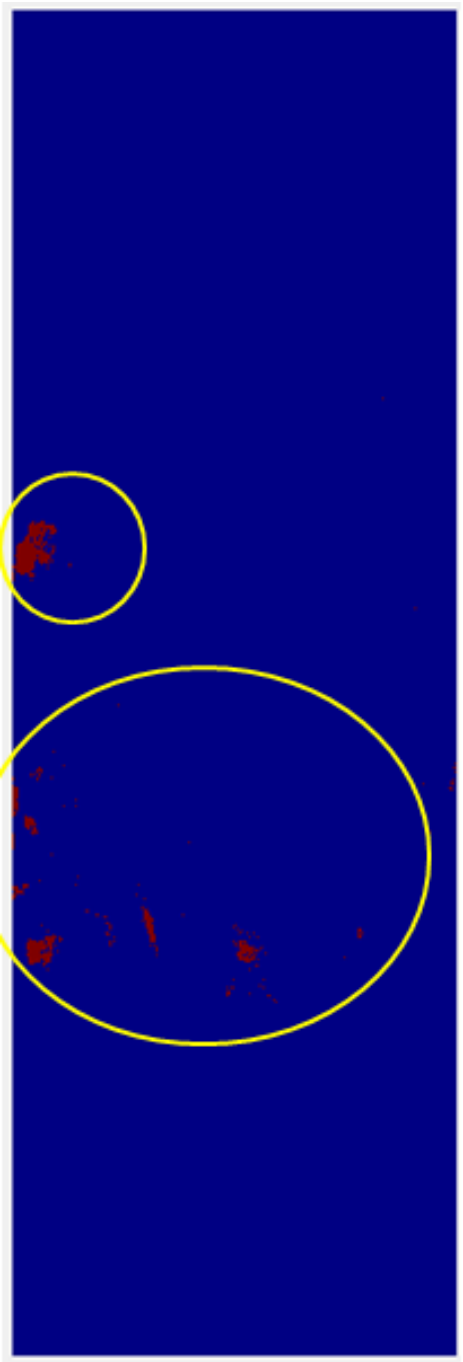

Figure B.15 - Image strip 2 from the AMS wildfire sensor of the Zaca Fire, with the fire pixels in red (yellow circle around them) and non-fire pixels in blue

Figure B.16- Image strip 3 from the AMS wildfire sensor of the Zaca Fire, with the fire pixels in red (yellow circle around them) and non-fire pixels in blue

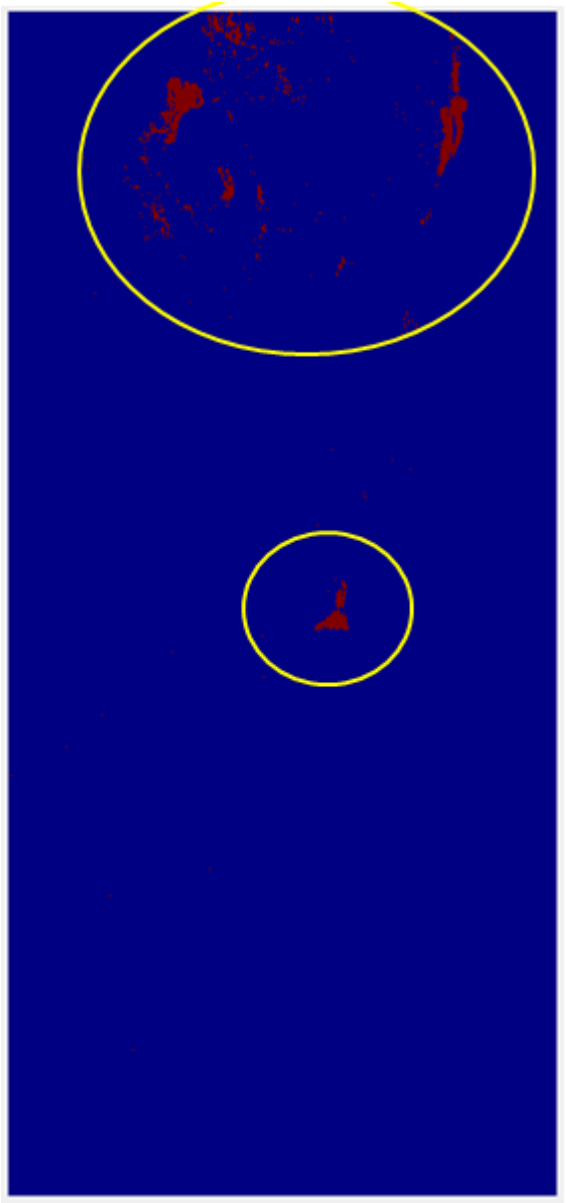

Figure B.17 - Image strip 4 from the AMS wildfire sensor of the Zaca Fire, with the fire pixels in red (yellow circle around them) and non-fire pixels in blue

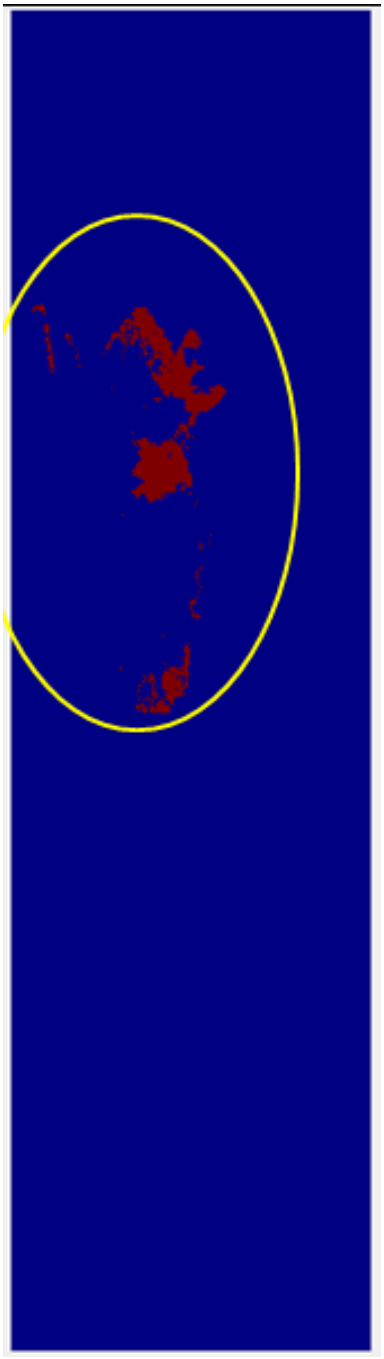

Figure B.18 - Image strip 5 from the AMS wildfire sensor of the Zaca Fire, with the fire pixels in red (yellow circle around them) and non-fire pixels in blue

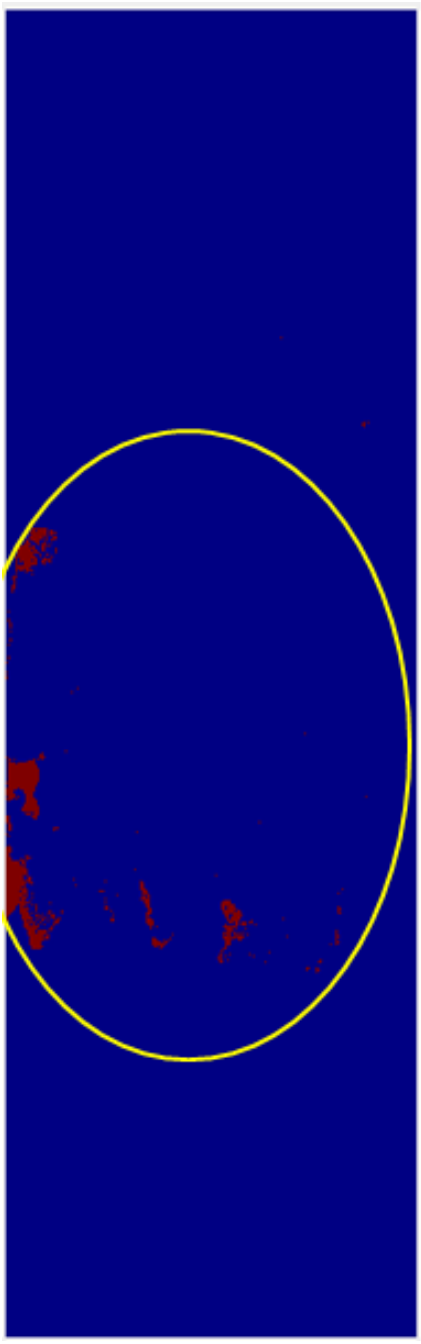

Figure B.19 - Image strip 6 from the AMS wildfire sensor of the Zaca Fire, with the fire pixels in red (yellow circle around them) and non-fire pixels in blue

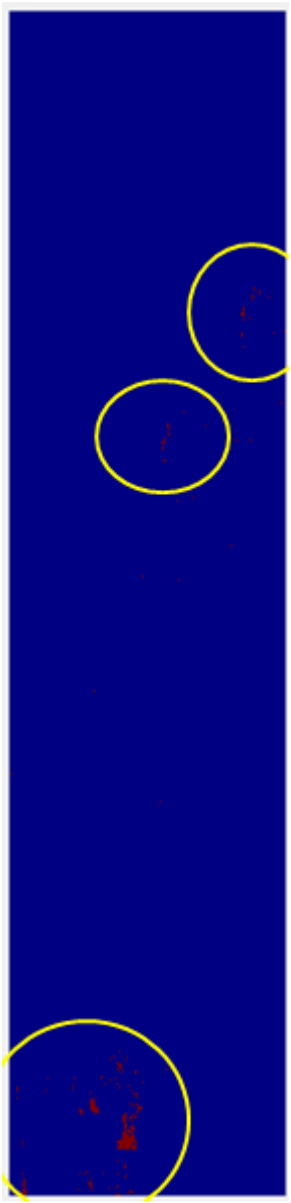

Figure B.20 - Image strip 7 from the AMS wildfire sensor of the Zaca Fire, with the fire pixels in red (yellow circle around them) and non-fire pixels in blue

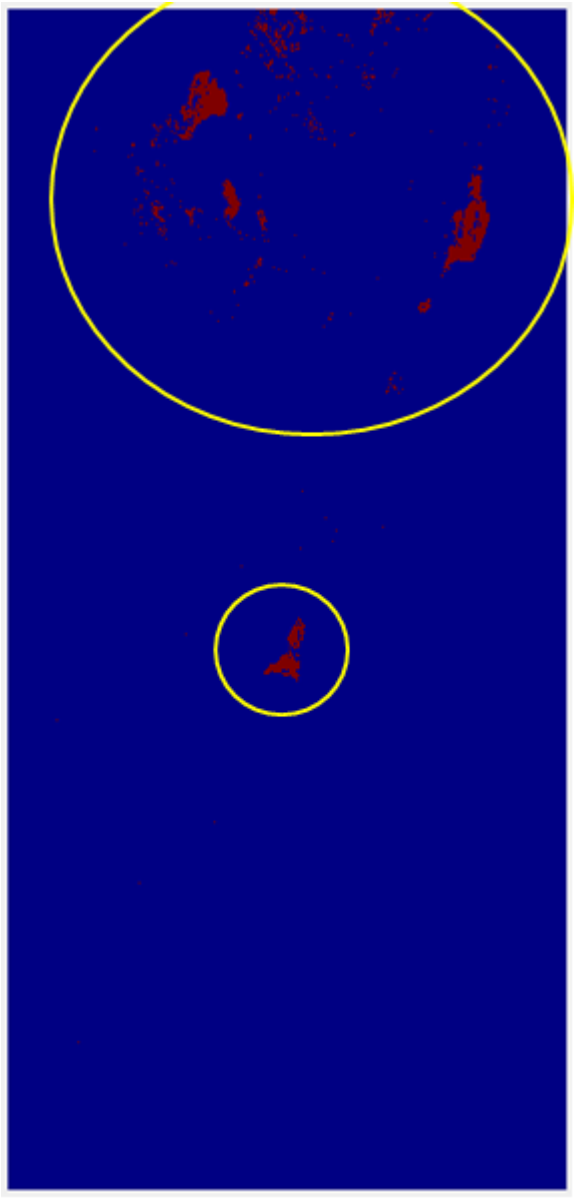

Figure B.21- Image strip 8 from the AMS wildfire sensor of the Zaca Fire, with the fire pixels in red (yellow circle around them) and non-fire pixels in blue